

Chlorophyll Fluorescence Spectrometer

Group 1

David Maria, Computer Engineering

Luke Preston, Electrical Engineering

Robert Bernson, Photonic Science & Engineering

Samuel Knight, Photonic Science & Engineering

Table of Contents

1. Executive Summary	1
2. Project Description.....	2
2.1 Motivation	2
2.2 Project Goals and Objectives	2
2.3 Requirement Specifications.....	3
2.4 Engineering Trade-Off Matrix	3
2.5 Block Diagram	5
3. Constraints & Standards	7
3.1 Standards	7
3.1.1 RoHS Compliance	7
3.1.2 Eye Safety.....	8
3.1.3 FDA Performance Standards for Light-Emitting Products	8
3.1.3 IEEE 802.15.1 - Bluetooth	9
3.1.4 ISO/IEC 9899 – The C Language.....	9
3.1.4.1 ANSI C (C89 / C90)	10
3.1.4.2 C99.....	10
3.1.4.3 C11.....	10
3.1.4.4 C18.....	11
3.1.5 Surface Quality for Optics.....	11
3.1.5.1 US Standard MIL-PRF-13830B (Scratch-Dig)	11
3.2 Constraints.....	13
3.2.1 Economic	13
3.2.2 Environmental	13
3.2.3 Social	14
3.2.4 Political.....	14
3.2.5 Health and Safety.....	14
3.2.6 Manufacturability	15
3.2.7 Sustainability	16
3.2.8 Time Constraints.....	16
4. Project Research.....	18
4.1 Similar Products	18
4.2 Light Source	18
4.2.1 Laser Module	20
4.2.2 Cuvettes	22
4.2.4 Chlorophyll Sample Preparation	23
4.3 Optics	24
4.3.1 The Slit	24
4.3.2 Collecting & Focusing Optics	25

4.3.3 Monochromator	25
4.3.3.1 Diffraction Grating.....	25
4.3.3.2 Monochromator Conclusions.....	27
4.4 Sensor System	28
4.4.1 Linear Sensor Arrays	28
4.4.1.1 AMS TSL1401CL.....	29
4.4.1.2 AMS TSL3301CL.....	29
4.4.1.3 Melexis MLX75306 3rd Generation.....	29
4.4.2 Square CCD Sensors	29
4.4.2.1 Renesas ISL29147	30
4.4.2.2 Texas Instruments OPT3002.....	30
4.4.2.3 ON Semiconductor AR0130CS Series	31
4.4.3 Sensor Comparisons	31
4.4.4 Sensor Conclusions.....	33
4.5 Electronics.....	33
4.5.1 Printed Circuit Board.....	33
4.5.2 PCB Design Software.....	35
4.5.3 CPU	35
4.5.4 ARM7	36
4.5.5 ARM Cortex-M	36
4.5.6 Power Delivery	37
4.5.7 Battery	41
4.5.8 Battery Charging Circuit	42
4.6 User Interface	44
4.6.1 Smartphone Application (Wireless)	44
4.6.2 Desktop Application (Wired)	44
4.6.3 On-Board Touch Screen	44
4.6.4 On-Board Display with Mechanical Buttons.....	45
4.6.5 User Interface Comparison and Final Selection.....	45
4.7 Wireless Communication	46
4.7.1 Bluetooth Classic.....	46
4.7.2 Bluetooth Low Energy.....	47
4.7.3 Wi-Fi.....	48
4.7.4 ZigBee Wireless Technology	49
4.7.5 Wireless Communication Comparison and Final Selection	50
4.8 Wired Communication	50
4.8.1 UART	51
4.8.2 I2C	52
4.8.3 SPI	54
4.8.4 Wired Communication Comparison and Final Selections	55
4.9 Bluetooth Module.....	56

4.9.1 HC-05	56
4.9.2 RN42.....	57
4.9.3 RN4020.....	58
4.9.4 ESP32	59
4.9.5 Bluetooth Module Comparison and Final Selection.....	60
5. Project Design.....	61
5.1 Hardware Design.....	61
5.1.1 Optical Housing Design.....	61
5.1.2 Optical Loss Calculations.....	66
5.1.3 Electronics Design.....	69
5.1.4 Laser Housing Design	76
5.1.5 Housing Design	76
5.2 Software Design	79
5.2.1 Embedded Software Design	79
5.2.1 Embedded Software Design	80
5.2.1.1 Block Diagram.....	81
5.2.1.2 Image Sensor Interaction	81
5.2.1.3 Bluetooth Sensor Interaction.....	83
5.2.2 Mobile Application Software Design.....	84
5.2.2.1 Block Diagram.....	85
5.2.2.2 Bluetooth Communication Design.....	85
5.2.2.3 Local Database Design	86
5.2.2.4 Graphical User Interface Design.....	87
5.3 Bill of Materials	90
5.4 Design Summary.....	90
6. Building and Testing.....	91
6.1 Introduction	91
6.2 Status Summary.....	91
6.3 Part Acquisition.....	92
6.4 Hardware Component Testing	92
6.4.1 RN4020 – Bluetooth Module Testing	92
6.4.2 AR0130CS – CMOS Monochromatic Sensor Testing.....	94
6.4.3 STM32F407VET6 – Development Board Testing.....	97
6.4.4 Newport 33066FL01-270R Diffraction Grating Testing.....	99
6.4.5 Laser Source Testing	100
6.4.6 Fluorescence Spectrum Testing.....	101
6.5 Software Testing	103
6.5.1 Development Board Emulation	103
6.5.2 Physical Measurements	104
6.5.3 Mobile Application Automated Testing.....	104
6.6 Building the Device.....	105

6.6.1 CFS Base and Walls	105
6.6.2 Posts, Mounts, and Holders	107
6.7 Integration Testing	107
6.7.1 Pixel Calibration	108
6.7.2 Camera Imagery and Spectrums.....	109
6.7.3 CFS Mobile Application Spectrums.....	110
6.8 Building and Testing Discussion.....	112
7. Operating Procedures.....	114
7.1 Sample Preparation	114
7.2 Mobile Application	114
8. Administrative.....	117
8.1 Milestones	117
8.2 Budget and Avenues of Financing	118
8.3 Division of Labor	118
9. Project Summary/Conclusion	120
Appendix A – References	i
Appendix B – Permissions.....	iii
Appendix C – Extra Tables and Figures	viii

List of Equations

Equation 1. Diffraction angle for a grating with light at normal incidence.....	26
Equation 2. Diffraction angle for a grating with light inbound from non-normal angle θ_i	26
Equation 3. Blazed grating equation.....	26
Equation 4. Calculating Power from Current and Voltage.....	41
Equation 5. Calculating Power from Energy and Time.....	42
Equation 6. Effective focal length of focusing mirror using slit size and angular dispersion.....	65

List of Tables

Table 1. Project deadlines	17
Table 2. Laser diode comparison	20
Table 3. Groove spacing vs incidence angle.....	27
Table 4. Diffraction grating comparisons	28
Table 5. Sensor Electro-Optic Specifications	32
Table 6. Processor table of comparison	37
Table 7. Estimate of power consumption	40
Table 8. User Interface Method Comparison.....	45
Table 9. Traditional Bluetooth Specifications	46
Table 10. Bluetooth Low Energy Specifications	47
Table 11. Wi-Fi Specifications	48
Table 12. ZigBee Specifications	49
Table 13. Wireless Communication Comparison	50
Table 14. Wired Communication Technology Uses.....	56
Table 15. HC-05 Technical Specifications	57
Table 16. RN42 Technical Specifications	58
Table 17. RN4020 Technical Specifications	59
Table 18. ESP32 Technical Specifications	60
Table 19. Bluetooth Module Comparison.....	60
Table 20. Mirror prices and other metrics	66
Table 21. Table of expected interface losses	67
Table 22. Bluetooth Module IO Connectors.....	72
Table 23. CMOS Sensor IO Connections	74
Table 24. Mobile Application Design Choice Summary.....	84
Table 25. Bill of materials	90
Table 26. Part Acquisition Timeline	92
Table 27. RN4020 Testing Results	94
Table 28. Monochromatic Sensor Testing Results	96
Table 29. Development Board Testing Results	99
Table 30. Diffraction grating spec test.....	99
Table 31. Tested Specifications for Laser Module	100
Table 32. Milestones for the CFS	117
Table 33. Budget details for CFS.....	118
Table 34. Division of labor for the CFS	119
Table 35. (Appendix) Efficiency and loss at relevant interfaces	viii

List of Figures

Figure 1. Engineering trade-off matrix	4
Figure 2. Block diagram and designation of responsibilities.....	6
Figure 3. Scratch-dig table of requirements.....	12
Figure 4. NFPA 704 diamond for acetone	15
Figure 5. Absorption spectrum of Chlorophyll <i>a</i>	19
Figure 6. Emission Spectrum of Chlorophyll <i>a</i>	19
Figure 7. Schematic including dimensions for MZH8340550D-AL01A laser module.	21
Figure 8. Measured emission spectra of Chlorophyll <i>a</i> in Acetone based on various excitation wavelengths from 405nm to 440nm.	22
Figure 9. From left to right: Chlorophyll <i>a</i> sample diluted with 150mL (high concentration), Chlorophyll <i>a</i> sample after diluted until OD<0.1, pure acetone.....	24
Figure 10. OPT3002 picture by TI.....	30
Figure 11. AR0130CS (ARDR) imaging sensor on a PCB	31
Figure 12. Internal Functioning of a 7805 linear regulator.....	40
Figure 13. Simplified schematic for the bq2970.....	43
Figure 14. UART Device Configuration	51
Figure 15. Serial over USB Communication	52
Figure 16. I2C Device Configuration	53
Figure 17. Multiple-Slave-Select SPI Configuration.....	54
Figure 18. Daisy Chain SPI Configuration.....	55
Figure 19. Dimensionless optical system design.	61
Figure 20. 90% sensor fill using the chlorophyll fluorescence spot.	63
Figure 21. Diffraction grating incidence angle vs angular dispersion at 600-700nm waveband .	64
Figure 22. Illustration of the geometric system between the diffraction grating and the focusing mirror (simplified)	64
Figure 23. Diffraction grating efficiency curve (source quality).....	68
Figure 24. ARDR Monochrome Sensor quantum efficiency curve vs wavelength.....	68
Figure 25. Battery Charging Management Circuit	70
Figure 26. CMOS sensor 1.8 Volt supply.....	70
Figure 27. CMOS sensor 2.8 Volt supply.....	71
Figure 28. Laser Diode 3.0 Volt Supply	71
Figure 29. ARM M-Processor and Bluetooth module power supply	71
Figure 30. Circuit schematic for the CFS	73
Figure 31. PCB Schematic.....	76
Figure 32. Dimensions of pump housing.....	77
Figure 33. Complete housing design with dimensions, angles, and labels.....	78
Figure 34. Use Case Diagram	80
Figure 35. Embedded Software Block Diagram	81
Figure 36. Timing Diagram for Reading Pixel Data.....	83
Figure 37. Mobile Application Block Diagram	85
Figure 38. Entity Relationship Diagram for Application Database.....	87
Figure 39. Initial GUI Design Sketch	88
Figure 40. Final Graphical User Interface	89

Figure 41. RN4020 Bluetooth Module	92
Figure 42. RN4020 Individual Module Testing.....	93
Figure 43. RN4020 Integration Testing.....	94
Figure 44. AR0130CS Monochromatic Sensor	95
Figure 45. Monochromatic Sensor Configuration Testing	96
Figure 46. STM32 Development Board.....	97
Figure 47. Flashing Development Board.....	98
Figure 48. Testing Development Board.....	98
Figure 49. Laser spectrum testing in a dark room	99
Figure 50. Setup for Measuring Laser Beam Spot Size.....	100
Figure 51. Grating diffracting fluorescent light from the slit	101
Figure 52. Laser light through the system and reflecting off the screen (two figures).....	102
Figure 53. Fluorescent light at the collimating mirror interface through the longpass filter.....	102
Figure 54. Longpass filter setup with light coming out of the focusing mirror.....	103
Figure 55. 3-D CFS design with slots.....	105
Figure 56. CFS baseboard housing design.....	106
Figure 57. Empty posts and holders (left); optics mounted in holders (right).....	107
Figure 58. Example of a spectrum before pixel calibration (with imagery).....	108
Figure 59. Green laser spectrum after pixel calibration.....	109
Figure 60. Red laser spectrum after pixel calibration.....	109
Figure 61. Fluorescence spectrum from Windows Camera app	110
Figure 62. Green laser source (left), red laser source (right)	111
Figure 63. Chlorophyll fluorescence tests: old sample (left), new sample (right).....	111
Figure 64. Chlorophyll fluorescence comparisons: graph only (left), qualitative (right).....	112
Figure 65. CFS Application Icon	114
Figure 66. Selecting Device in CFS Application.....	115
Figure 67. Conducting Analysis Via CFS Application.....	115
Figure 68. Viewing Stored Results in the CFS Application	116
Figure 69. Measuring Plant Health in the CFS Application	116

1. Executive Summary

Plants are vital to human culture. They form the backbone of cultural ceremonies, social situations, medicines, decorations, food sources, oxygen production, and agriculture. It is important that plants stay healthy for all these applications. However, sometimes a plant might not be healthy even if its leaves aren't wilting. Ways of testing for plant health include soil examination, chemical analysis, and even trial-and-error horticulture practices. However, by using chlorophyll fluorescence spectroscopy, a general idea of plant health can be gained in only a few minutes.

A chlorophyll fluorescence spectrometer (CFS) tests for the presence of chlorophyll in flora by pumping a sample with low blue/high ultraviolet light. This spectrometer is designed with portability and cost in mind. The device shines light from a laser module through a chlorophyll sample. The fluorescent light is set parallel to a vertical slit that has been placed at the focal length of a curved collimating mirror. The collimating mirror directs the light to a reflective diffraction grating that splits the light into its component wavelengths and sends it to a focusing mirror. The focusing mirror directs the light to a square CMOS sensor. The signal is then processed from analog to digital by the sensor and sent to the processing unit where the sample's spectrum is shown on a mobile phone screen.

Chlorophyll fluorescence gives information about the Photosystem II (PSII) protein complex, which is the first protein group chain involved in photosynthesis. Chlorophyll fluorescence intensity reveals information about how well PSII is using light energy absorbed by chlorophyll to power photosynthesis, and since PSII's efficiency is a general indicator of photosynthetic performance, chlorophyll fluorescence is the fastest method of testing the state of PSII. This spectrometer thus relies on the function of the PSII protein complex in plants to give meaningful data about the plant's health. If a certain plant's chlorophyll sample fluoresces lower than a known healthy plant, there could be evidence of stress, disease, infestation, or malnutrition. This device acts as a first indicator, preventing the need for lengthy chemical tests. Since light covers a large area, the device can also be used to judge the general health of plants in its vicinity, assuming all factors constant, which is a boon for greenhouses with strict environment and climate conditions.

This report documents the design process of the CFS. It starts with the description of the project and the motivations for choosing the topic. It describes requirement specifications such as cost, power supply, and device dimensions. There is a research section describing each part chosen for the design and why that part was chosen. It also briefly describes the trade-offs associated with the chosen parts compared to other considered parts. The report then discusses the design constraints and engineering standards pertinent to the design. There is a section following this describing the hardware and software design of the project with accompanying research. The report then details the administrative side of the project, such as budget, financing, and the project schedule template. The report concludes with necessary references and an appendix for further references or for any material not significant enough to include in the body of the text.

2. Project Description

A CFS is an important tool for home horticulture enthusiasts, farmers, and pharmaceutical companies. It can accurately give a quick measure of a plant's overall health by observing how strongly a sample's chlorophyll fluoresces. The section herein describes the goals, motivations, requirements, and trade-offs associated with the CFS.

2.1 Motivation

Plants are an integral part of human culture. They help cure sicknesses, decorate space, are critical in art and architecture design, exchange carbon dioxide for oxygen, and many other functions. Like animals or family members, taking care of plants is a human imperative. It is important to understand when plants are stressed, sick, infested, or in need of different amounts of sunlight. The CFS is a tool that will provide a first-response overview of plant health, like a thermometer for a feverish toddler. Of course, once it has been established that a plant is unhealthy, then more specific measures can be taken to ensure the plant recovers adequately. The initial screening is the important part. Without it, it may be impossible to tell a plant is unhealthy until it is too late to save the plant.

2.2 Project Goals and Objectives

The goal of this project was to build a portable, cost-effective prototype of a fluorescence spectrometer that focuses mainly on measuring chlorophyll fluorescence. The prototype that was built met the following goals.

Cost – The device cost less to build and use than models currently on the market while performing the same tasks. The idea for this goal was to allow access for anyone who wants to monitor their plants' health and not limit it to only those with large or corporate budgets.

Size – The device was portable and not overtly large, bulky, or cumbersome. The idea for this goal was to make the device easy to transport and store. Size is an important consideration for this device since many similar products are small enough to fit in the palm of a user's hand.

Ease of Use – The device was simple, modest, and not over-designed. The device's interoperability with wireless communications prevented the need for bulky cables and external storage. The idea for this goal was to make the device usable by anyone who has a smartphone. This goal went in-hand with the Size and Cost goals.

Robust Quality – The device was able to sustain normal wear-and-tear, was water resistant, and was housed in material that protected the delicate optics and electronics inside. The idea of this goal was to ensure that the sensitive optics and electronics did not get ruined or shifted out of place when the device was moved.

Utility Analysis – The device was able to give a general classification of the sample’s health after analysis. The idea of this goal was to make it easier for the user to understand the data. Some examples were “Good health”, “Average health”, and “Fair health”.

2.3 Requirement Specifications

This section details the requirement specifications for the CFS before the build commenced.

- The device will cost less than 500 USD to build to completion. This value includes all optics, electronics, computer hardware, software, and housing materials used for the final product. This value does not include test materials, simulation or design software used on license agreements, or previous prototypes.
- The device’s total volume will be less than or equal to 4000 cubic centimeters.
- The device’s total power delivery to all power-requiring components will be less than or equal to 5 Watts. Originally, the power delivery was 115 Watts due to the light source being two gas-based light bulbs. This specification was redrafted after the device was redesigned to work with a laser diode.
- The device will house a wireless standard Bluetooth 4.0 Bluetooth Low Energy (BLE) mechanism which will provide fundamental communication for the user.
- The device’s radio power consumption will be less than 50 microWatts.
- The total analysis time required to produce spectrum data for one sample will take less than 60 seconds.
- The device will image at least the 600 to 700 nm waveband.

From the above requirement specifications, the following three were chosen as demonstrable specifications for the demonstration of our product.

- The device will house a wireless standard Bluetooth 4.0 Bluetooth Low Energy (BLE) mechanism which will provide fundamental communication for the user.
- The device will produce an analysis from start to finish in less than 60 seconds.
- The device will image at least the 600 to 700 nm waveband.

2.4 Engineering Trade-Off Matrix

The engineering trade-off matrix for the CFS was designed to show the relationship between its engineering and marketing requirements. Fig. 1 is the matrix used for the CFS and is followed by a key describing the symbols used. An explanation with examples from the matrix follows Figure 1’s key.

The engineering requirements list the needs of the system from the point of view of a developer or engineer. Dimensions describes the volumetric size of the CFS in cubic centimeters and should be decreased to make the device portable. Power delivery shows how much power will be delivered to the circuits within and should be decreased so the

device is economical and doesn't heat up. Power consumption describes how much power the internal battery will consume while powering the circuits and components within the device. This metric should be decreased so that the device lasts long amounts of time before needing a recharge. Cost describes how much money it will take to build and test the device and should be decreased for financial reasons. Wireless communication describes how wireless the device is, so this metric should be increased as much as possible. Total analysis time is the time spent analyzing information passed from the device to the processor and passing that on to the user, so it should be decreased.

			Engineering Requirements					
			Dimensions	Power Delivery	Power Consumption	Cost	Wireless Communication	Total Analysis Time
			-	-	-	-	+	-
Marketing Requirements	Cost	-	↑	↑	↑		↓	↓
	Size	-	↑					
	Ease of Use	+	↑			↑	↑↑	↑↑
	Robust Quality	+	↓			↓	↑	
Targets for Engineering Requirements			≤ 4000 cubic meters	≤ 5 Watts	6 hours of battery life	≤ \$500	Bluetooth 4.0 Bluetooth Low Energy (BLE)	< 60 seconds

Figure 1. Engineering trade-off matrix

Key

↑↑ = Strong positive correlation. Advancing both metrics can be done without sacrifices and will produce corresponding net positives.

↑ = Positive correlation. Advancing both metrics can be done without sacrificing anything from either.

↓ = Negative correlation. Advancing one metric causes a sacrifice in the other correlated metric.

↓↓ = Strong negative correlation. Advancing one metric causes great sacrifices in the other correlated metric.

- = Negative polarity. This metric aims to be decreased in the project.

+ = Positive polarity. This metric aims to be increased in the project.

Green = Engineering Requirements chosen for demonstration.

The marketing requirements detail the qualitative metrics that the CFS aimed to reach during the design process. Cost, as previously discussed, describes how much the device will cost. It is important that this metric is decreased as low as it can go. Users of the CFS will appreciate a cheaply priced, quality product. Size is the same as the engineering requirement's Dimensions, but for marketing requirements, it describes the general size of the device. Users of the CFS will want a device that isn't cumbersome or bulky—something they can carry around or install in place without disturbing their daily routines. Ease of Use describes how accessible the CFS is for the lay user. Since the CFS has built-in wireless capabilities, it is easy to sync up a data stream with the user's smartphone rather than having them deal with installing a program on their computer and offloading data using hard wires or cables. Robust Quality says that the product should be resistant to damage, stable, and not easily broken. Since the CFS houses sensitive optics and communication technologies, robustness is a very important metric.

Consider the Dimensions engineering requirement and the Size marketing requirement shown in Figure 1. Size and Dimensions both have a negative direction. Their correlation is ↑. As the Size of the device is decreased in its negative direction, the Dimensions of the device will also decrease in its own negative direction. They are positively correlated with ↑ since either metric can be advanced in their direction without sacrificing anything in the corresponding metric.

Now consider the Wireless Communications engineering requirement and the Cost marketing requirement in Figure 1. Cost has a negative direction and Wireless Communications has a positive direction. Their correlation is ↓. If Cost is decreased, or advanced negatively, Wireless Communications will be harder to implement and will also decrease negatively, which is the opposite of Wireless's positive direction. On the other hand, if more Wireless Communications are added, advancing the direction positively, the Cost of the device will increase, advancing Cost positively (or in the negative of its negative direction). For this reason, the correlation between these two metrics is ↓.

2.5 Block Diagram

Figure 2 shows the division of responsibilities and overall schematic of the chlorophyll fluorescence spectrometer. The device starts with an input optical source that excites a sample of isolated chlorophyll diluted in acetone. The fluorescent light is directed into the

optics area of the device by a slit. The optics separates the spectrum and passes it to the sensor array. The light is converted from an analog signal to a digital signal by the sensor and is sent to a central processing unit. The unit will feed the information into a software interface which will display the spectrum and allows the user to store, review, and compare analyses. The CFS also has an option to offload data using external storage. Even though the device communicates wirelessly, the team wanted the CFS to give the user an option to port the information over to a personal computer or other device for analysis.

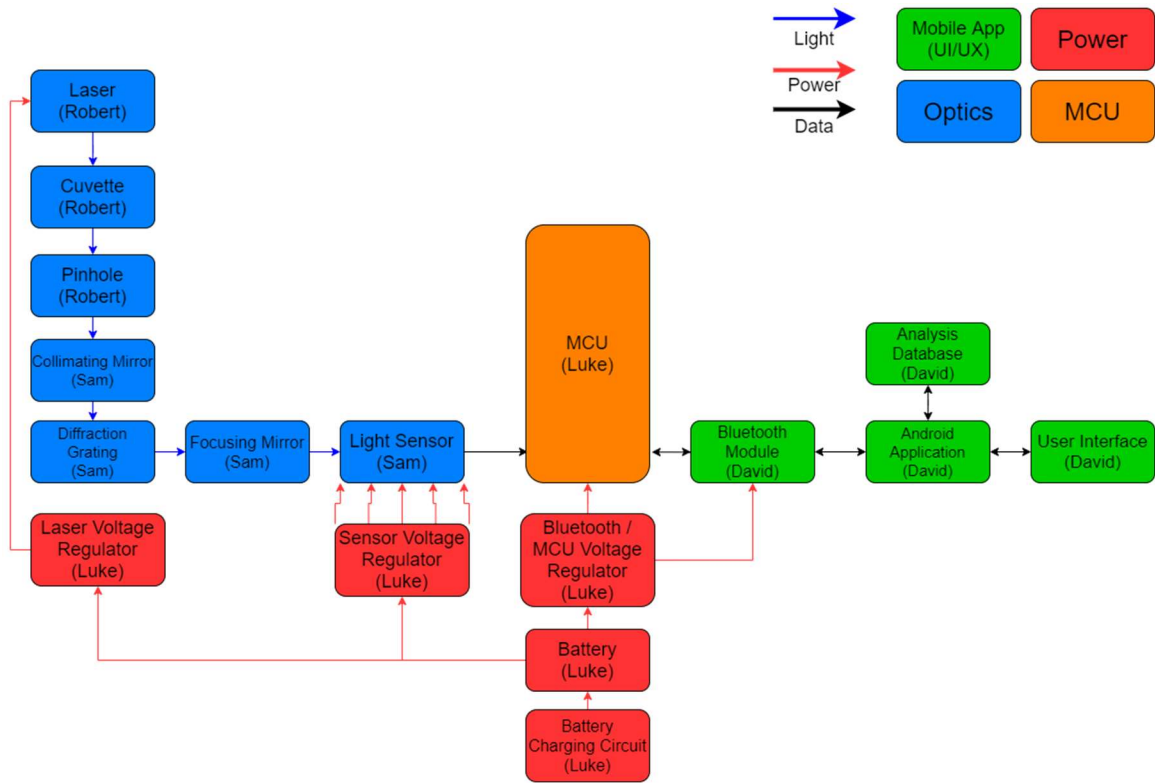


Figure 2. Block diagram and designation of responsibilities

3. Constraints & Standards

The section that follows details the constraints and standards applicable to the CFS. The standards section describes guidelines by which the CFS was engineered. The constraints section describes rules which the CFS follows. Together, these two engineering requirements promotes a sturdy product that is built to last, is marketable, and is not dangerous to introduce to the market.

3.1 Standards

A standard is an established way of doing things that ensures interoperability. Without engineering standards, the use of technology in the engineering industry, including the CFS, would be severely limited. The wide variance in how products are built and operated would cause vendor mismatches in the markets. Products that should work naturally together, such as bolts and ceiling fans, home plumbing fixtures, and the modules in a modern computer would not work together if standards were not around.

Standards ensure the health and safety of the people who work with and use the product every day. Standards also ensure that the product itself is safe and does not cause undue harm to those who seek to operate it. According to senior engineers and standard accreditation organizations, following and identifying standards is an expected part of good engineering practice. As such, a working list of considered standards for the CFS has been listed below. Each standard is highlighted, is overviewed, and is briefly discussed with respect to its relevance to the project. Following the standards section is a discussion on the engineering constraints for the CFS.

3.1.1 RoHS Compliance

The Restriction of Hazardous Substances Directive (RoHS) is a European Union directive which was ratified in 2003. The RoHS restricts the amounts of certain materials which are allowed to be included in electronic devices. The RoHS is related to the Waste Electrical and Electronic Equipment Directive, which categorizes electronics and sets recycling goals. There are ten chemicals listed in the RoHS standard, which are lead, mercury, cadmium, hexavalent chromium, polybrominated biphenyls, polybrominated diphenyl ether, bis(2-ethylhexyl) phthalate, butyl benzyl phthalate, dibutyl phthalate, and diisobutyl phthalate. Prior to July 2019, only the first six materials were restricted. The changes were made with the release of RoHS 3. Exemptions in the RoHS allow lead for use in high temperature solders as well as solder for use in servers, storage and network equipment.

We used RoHS compliant solders for this device—specifically, when soldering the image sensor. In order to achieve RoHS compliance, we used lead-free solder and screened each component and material to ensure that none of the listed hazardous materials made their way into the device.

3.1.2 Eye Safety

Whenever a light source is involved, it is important to wear proper protective equipment to reduce injuries to the eye. Our CFS incorporates a laser diode as the light source, so it is important to recognize the standards of operation when operating a laser. The American National Standards Institute (ANSI) has written the ANSI Z136 set of standards to outline the safe use of lasers. ANSI has put categorized lasers into four main hazard classifications:

- Class I: Incapable of producing damaging radiation levels during operation
- Class II: Emits light in the visible portion of the spectrum
- Class III (a and b): Medium-power laser, may be hazard under specific viewing conditions, does not pose a fire or diffuse-reflection hazard
- Class IV: High-power laser, the direct beam can be hazardous to the skin and eye, may also pose a fire or diffuse-reflection hazard

The laser diode used in this CFS fall in the category of a Class 3b laser. This means while the laser is turned on and used for testing, proper eyewear must be worn such as UV blocking lenses. Besides eye injury, the laser does not pose much risk of injury.

3.1.3 FDA Performance Standards for Light-Emitting Products

The laser module we ordered came from a company outside of the United States. While this product was being shipped to the United States, we were required to fill out two forms: one which identified the importer to the Department of Homeland Security and another that ensured the radiation standards of the imported equipment were up to date.

To fill out the form of “Declaration for Imported Electronic Products Subject to Radiation Control Standards,” it was necessary to locate the correct part of the Electronic Code of Federal Regulations, specifically Part 1040.10 on Radiation-Emitting Electronic Products. Part 1040 provides a general overview of both medical and non-medical radiation-emitting electronic products and the requirements the FDA must both verify and enforce when these products are imported into the United States. The FDA “defines a radiation-emitting electronic product as any electrically-powered product that can emit any form of radiation on the electromagnetic spectrum.” The laser module for our device fitted this definition.

In order to ensure that our laser module met FDA standards, the applicability section of Part 1040.10 on laser products was referenced. Our group was manufacturing an electronic product (the CFS) and was using the laser module as a component in the final product. Therefore, our laser module met the required standards due to Part 1040.10 clause (1) which states that lasers manufactured or assembled after August 1, 1976 meet standards if they are “sold to a manufacturer of an electronic product for use as a component in such electronic product.” [eCFR]

3.1.3 IEEE 802.15.1 - Bluetooth

IEEE 802.15 is a set of standards from The Institute of Electrical and Electronics Engineers (IEEE) which defines standards related to Wireless Personal Area Networks (WPAN). While there are 10 major working areas under the IEEE 802.15 group, only the 802.15.1 substandard is relevant to this project. This standard is relevant to this project because we used Bluetooth Low Energy, which is a wireless communication technology that falls under the 802.15.1 standard, to send analysis results from our device to a user-controlled device that served as the main user interface.

The IEEE project 802.15.1 has defined a WPAN standard specifically based on the Bluetooth Foundation Specifications. The latest version of this standard, the IEEE Std 802.15.1™-2002, was published in June 2002, and mainly focuses on defining the physical layer and media access control specifications for Bluetooth communication.

3.1.4 ISO/IEC 9899 – The C Language

ISO/IEC 9899 is an international standard which defines the C Programming Language. This standard was jointly defined by International Electrotechnical Commission and the International Organization for Standardization. The standard for the C language defines the syntax and constraints of the language and the semantic rules for the language.

For this reason, it is important for users of the language to be familiar with the different version of the C standard, and their differences, so that they can know what syntax and features are supported by the C standard version that they are implementing. This standard is relevant to our project because a large portion of the software that was written for this project was embedded software written using the C programming language. Because we wrote in C code, it is considered good practice to choose a single version of the C standard to target and adhere to the restrictions of that standard to avoid portability issues.

Although this standard defines the syntax and constraints of the language, there is no official standardized style guide for the C language. Having a set of defined style standards is important when developing an application to ensure that the code that is being written is all consistent style-wise. Style consistency increases the readability of the code and can make sure that best practices are followed when formatting code to avoid common mistakes. Because the C language has no official style guide, will define our own style guide for the development of this project. The code formatting standard that our team has defined for ourselves includes restrictions such as requiring meaningful names for all constants and variables, restricting the use of camelCase, defining indentations to be 4 spaces wide, requiring open braces be on the same line as the conditional or function, and other style restrictions.

The following sections of this report contains details about the major versions of the C standard, and the main differences between them. For this project we adhered to the C99 standard, for portability reasons.

3.1.4.1 ANSI C (C89 / C90)

ANSI C is a term commonly used to refer to the original group of C standards, also known as C89 and C90. Although these are the original C standards, they are not commonly used due to being outdated and lacking compatibility and usability features that were introduced in later versions of the C standard. The ANSI C standards have been officially withdrawn by their authors.

3.1.4.2 C99

The C99 standard was adopted in March 2000 by ANSI and is known to be the most portable version of the C standard. The portability of this standard means that code compiled using the C99 standard is more likely to be supported on a wider array of devices than code compiled using later version of the C standard, which may have features that are too advanced or for which support was never implemented for some devices. This is especially important when dealing with Embedded programming, since many devices have been around for a long time and are not frequently updated. This version of the C standard improved the language by adding new data types and core language features, as well as improved compatibility with C++. A more detailed list of the additions made in this standard can be found in the list below.

- Better support for IEEE floating point standard
- Added the following built-in data types:
 - Long
 - `_Bool`
 - `_Complex`
 - `_Imaginary`
- Added new core language features:
 - static array indices
 - designated initializers
 - compound literals
 - variable-length arrays
 - flexible array members
 - variadic macros
 - the “restrict” keyword
- Improved compatibility with several C++ features

3.1.4.3 C11

The C11 standard was published in 2012 and is currently the previous version of the C standard. The C11 standard attempted to modernize some of the aspects of the language by doing things like improving Unicode support for the language, adding the “Generic” keyword, add a multi-threading API, and adding support for Atomic types. These additions work to modernize the language and make it fit in to the modern programming language

landscape. Although these features modernize the language, 2012 is fairly recent as long as hardware manufacturing goes so the C11 standard is not as portable as the C99 standard, as not all hardware, especially embedded, has caught up with this standard.

3.1.4.4 C18

The C18 standard was published in 2018 and is mainly a “bug fix” release. No new features were added in this release over the previous C11 standard, as the only purpose of this release was to fix bugs that were introduced in the previous standards and make the programming language more stable.

3.1.5 Surface Quality for Optics

Optics are incredibly sensitive instruments since light is very sensitive to any effects imposed on it. A major effect for consideration, especially when lenses and mirrors are considered, is the surface quality assured by the supplier of an optical component. In this section, the surface quality standard will be examined and discussed with respect to its relevance to the project.

3.1.5.1 US Standard MIL-PRF-13830B (Scratch-Dig)

The United States Military Standard Performance Specification MIL-PRF-13830B classifies optical surface quality using a “scratch-dig” system found in just about every optical manufacturer’s catalog. Optics must both comply with the standard listed above if either is desired by the manufacturer for use in military systems. Considering this is where an immense amount of money is made in the optics field, following this standard is good economic practice.

Following this standard is also good safety practice since a scratch or dig in an optic, particularly in laser applications, can cause immense laser-induced damage to a system, especially in ultrafast applications. Since the CFS uses a laser as its pump source, all optics should comply with the scratch-dig standards set forth in the MIL-PRF-13830B document to prevent any laser light from interacting with or damaging components within the optical housing.

“Scratches” are marks on the surface of the optic. They are quantified with one of five numbers: 10, 20, 40, 60, and 80, with 10 being the lightest class of scratch and 80 being the darkest class of scratch. There is no metric given for the scratches; the scratches are arbitrary numbers that a human inspector assigns to a scratch under certain illumination conditions not described in the MIL-PRF-13830B document. The sum of all the lengths of all scratches in a single scratch brightness class cannot exceed one-quarter of the diameter of the optic as described in MIL-PRF-13830B 3.5.2.1.

“Digs”, as defined in section 3.5.3.1 of MIL-PRF-13830B, are the physically allowed diameters of the defect in units of 1/100 mm. If a dig is irregularly shaped, the average of the length and width is used as the dig magnitude. These dig numbers are then converted from 1/100 mm to a numeric signified with a pound sign. For example, if a dig is 0.8mm in diameter, it has Dig # 80. According to 3.5.3.2, the total number of digs cannot exceed one per 20mm of diameter or the total additive dimensions cannot exceed 1/20 of the total optical diameter. The reason these metrics are so important is the level of scrutiny at which it forces manufacturers to quality control their optics. The higher the numbers are in the scratch and dig classifications, the less likely the chance the optic has at being used in a government system, which will cost the company a lot of money.

The ideal optic has no scratches and no digs, but due to how optics are manufactured, even optics designed for immense precision will not have 0-0 classifications. In fact, the closest to a 0-0 classification is 10-5 standard used for laser cavity mirrors, particularly in the ultraviolet but less so in the infrared. The ideal 0-0 optic would also have ideal lossy surfaces that only lose power based off their reflectance of light. While these optics simply do not exist, the discussion of their effects and their close neighbor (the 10-5 standard) is pertinent to show how important scratch-dig is to the selection of optical components.

The most common standard for commercially available optics is 40-20, circled in Figure 3. This is a scratch class of 40 and Dig # 20. As can be seen in Figure 3, there is no magnifying power or focal length requirement for the optics in this category, leading to an immense amount of freedom for the optical designers to manipulate.

TABLE I Surface Quality Requirements

Focal planes and near focal planes			Central zone 1/2 diameter of surface		Outer Zone	
Beam diameter (mm)	Magnifying power	Focal length (mm)	Scratch	Dig	Scratch	Dig
Over 5.....	80	50	80	50
4-5.....	60	40	60	40
3.2-4.....	60	30	60	40
2.5-3.2	40	20	60	40
2.1-2.5.....	40	15	60	30
1.6-2.1.....	30	10	40	20
1.0-1.6.....	20	5	40	15
0.6-1.0.....	15	3	30	10
0.4-0.6.....	10	2	20	5
0.2-0.4.....	10	1	15	3
0.2.....	20-10	12.5-25	10	1	15	3
0.4.....	10-5	25-50	10	2	20	5
0.6	5-3.3	50-75	15	3	30	10
1.0.....	3.3-2	75-125	20	5	40	15
1.6.....	2-1	125-250	30	10	40	20

Figure 3. Scratch-dig table of requirements

Republished under AMSC N/A FSC 6650 Distribution Statement A (Approved for public release; distribution is unlimited).

Precision and ultrafast lasers usually require 20-10 minimum due to how sensitive a laser is to light propagation and reflection. The CFS, not requiring too much precision, uses 40-20 optics since these are the most commercially available components. 40-20 optics are low cost, meet United States military specifications, and are readily available for purchase which translates to low lead times on shipping and arrival.

3.2 Constraints

Constraints are design decisions imposed by the environment or designer that impacts or limits the design. They act as pseudo-guidelines for the CFS. Constraint requirements often violate the abstractness property of engineering requirement specifications, but in this section, they are treated as guidelines for ethical, safe, and intelligent engineering work.

3.2.1 Economic

Economic constraints were an important limitation for our senior design project. We were not sponsored by a private company or by the University; the CFS in its entirety was financed by the group. For this reason, great care and deliberation was taken to reduce the cost as much as possible. We decided to split the cost equally across the four engineers. In order to keep the cost down, we avoided overdesigning and chose components which met our needs, not necessarily the highest quality components money can buy.

It is possible to spend thousands on a high-speed CPU. However, in the case of the CFS, that would not result in a higher quality device for measuring chlorophyll content. Running over budget and being unable to complete the project is a danger that we avoided. The marketability of our device also improved since we kept costs lower. If the CFS were to be manufactured for sale, the lower cost of the device makes the product more attractive to customers and improves the volume of sales. The budget for our device was limited to \$500 and includes all components, electronics, hardware, software, optics and materials that we used in the final design.

3.2.2 Environmental

Environmental constraints are factors in which the testing and development of a device is limited by its surrounding environment. For chlorophyll to fluoresce and for the emitted light to be collected properly, certain environmental conditions must be met. There must be little to no natural or randomly polarized light interfering with the fluorescent light. This can cause destructive interference to occur and prevent the desired signal from reaching the detector. It should be noted that the samples we tested are constrained by environmental factors. We only tested samples that were easily found in our immediate location. However, our device can test and monitor plant health for any sample in an environment where chlorophyll extraction is possible.

Another environmental constraint to consider is how our procurement of samples will affect the health of a plant. A leaf or leaves are going to have to be removed from the tree or bush to be sampled in the CFS. This affects the plant's health in a way that must be examined. Generally speaking, removal of plant leaves is not unhealthy for a plant. It does not affect plant growth, internal health, or susceptibility to diseases and infections. In fact, removing leaves from a plant is considered a healthy part of maintenance, similar to getting a haircut. Proper removal of plant material helps a plant continue to grow without becoming deformed, bent, or unruly. [HGIC] As such, removal of plant material for the purposes of integration into a sample for the chlorophyll fluorescence spectrometer has no environmental constraints because its own sampling activity benefits the environment.

3.2.3 Social

Social constraints are patterns of societal and cultural behavior which can impede the development of a device. The CFS does not have any major social constraints limiting it; however, there are government regulations applicable to the operation of the optical source used in the CFS. These standards are discussed in more detail in 3.1.2 Eye Safety, the subsection of 3.1 Standards.

3.2.4 Political

Political constraints include limitations on the project placed by the government policies and political weather in the area the project is being designed. After researching the political cloud surrounding chlorophyll fluorescence spectrometers, it was determined that no political constraints are applicable to the CFS. There are, however, political constraints that prevent the importation of laser sources and parts from certain overseas countries.

3.2.5 Health and Safety

A first thought for health and safety should be how the chlorophyll is extracted. Primarily, for preparing samples, acetone was used to extract chlorophyll from plant samples such as pine needles, leaves, and flowers. Acetone is a flammable, volatile liquid compound with a strong odor. It is dangerous to drink and has non-zero NFPA 704 codes outlined in Figure 4. Acetone 1 in the Health code, meaning "Exposure would cause irritation with only minor residual injury."

Acetone ranks 3 in the Flammability code, meaning that acetone is a "Liquids and solids (including finely divided suspended solids) that can be ignited under almost all ambient temperature conditions." Acetone ranks 0 in the Instability-Reactivity code, meaning that it is "Normally stable, even under fire exposure conditions, and is not reactive with water." It is important, therefore, when preparing solutions for testing that the acetone is kept away from open flames, is used in a well-ventilated area, and is not allowed to contact the skin, eyes, or mouth.

Acetone can be toxic when inhaled and therefore should only be used to create chlorophyll solutions in a well-ventilated area. It is also dangerous to ingest or drink, but only in large quantities since the body is naturally adept at breaking down large amounts of acetone. [HL.A] As such, the acetone used for the project was labeled at all times and no drinks were allowed in sample preparation areas. This prevented cross-contamination of safe liquids with the unsafe acetone.



Figure 4. NFPA 704 diamond for acetone

Republished under public domain use.

There is also concern with the battery and power supply of the device. A battery which operates at too high voltage will heat up quite a lot and could either overheat the device, causing a burn on someone handling it, or the battery could simply explode. The power supply has a similar problem; if too much voltage is supplied to any one part of the device, that device may burn out, fail, and/or cause a fire. As such, the power supply was designed very carefully using the power constraints given in the data sheets of the chosen components to prevent the possibility of explosions.

The light source for the CFS is centered in the low visible, upper ultra-violet range. The eye cannot see ultraviolet light and thus cannot contract the pupil to protect the rods, cones, and retina from damage. It was therefore important that the light source was encased in the CFS such that stray light did not leak out and damage the eye. This is covered in greater detail in 3.1.2 Eye Safety, the subsection of 3.1 Standards.

3.2.6 Manufacturability

Manufacturability constraints are design constraints that limit our design based on the ease with which the design can be constructed or mass-produced. “Design for manufacturability”, or DFM, is a common engineering practice which requires the engineers designing a product design the products to maximize the ease with which those products can be manufactured. This engineering practice is necessary for commercial products to increase profit margins and reduce the possibility of quality issues arising due to a difficult to manufacture product.

For the CFS, the main manufacturability constraint which we complied with was following Design for Manufacturability best practices for our PCB design. Designing a PCB with manufacturability in mind reduces the cost of our PCBs and allowed us to design more copies of the PCB in a shorter amount of time. Having a short design time for our PCB was

important because it provided us with a quick turnaround time just in case we found an issue with our PCB during the testing phase and needed to make changes to the PCB design and order a new one. The cheaper cost associated with a manufacturable PCB allowed us to order more copies of the PCB for use in prototyping and testing. An example of PCB design manufacturability best practice was to choose components that can be placed and soldered by machines in the factory, which was cheaper, faster, and more precise than using components that must be soldered by hand.

While we followed Design for Manufacturability constraints for our PCB design, we did not constrain our general product assembly to manufacturability constraints. We chose not to complicate our design by requiring a chassis design that can be manufactured at scale due to the fact that all of the assembly for our project was done by hand. However, if the CFS were to be a commercial product, a re-design would be necessary to allow for automated assembly and increased manufacturability.

3.2.7 Sustainability

Sustainability constraints are design constraints that limit our design based on the reliability and durability of the product over a long period of time. The lifespan of a device is an important aspect to potential customers, and it is important for us to constrain our design in such a way that we can ensure the longevity and durability of our product.

The main sustainability constraint for the CFS is that our design must be water-resistant. This is because our CFS may be used in many different environments and will likely be used around plants. Areas with plants are generally either outdoors or near sprinkler systems, both of which put the sensitive electronics on-board the device at risk of being water damaged.

Another constraint for this device is that the device must be secured in such a manner that small drops or impacts will not compromise the integrity of the chassis. This is important because the optical elements within the measurement device are extremely sensitive and could quickly become damaged beyond repair if the chassis of the device were to be opened.

3.2.8 Time Constraints

Time constraints was one of the biggest challenges for our design team. We had two semesters to research, design, build, test, and present our device. During this time, we each had other obligations in our schedules and were compelled to dedicate time to developing this project every week. Procrastination was an easy way for us to waste our time and end up with nothing to present at the end of Senior Design 2 and receive a failing grade. Thankfully, procrastination did not occur in any major capacity and our presentation at the end of Senior Design 2 was a success.

The possibilities for our design was potentially endless and for that reason it was important that we limit the scope of our project early on. This way, we did not have an ever-expanding list of features to add which became more than we could realistically produce in the 8 months allotted to work on the project. Time constraints related to milestones and deadlines for this project were dictated by the senior design curriculum at UCF. By the end of the first semester, we aimed to have our design completed and a prototype built. The design was complete at the end of the first semester.

At the end of Senior Design 2, we aimed to have a final project fully completed with all features as designed and ready to present. Having the PCB designed as early as possible was extremely important because it required a couple weeks from the time the board was ordered until it arrived. If there were any errors or if the board needed to be redesigned or adjusted, it was important that we have time to do that because the PCB was central to the design of the CFS. An exhaustive list of our deadlines is included in Table 1.

Table 1. Project deadlines

Deadline Name	Due Date
Divide and Conquer Project Document	September 20th, 2019
Divide and Conquer Project Document v2	October 4th, 2019
60-page Draft Senior I Design Document	November 1st, 2019
100-page Draft Senior Design I Document	November 15th, 2019
Functioning Prototype with Microcontroller	November 30th, 2019
Senior Design I Final Paper Deadline	December 2nd, 2019
Begin Sectional Testing	February 1st, 2020
PCB Design Complete/Ordered	February 8th, 2020
Begin Integration Testing	March 1st, 2020
Begin Machining of Device Housing	March 1st, 2020
Final Project Complete	April 10th, 2020

4. Project Research

This section describes how the project combined the design constraints and standards with the stated goals in order to meet the desired outcome. Hardware and software components are judged against the stated standards and comparisons are made.

4.1 Similar Products

Unsurprisingly, other companies understand the importance of chlorophyll fluorescence and have created products similar to the CFS. These products were observed by the design team and were used as starting points for the general idea of the CFS. The two main companies who have deployed chlorophyll fluorescence spectrometers in the past are NASA and Spectral Evolution.

NASA's CFIS (chlorophyll fluorescence imaging spectrometer) was built at the Jet Propulsion Laboratory (JPL). Its mission purpose is to monitor solar-induced fluorescence from the Orbiting Carbon Observatory-2 (OCO-2), specifically the O₂ A-band in the mid-700-800 nm waveband. Successful reports from the CFIS include showing that there are higher solar-induced fluorescence values in soy fields than there are in corn fields.

Another product is Spectral Evolution's SR-3500 full range UV/VIS/NIR field portable agricultural spectrometer. It is a handheld, wired device that is designed to test for nitrogen, phosphate, potassium, and chlorophyll content. The samples are excited with a 532 nm green laser and a full imaging system observes the spectrum from 350 to 2500 nm. The exact details of the internals of the device are not public knowledge, but it is expected that the imaging system is designed to be broadband. This contrasts with the CFS, which is designed to be shortband and is only focused on the fluorescence response found in exciting a chlorophyll sample with a source near 430 nm.

4.2 Light Source

There are three possible processes that could occur when chlorophyll molecules absorb light energy: the energy could be used for photosynthesis to provide the plant with sustenance, the excess energy could dissipate as heat, or the plant could re-emit the light. This last process is known as chlorophyll fluorescence.

In general, fluorescence occurs when a material absorbs light of a certain wavelength and re-emits light at a longer wavelength than the original source. By studying and comparing the fluorescence emission spectrum of Chlorophyll *a* from various samples, it is possible to have a general understanding of the relative health of the samples.

Chlorophyll *a* fluoresces at a peak wavelength near 670nm when it has been excited by a light source emitting near 420nm. Figure 5 and Figure 6 each respectively display the absorption spectrum and the emission spectrum of Chlorophyll *a* samples in methanol. The

graphs of the spectra were created by Scott Prahl, PhD Professor at the Oregon Institute of Technology. Prahl obtained the data for the graphs from the PhotochemCAD package, version 2.1a which is a database containing the spectral information for various chemicals including Chlorophyll a. The absorption measurements were originally recorded by J. Li et al, Department of Chemistry at North Carolina State University, on December 11, 1997 using a Cary 3 and were later refined by J. Dixon et al from the same department in 2005. Similarly, the measurements for the emission of Chlorophyll a was obtained and refined by the same groups using a Spex FluoroMax.

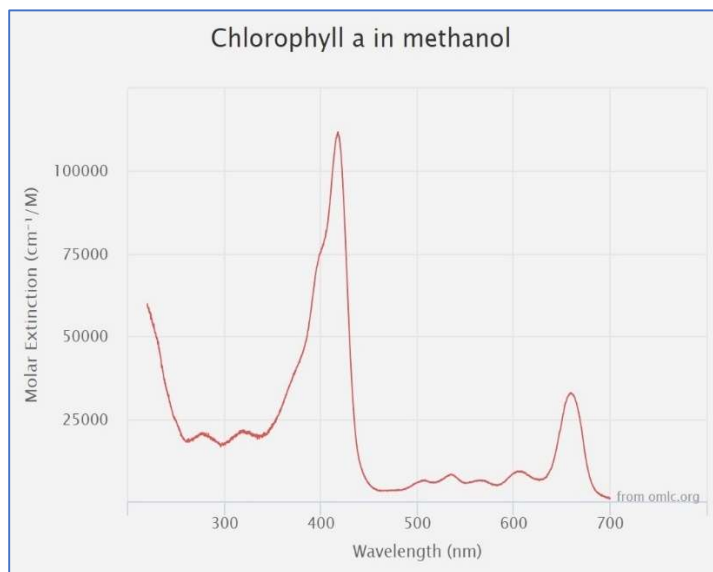


Figure 5. Absorption spectrum of Chlorophyll *a*
Reprinted with permission from Dr. Scott Prahl, OIT.

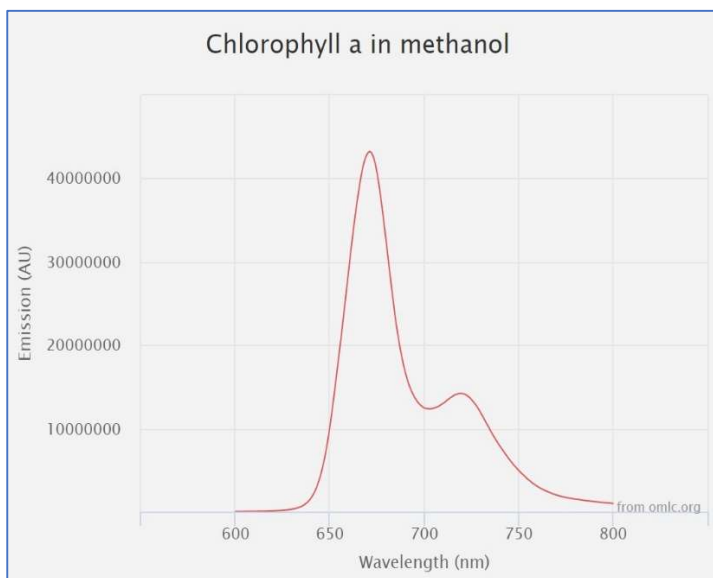


Figure 6. Emission Spectrum of Chlorophyll *a*
Reprinted with permission from Dr. Scott Prahl, OIT.

The light source needed for the CFS needs to have a small bandwidth with a high intensity around the 430nm wavelength. Common sources which fit these constraints and are cost-effective include a laser and an LED. After reviewing options, a laser module was selected for this project.

4.2.1 Laser Module

Laser diodes have some inherent disadvantages when compared to LEDs: they have a more complicated design, generally more expensive, and have a greater temperature dependence. However, regarding chlorophyll fluorescence spectroscopy, the advantages in using a laser diode over an LED outweigh the disadvantages. While LEDs have a narrow bandwidth when compared to traditional sources like a halogen bulb, the laser diode's bandwidth is much narrower making the source more monochromatic than an LED.

The laser diode has a tighter beam and therefore smaller spot size than the LED, it will be easier to focus the laser onto the sample. The intensity of the focused light on the sample will also have a much greater intensity than the LED allowing the Chlorophyll *a* to yield higher fluorescence. The emitted light from the sample will also be tighter allowing it to be passed through the focusing optics and onto the detector more easily.

If we wished to measure the full emission spectrum based on various source wavelengths than an LED or a lamp would be more suitable for fluorescence spectroscopy, but since we only care about a single excitation wavelength and a narrow emission bandwidth, the monochromaticity of the laser diode makes it the most suitable light source for this CFS. Several different diodes were considered and are shown in Table 2.

Table 2. Laser diode comparison

Laser Model	Manufacturer	Price	Peak λ	Power
FVLD-415-45S-AR	Frankfurt Laser Co.	~\$5000	415nm	65mW
TG430	RPMC	\$500	430nm	50mW
LD2008	Power Technology Inc.	\$6310	420nm	120mW
MZH8340550D-AL01A	MZLASER	\$12	405nm	50mW

The laser module chosen for this product will be a CW 50mW laser with a 405nm center wavelength. This laser can be operated between -10°C and +50°C and stored between -40°C and +80°C with a wavelength drift of 0.25nm/°C . The beam size at a distance of 10 m is about 5x8 mm. It requires an operating voltage between 2.8-5.5V and an operating current < 160MA. The drive type is ACC and the service life is given to be over 8,000 hours. The casing for the module is made from Aluminum and is approximately 32mm in length with an 8mm diameter.

Although the absorption spectrum for Chlorophyll *a* has a peak near the 430nm wavelength, we decided on the 405nm wavelength due to cost. Most lasers centered at

430nm were very expensive ranging from \$500-\$5,000; however, lasers centered at 405nm are much less expensive and more readily available. The MZH8340550D-AL01A laser we ordered from MZLASER only cost \$12.00 per unit including shipping which is over a 97% decrease in price. A schematic of the laser and its dimensions can be seen in Figure 7.

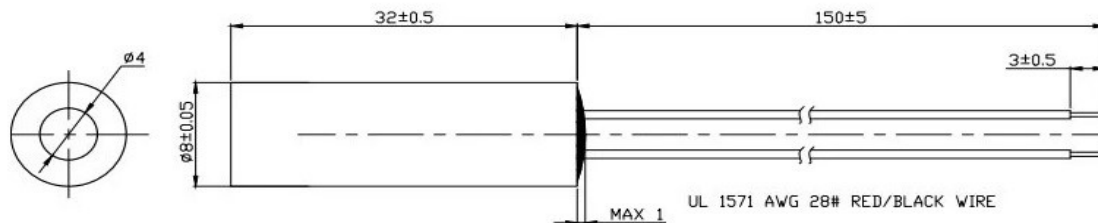


Figure 7. Schematic including dimensions for MZH8340550D-AL01A laser module.
Provided by Zhuhai MZLaser Technology Co. Ltd.

The main drawback to using the shorter wavelength is that we will have a lower intensity of emitted light. In order to ensure we still had enough light being emitted we created samples of Chlorophyll *a* diluted in Acetone until we reached an optical density <0.1 . After our sample was deemed adequate, we placed it inside a Spectrofluorometer to see the emission spectrum of our sample based on different excitation wavelengths. We recorded our results and they are displayed in Figure 8.

From the following graph it can easily be seen that the 430nm excitation source provides the greatest amount of fluorescence intensity. The 420nm excitation wavelength shows about an 20% reduction in intensity, and the fluorescence intensity from the 405nm source has a very similar emission spectrum comparatively. In contrast, if the wavelength is increased to 440nm, there is a much more drastic reduction in peak fluorescence intensity by approximately 55%.

These measurements make sense because they correspond to the absorption spectrum of Chlorophyll *a* seen previously in Figure 5. The peak of the absorption spectrum is at 430nm this excitation source can be expected to produce the greatest emission intensity. The 420nm and 405nm sources had similar absorption values, and both were slightly lower than the peak at 430nm. The absorption at 440nm was by far the lowest compared to the other sources so it should be expected to produce the least amount of fluorescence.

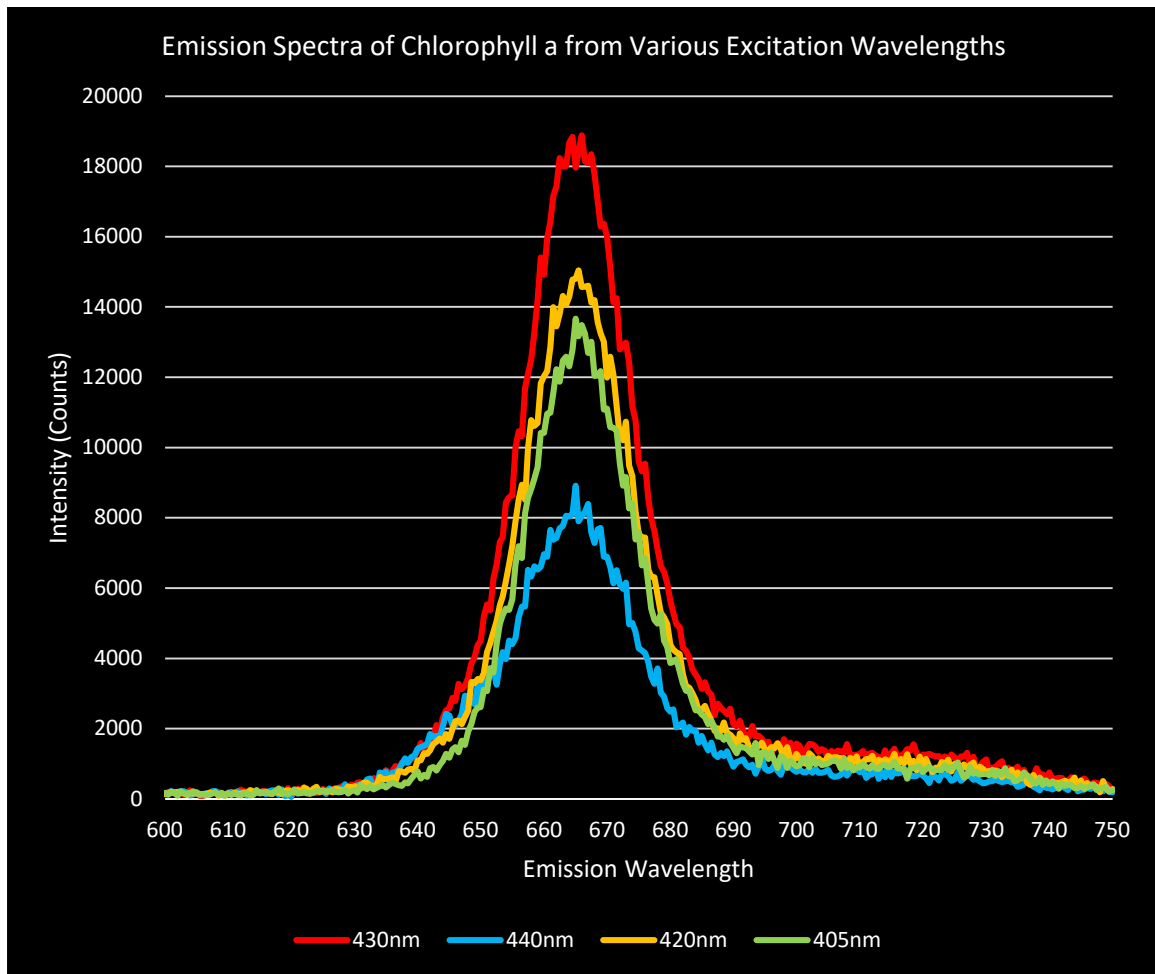


Figure 8. Measured emission spectra of Chlorophyll a in Acetone based on various excitation wavelengths from 405nm to 440nm.
The measurements were recorded by Samuel Knight and Robert Bernson on the spectrofluorometer at the College of Optics and Photonics at the University of Central Florida. The graph was reconstructed from the measurements by Robert Bernson.

4.2.2 Cuvettes

The container holding the sample of Chlorophyll must also have the correct dimensions. If an LED were to be used, a lens would be utilized to focus the light emitted from the LED into a spot size which could illuminate as much of the sample as possible with a high enough intensity. However, we have decided to use a laser which simplifies this process. The beam from the laser should have enough intensity and focus without the use of a lens to make the sample inside the container fluoresce with a great enough intensity to be detected.

The use of the laser diode places fewer constraints on the kind of cuvette used in the CFS. Spectrophotometric cells come in different styles but there are three main categories: rectangular, cylindrical, and flow cells. Rectangular cells are the most basic and also the most common cuvette used in UV/VIS spectroscopy. Cylindrical cells are mainly used when the excitation source has a large circular beam and the volume of the sample is less important. Lastly, flow cells are used for which it is important to keep the samples constantly moving or flowing.

We are trying to incorporate the most basic design in our CFS to reduce costs and therefore will be using a screw top, micro rectangular cuvette which will have a volume between 1mm^3 and 6mm^3 . The spectrofluorometer which recorded the measurements held housing for cuvettes with a 1mm^2 base, but the cuvettes could have varying heights allowing for different volumes to be used if the base of the cuvette was the same. This idea could also be utilized in our design; however, a standard cuvette size could reduce the cost of the device and any replacement parts.

The material of the cuvette is also important. The fluorescing light needs to path through the cuvette as well so the material must have enough transmission for both the excitation wavelength and the emission spectrum. In order to ensure the sample is excited with maximum intensity from the source we will be using a quartz cuvette which allows for adequate transmission between 300-800nm which completely cover the necessary range of wavelength to meet our design specifications.

We are currently borrowing a quartz cuvette from UCF as it is a very expensive piece of equipment. We are currently determining if we will order ourselves for the next phase of the design process.

4.2.4 Chlorophyll Sample Preparation

In order to obtain the measurements used to construct Figure 11, samples of chlorophyll a need to be obtained. Likewise, our device will make similar samples fluoresce and the preparation of these samples needs to be done in the same manner to ensure accuracy. The original samples can be used as a reference for a typical spectrum of Chlorophyll *a* which allows any new samples obtained to be compared to the reference. Also, if we compare the emission spectrum obtained with our device to the emission spectrum of the spectrofluorometer we can ensure our CFS is working properly.

In order to make our reference sample we followed a specific procedure:

1. Picked leaf from a *Tilia platyphyllos* plant (a healthy plant in Samuel Knight's yard)
2. The leaf was torn into smaller pieces and placed in a measuring cup
3. The cup was filled with 150mL of acetone
4. The pieces of leaf were grinded down inside the acetone
5. The solution was poured through a filter to remove the small pieces of leaf
6. A small portion of the sample was added to the cuvette

Results of our sample preparation can be seen on Figure 9 below.



Figure 9. From left to right: Chlorophyll *a* sample diluted with 150mL (high concentration), Chlorophyll *a* sample after diluted until $OD < 0.1$, pure acetone.

The samples were prepared by Samuel Knight and the photograph taken by Robert Bernson

4.3 Optics

The optics in this device will be primarily utilized for the emitted light from the sample of Chlorophyll *a*. The light from the sample will pass through a vertical slit. The image of the slit will be projected onto a collimating lens which collects the light and transfers it onto a reflective diffraction grating or prism. The grating or prism will diffract the light so only the desired wavelengths reach the focusing lens. This lens then focuses the light onto the detector which passes the spectral information of the emitted light to a computer software program which can be interfaced by the user of the CFS. Optical components can be quite expensive, so it is necessary to research and plan which optics are required, and which are available within the project's economic constraints.

4.3.1 The Slit

Once the excitation source has interacted with the sample and fluorescence emission occurs, the light exits the initial chamber through a narrow vertical slit. The width of the slit is an important factor when designing the resolution of the CFS. A larger width means more optical power which can reduce the amount of time required to obtain an accurate

reading. However, the larger the slit, the narrower the resolvable bandwidth of the emission spectrum. There is a very wide width of range of possible slit widths to use ranging from $5\mu\text{m}$ up to $800\mu\text{m}$. For our design we chose a $350\mu\text{m}$ slit width. This width was chosen from the ideal pinhole equation $d = 1.9\sqrt{t\lambda}$, where t is the distance from the slit to the image and λ is the wavelength of maximum transmittance (683nm for the CFS). As seen in 5.1.1 Optical Housing Design, the collimating mirror is $t = 50\text{mm}$ from the slit. Since $350\mu\text{m}$ slits cannot be purchased for cheap or must be manufactured, we reduced our slit size to $200\mu\text{m}$ since this size was commercially available for a low price.

The vertical size of the slit is less important as long as it is much larger than the slit width. Typical slit lengths range in between 1mm and 2mm with the typical length being 1mm . Our design incorporated a 1mm length slit. Our group started to research the possibility of using a slit with an adjustable width as we have seen in use on the CREOL spectrofluorometer but decided not to pursue it due to the complicated nature of adding moving parts to a simple system, violating the Robustness goal of the project.

4.3.2 Collecting & Focusing Optics

Lenses and mirrors are part of the hardware design of the system. They are tools which are picked while the system itself is being designed and require no intense or stringent research to be done except in the cases of F-# matching, effective focal length, and curvature. For focusing, a concave mirror and a convex lens is used. For diverging, a convex mirror and a concave lens is used. The other characteristics such as focal length and diameter are all covered in the hardware design section 5.1.1 Optical Housing Design. The collecting and focusing optics chosen for the project are itemized in Table 25. Bill of materials.

4.3.3 Monochromator

There were two monochromators that were considered for the analysis of chlorophyll's fluorescence spectrum: a diffraction grating or a prism. The chosen monochromator needed to be able to disperse the incoming optical signal to a resolution of at least 5nm , a metric which this device shares with the sensor system. However, there are some detracting considerations to be made when it comes to prisms. The primary factor is its design flexibility. In order to use a prism, it would have to be custom machined for our purposes, which is expensive and time-consuming. Due to this constraint, we decided not to use a prism in our device and have instead chosen to use a diffraction grating in our device.

4.3.3.1 Diffraction Grating

A diffraction grating is an optical component that splits light into its component frequencies. Diffraction gratings make use of the multi-slit configuration where the ruling or grating of the diffraction grating acts as a means of self-interference for incident light, causing light to interact with itself and diffract its spectrum appropriately.

Gratings are made by etching or ruling a piece of glass or reflective material in a periodic manner such that the light undergoes self-phase modulation. This type of grating is called “ruled.” Gratings can also be made using photolithography; these are called “holographic.” [TL.dfg] Traditionally, there are two types of diffraction gratings: reflective and transmissive. A reflective grating has a mirrored surface behind a reflective film that acts as a mirror in the geometric system. A transmissive grating allows light to pass through it and interact with its etchings, acting as a lens in the geometric system. [Hct]

It is important to remember that a grating diffracts light in orders, a notation marked with m in Equation 1 and Equation 2. Each order is more diffracted than the last, but also carries less intensity. For example, the 1st order diffraction from a transmissive grating is much more intense than the 13th order diffraction. Generally, the equation for how strongly light diffracts from a diffraction grating is given by Equation 1. This equation works only for light at normal incidence and works for both reflective and transmissive gratings. When light enters a diffraction grating at an angle θ_i , the equation for its subsequent diffraction is given by Equation 2. In both equations, a is the diffraction grating groove or ruling spacing, m is the order number, λ is the wavelength of incident light, and θ_m is the light diffracted angle, signified by the order m in its subscript.

$$a \sin \theta_m = m\lambda$$

Equation 1. Diffraction angle for a grating with light at normal incidence

$$\sin \theta_m = \frac{m\lambda}{a} + \sin \theta_i$$

Equation 2. Diffraction angle for a grating with light inbound from non-normal angle θ_i

When designing the system, it is important to keep the blaze angle in mind. The blaze angle is a property of a blazed diffraction grating which sets a maximum wavelength of efficiency for certain applications. Blazed diffraction gratings eliminate all but one selected diffraction order, including the zeroth order if it is not selected. These gratings seek to optimize grating efficiency, a metric given as $\eta = P/P_0$, where P is the diffracted power of light and P_0 is the incident power of light. Since gratings are not lossless devices, it is very important to have a high grating efficiency so that the system achieves maximum signal throughput.

The grating should be blazed at the angle of maximum efficiency for Chlorophyll a . To find this, use Equation 3 with the parameters $m = 1$ and $\lambda = 683\text{nm}$. m is the desired diffraction order, λ is the peak wavelength of incident light, and d is the line spacing of the diffraction grating (convertible from grooves per mm). Since d is typically a standardized number, this can be varied with those known quantities to produce a blaze angle that matches the m and λ values.

$$\theta_B = \sin^{-1} \frac{m\lambda}{2d}$$

Equation 3. Blazed grating equation

Typically, vendors will list either the blaze angle or the wavelength of maximum efficiency. This, coupled with the grooves per mm, will narrow down the choices of

diffraction gratings. Ideally, the CFS should use a diffraction grating that provides a significant angular dispersion without having such a large θ_m (Equation 2) that its diffractive order is impossible to calibrate with a focusing mirror. So, choosing a groove spacing that is close to the longest desired wavelength is not the ideal choice. Propagation of the light from the diffraction grating should spread the spectrum out a bit, preventing it from being so condensed that the sensor cannot differentiate between wavelengths.

There are a couple of known groove spacings: 300 gr/mm (3.33 μ m spacing), 600 gr/mm (1.66 μ m spacing), and 900 gr/mm (1111nm). Using Equation 2, light on the grating will diffract at the following angle: $\theta_m = \sin^{-1} \left(\frac{m\lambda}{a} + \sin \theta_i \right)$. Since only the first order of the grating is considered, $m = 1$. The wavelength of peak intensity for the CFS is $\lambda = 683 * 10^{-9}$ m. Now, consider a few groove spacings and their effect on the diffraction angle at various incidence angles θ_i in Table 3.

Table 3. Groove spacing vs incidence angle

	300 gr/mm	600 gr/mm	900 gr/mm
θ_m ($\theta_i = 15$)	27.64°	42.09°	60.87°
θ_m ($\theta_i = 30$)	44.84°	65.70°	OoR*
θ_m ($\theta_i = 45$)	65.81°	OoR	OoR

*OoR = out of (calculable) range

While the incidence angle will affect how strongly the diffraction grating diffracts the light and at what angle, the groove spacing is what gives the incredible flexibility in diffraction angle. For the diffraction grating for the CFS, a groove spacing of 300 gr/mm is fine, but since the hardware can be designed so the diffraction grating can be at any angle, 600 gr/mm is also fine. 900 gr/mm diffracts strongly at the ideal wavelength and groove spacings in-between 600 and 900 are often custom-made and cost extra.

4.3.3.2 Monochromator Conclusions

Table 4 displays a few gratings that have ideal groove spacing, physical size, and wavelength of closest maximum efficiency required for the CFS. The group decided not to use prisms due to the high cost associated with custom machining and the long lead time for just one piece. A grating was simply easier to integrate into the planned optical system. Since the light from chlorophyll will be passing through a slit and will not diffract much in the vertical direction, there is no need to pay extra for the extra surface area. The horizontal area should be maximized without breaking the budget, hence the dimensions being 12.5 x 25 mm, which narrowed the choice to the 33066FL01-270R. Newport's 33066FL01-270R was chosen from the table below, highlighted in green.

Table 4. Diffraction grating comparisons

Name	Manufacturer	Grv/mm	Range	Max Efficiency	Size	Type	Price
33009FL01-270R*	Newport Corporation	300	300 – 1000 nm	500 nm	25 x 25 mm	Plane ruled, reflective	\$109
33066FL01-270R	Newport Corporation	300	300 – 1000 nm	500 nm	12.5 x 25 mm	Plane ruled, reflective	\$89
GR25-0305*	ThorLabs	300	200 – 1100 nm	500 nm	25 x 25 mm	Plane ruled, reflective	\$117
GR25-0605*	ThorLabs	600	250 – 1300 nm	500 nm	25 x 25 mm	Plane ruled, reflective	\$117

*Different size available for lower cost.

4.4 Sensor System

The sensor is arguably the most important optical device in a spectrometer. A sample can be illuminated, have its light transferred by collecting and focusing optics, and have its spectrum split up by a diffraction grating or prism, but if there is no system in place to analyze the incident light, the spectrometer is useless.

In this section, several sensors were analyzed for their possible effectiveness in the project. Some features examined are on-board ADC conversion, sensitivity, pixel pitch, supply voltage, and more. The primary metric used for choosing the sensor for the CFS was the sensor's ability to obtain good resolution for an incident beam of light over the 600 to 700 nm waveband.

4.4.1 Linear Sensor Arrays

A linear sensor is a 1xN dimensional pixel array used in most spectrometers. Commonly, linear arrays only output analog signals and require an outside analog-to-digital converter (ADC) to convert the data from spectrometry into digital bits processable by computer programs. Many microcontrollers and central processors have built-in ADCs in their hardware, making this design choice easy to implement, but that came with some costs, primarily with issues with bit conversion since the data takes longer to transmit and convert, increasing the bit-error ratio.

Building an ADC was out of the scope of this project, so the ideal sensor should have a built-in ADC or be compatible with a microcontroller that has a built-in ADC. Therefore, it was imperative to put great consideration on linear array sensors with an on-board ADC. However, a sensor that does not have a built-in ADC was not automatically excluded from the project if its other metrics outperformed other sensors in consideration.

4.4.1.1 AMS TSL1401CL

The TSL1401CL by Austria Mikro Systeme (AMS) is a linear sensor array with a sensitivity curve spanning 400nm to 1000nm with peak wavelength sensitivity around 780nm. The TSL class of sensor arrays offered by AMS consists of linear arrays, light-to-frequency converters, ambient light sensors, and proximity detectors. The TSL1401CL was chosen for review for its low cost per unit, short length, and low supply voltage. The TSL1401CL matches three of the seven engineering requirement specifications for the CFS—cost, dimensions, and power delivery. This sensor is also RoHS compliant.

4.4.1.2 AMS TSL3301CL

The TSL3301CL by Austria Mikro Systeme (AMS) is a linear sensor array with a sensitivity curve spanning approximately 300nm to 1100nm with a normalized peak wavelength of 660nm. The TSL3301CL was chosen for review for its good rise time, low dark noise, high clock frequency, and on-board ADC converter. Additionally, due to its low cost per unit, short length, and low supply voltage, the TSL3301CL matches three of the seven engineering requirement specifications for the CFS—cost, dimensions, and power delivery. This sensor is also RoHS compliant.

4.4.1.3 Melexis MLX75306 3rd Generation

The MLX75306 3rd Generation linear sensory array by Melexis is the third linear sensor array that is being considered for observing the spectrum of the chlorophyll fluorescence. The sensor has an operating wavelength of 400 to 1000 nm. It has a peak wavelength sensitivity at 880nm, which is longer than the ideal sensitivity of 683 nm for chlorophyll fluorescence. The MLX75306 was chosen because it has an on-board ADC, a very small active length, low dark noise, and a small supply voltage. The device is also RoHS compliant.

4.4.2 Square CCD Sensors

Square sensors offer a few attractive advantages over their linear array counterparts. Square sensors are thoroughly documented, have a very large market which makes for a diverse variety of products to choose from, are easily integrable with common microcontrollers and processors, typically operate at low power, and offer more room for a margin of error in vertical dispersion smearing. For example, in a linear array, if a pixel's dimensions are 10-by-10 μ m and the dispersed light has a real height of 1 mm, the pixel is losing over 30dB of information.

To retain all this information and boost signal strength, it would be better practice to have a large square sensor which can retain all the information from the dispersed light. From here, the back-end software of the system can vertically sum all the pixels to create a pseudo-linear array where there is very little signal loss from the pixels being too small.

There, of course, will be some losses from the pixel pitch being a non-zero number, but that is the nature of every marketed sensor. It is an un-mitigatable characteristic if the designer wants to use pixel arrays to solve a problem.

Square sensor arrays are typically not used in commercial spectrometers. Those devices use linear arrays which have been carefully engineered to match the full waveband of a fan of incident light. Ideally, the CFS would mimic the exact design of a commercial spectrometer, including the linear array, but as research was done on the effectiveness of linear arrays in previous projects, it was learned that many groups struggled to implement the linear array into their own projects. Some of these projects were spectrometers operating in a very wide waveband, effecting the capability of their budget linear arrays to produce a spectrum. With this known pitfall in mind, research was conducted on square sensor arrays of interest and their metrics were compiled into the following sections for review by the designers.

4.4.2.1 Renesas ISL29147

The Renesas ISL29147 is a square sensor array with a peak spectral sensitivity at 575 nm. This sensor offers some very promising metrics that are attractive to the CFS. It has a minimum supply voltage of 2.25 V and a maximum of 3.63 V. The device has a 12-bit resolution for its on-board ADC. It has a very low price per unit. Its minimum lux range is 56.25 lux, which puts it roughly in the area for sensing the low light of fluorescence. It has a dark noise coding error of 1 LSB and interfaces with I²C outputs. The device is approximately 2.04 x 4 mm in size, making it easy to fit into the device but a little challenging to image onto.

4.4.2.2 Texas Instruments OPT3002

The Texas Instruments OPT3002 (shown in Figure 10) is a low-cost, dynamic light-to-digital sensor with an effective wavelength range of 300 to 1000 nm. It has a peak sensitivity at 505 nm and varies between 60% to 80% quantum efficiency in the 600 to 700 nm waveband—the imaging waveband for the chlorophyll fluorescence spectrometer. It is compatible with I²C and SMBus, can be operated in continuous or single-shot mode, and has a less than 1 μ W power consumption from a 1.8V power supply.

The device met three of the seven engineering requirement specifications—cost, dimensions, and power delivery. The cost per unit is less than \$3 and thus the device can be easily picked up by even the most frugal team. The device has a physical body size of 2.00 x 2.00 mm, which makes it easily integrable into the system. The one obvious issue for such a small active area will be compressing the light from the monochromator such that it fits on to the active area. To solve this problem, simply choose a focusing mirror with a certain effective optical power such that the imaged beam width fits on to the sensor's active area. As

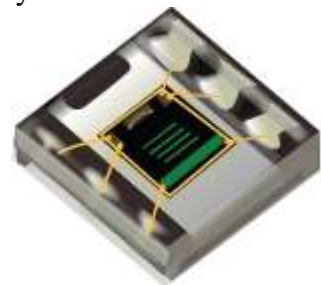


Figure 10. OPT3002 picture by TI

mentioned previously, the OPT3002 requires very low operation power and has an operating power supply voltage that rivals or exceeds that of all the linear sensor arrays previously listed. This made it an incredibly attractive choice for the project.

4.4.2.3 ON Semiconductor AR0130CS Series

The ON Semiconductor AR0130CS Series is a line of CMOS image sensors that come in monochromatic and RGB color scales. Depending on the exact model of the AR0130CS, the color scale may change. All sensors in the AR0130CS line shares the same electrical and optical characteristics, namely spectral efficiency, on-board ADC, supply voltage, and RoHS compliance. The main differences are pixel array dimensions, pixel size, and cost.



Figure 11. AR0130CS (ARDR) imaging sensor on a PCB

The primary sensor reviewed is the AR0130CSSC00SPBA0-DR, or ARDR for short, shown in Figure 11. The ARDR is a monochromatic CMOS image sensor with an active pixel array area of $4.86 \times 3.66 \text{ mm}^2$. It comes with an on-board 12-bit ADC, peak spectral efficiency at 570nm, a required supply voltage of 1.8 or 2.8 V depending on the application, automatic dark current and shot noise correction, and a responsivity of 6.5 V/lux-s. A monochromatic sensor was chosen for review since it makes the creation of an intensity profile easier. The idea with the ARDR sensor, as mentioned before, is to sum up the pixels vertically to produce a 1-D intensity profile. This will be used to create the spectrum of the fluorescing chlorophyll.

4.4.3 Sensor Comparisons

It was soon discovered that previous groups performing work with linear arrays suffered certain setbacks. Some groups were unable to complete any spectral analysis with a linear array due to electronic clock timing problems and difficulty coupling light onto the small area. Those groups defaulted to using photodiodes and power meters tuned to a known wavelength instead of observing the full spectrum of their samples. After reviewing the linear arrays and consulting with faculty advisors, it was decided that the group should discard linear sensors and review CMOS and CCD sensors instead. CCD and CMOS devices are compatible with any number of computing systems, are easily understood by most users, are well-documented, robust, and can be adapted to perform imaging work if necessary. This makes them attractive to the project.

The first square sensor array to be reviewed was the Renesas ISL29147. It has a low supply voltage of 2.25 to 3.63 Volts, 12-bit ADC conversion, and its active area is approximately 9.6 mm^2 , giving the sensor plenty of room to image a scene. However, while reviewing the sensor more closely, the spectral efficiency curve of Renesas's ISL29147 square sensor array has less than 10% quantum efficiency in the 650 to 700 nm waveband, the area where Chlorophyll *a* fluoresces the strongest. A drop of that size in quantum efficiency at that

range was too poor for the CFS to consider. Reviewing the physical price of the device also brought up some concerns. Though the price per unit is slightly below \$2, the minimum purchasable quantity is 1000, meaning the team would have to spend over \$2000 just to get one device worth using, severely violating the cost engineering requirement. These reasons made the ISL29147 too unattractive and it was discarded from consideration for the project’s sensor. The OPT3002 by Texas Instruments was then considered.

The TI OPT3002 has low price of \$1.60 per unit, an operating supply voltage at 3.6 Volts, and a waveband from 200 to 1000 nm. It has tremendous ADC bit depth at 23. Its main detriment is the small active area of 4 mm², a dimension which scrapes the boundary of the previously mentioned limiting size of a considered sensor. The OPT3002 excels in so many categories that it was considered a no-brainer for the project and was purchased. However, it was immediately discovered that the TI OPT3002 is merely a power sensor. It cannot measure spectrum. For this reason, the TI OPT3002 was relegated to testing for emitted power from chlorophyll fluorescence only, but its purchase was included in the budget as a test device. ON Semiconductor’s AR0130CSSC00SPBA0-DR was reviewed next.

The price of the ARDR is \$8.38 per unit. The active area is 17.78 mm², which is plenty of space to image the chlorophyll spectrum. Its supply voltage can be 1.8 or 2.8 Volts, depending whether the device operates in I/O (either), digital (1.8 V), or analog mode (2.8 V). Its operating wavelength is 300 to 950 nm. The ARDR has an on-board ADC with a bit depth of 12 bits. All of these made the ARDR seem like the ideal sensor for the project.

The ARDR excelled in all areas that the group looked at for finding a good sensor. The ARDR sensor matches all the relevant engineering requirement standards in cost, dimensions, and power delivery. These characteristics made the ARDR our chosen sensor for the project, shown in Table 5 and highlighted in green.

Table 5. Sensor Electro-Optic Specifications

Specification	ISL29147	OPT3002	ARDR
Manufacturer	Renesas	Texas Instruments	ON Semiconductor
Price per unit	\$2 (min: 1000)	\$1.60 (min: 20)	\$8.38
Active Area	2.4 x 4 mm	2 x 2 mm	4.86 x 3.66 mm
Supply voltage (V)	2.25 – 3.63	3.6	1.8 or 2.8
Operating wavelength (nm)	475 – 650	200 – 1000	300 – 950
Dark Noise	-	0 – 3 LSB	-
ADC Depth (bits)	8 or 12	23	12

*The notation “-” means a spec was not listed on any datasheet, website, or white paper.

4.4.4 Sensor Conclusions

The group ultimately chose ON Semiconductor's ARDR for its monochromatic response, great power supply requirements, wide operating waveband, excellent responsivity, cost, effectiveness, and built-in ADC. The ADC in particular eliminated a lot of potential sources of bit error from occurring at the digital processing stage. The ARDR was also the only sensor that didn't disappoint after further research was accomplished on it. It was not listed as a challenge to overcome in other group's projects like linear arrays, it did not turn out to be a power detector like the OPT3002, and it was not necessary to purchase the device in quantities of thousands from a foreign manufacturer like the Renesas ISL29147. The ARDR was everything the CFS needed for an image sensor.

4.5 Electronics

Our electronics design includes our processor, memory, storage, sensors, light source, power supply, battery, charging circuit and wireless networking hardware. These will all be integrated onto a single printed circuit board. Integrating each of these components together will require a collaboration of photonics, electrical, and computer engineering. With further research, our design may also include a data and power transfer via USB cable.

4.5.1 Printed Circuit Board

A printed circuit board is the primary technique for connecting electronic components in an electronic device. A printed circuit board (PCB) is made using a substrate such as paper combined with resin, or fiberglass with copper traces to connect the components. A PCB can be made from one or more layers depending on the complexity of the system. Copper traces allow power and signal to propagate across the board, connecting systems together in order for the components to function as designed. The resistance of a copper trace is calculated by multiplying the resistivity which is a parameter of the material used multiplied by the length of the conductor and divided by the cross sectional area. A PCB can be populated by hand or for more complicated designs with a CNC machine called a pick and place machine.

For components with large enough contacts to solder by hand, a soldering iron is used. 805 and 603 size components are ideal for this project because they are large enough to be easy enough to solder by hand and small enough that they will not have a very large footprint on the printed circuit board. A soldering iron can produce high quality connections that provide a low resistance electrical connection as well as a strong structural joint. Surface mount components which are too small, delicate or complicated to solder by hand will require the use of a pick and place machine. Surface mount components are generally smaller than their through hole counterparts and so have seen increased use as devices tend to get smaller and more densely packed with electronics. Another advantage of surface mount technology is that components may be placed on both sides of the printed circuit board.

Smaller connections on surface mount components mean lower resistances and reactances which can produce noise and voltage attenuation. Drilling holes in the PCB is an expensive process, which makes through hole mounting of components more expensive. A pick and place machine is the fastest way to populate a PCB with components. Both techniques can be used on the same product with larger power diodes, op-amps and transistors still being installed as through hole components. A printed circuit board that is designed to be populated with surface mount parts will usually have solder pads which are flat contacts made of tin, lead-tin or copper.

Solder paste, which is a mixture of flux and solder particles, is applied to the contacts to be soldered. There are two ways that this can be done, either applied with a stencil or a CNC applicator which is similar to the operation of an inkjet printer. The components are then placed in the correct orientation by the pick and place machine before the part is put in a solder reflow oven. It is the heat of the oven which causes the solder to melt, simultaneously soldering all of the components on the printed circuit board.

It is common practice to wash the printed circuit boards with a solvent after soldering to remove flux residue. There are vendors available which are capable of building a printed circuit board as well as populating the boards with surface mount components based on our designs. We will order 2 or 3 PCBs providing for the event that we fail in assembly. Having a PCB made for us should cost somewhere in the range of \$20-\$30. The lead time for producing a PCB varies from vendor to vendor and can vary from 2 weeks to 24 hours. Getting a printed circuit board made in a hurry has a higher cost than if you are willing to wait a little longer.

When soldering it is important that the device not exceed its maximum soldering temperature. This value can be found on the product datasheet and is different from the operating temperature. Exceeding the rated temperature while soldering can result in a device which no longer works or no longer works as intended. This can result in a cascading failure and damage other parts in the circuit, even if they were originally unaffected.

A printed circuit board provides electrical connections for data and power transmission as well as providing structural rigidity, keeping the components in a precise orientation. Since we are building a portable electronic device, it is important that it maintains structural integrity. The basic components mounted on printed circuit boards are resistors, inductors, capacitors, transistors, diodes, op-amps and integrated circuits built using networks of these components on a single silicon wafer using photolithography, often becoming very complicated. A printed circuit board will often be treated with a conformal coating after soldering.

The function of conformal coating is to protect sensitive electronics from dust, moisture, heat and corrosion and is particularly important in electronics which will be in service for a prolonged period of years. Conformal coating can be composed of acrylic, parlyene, silicone or urethane. There are multiple methods of application for conformal coating, being brushing, dipping or spraying.

4.5.2 PCB Design Software

There are several software tools available to aid in the design of embedded circuits. One such application is Kicad. Kicad is an open source free software platform distributed under a GPL v3+ license. Kicad allows for the design of complex electronic circuits and facilitates the conversion to a PCB layout. Kicad also has tools for creating bill of materials, gerber files, 3D views and component diagrams. Being built on C++, Kicad will run on essentially any modern computer architecture and operating system. The PCB design utility PCBNew allows for up to 32 layers and stores dimensions in nanometers as a 32-bit integer which allows for a PCB up to 2.14 meters which is far more than we require for this project.

Another Electronic Design Automation (EDA) software which we can use to design our PCB is Autodesk EAGLE. Autodesk EAGLE is a commercial engineering software sold on a subscription model. Autodesk EAGLE will run on Windows, Linux and Mac. Autodesk EAGLE consists of a schematic editor, a PCB layout editor, gerber file support and a graphical user interface for project management. We have chosen to use Kicad because its free and open source nature makes it more accessible as well as it being easy to use. Since we already have some experience modelling using Kicad, there are fewer new skills needed in order to complete this project. Being available for free is an advantage over most commercial software for this purpose because it helps us keep the project's budget under the limit.

4.5.3 CPU

The Central Processing unit, or CPU is one of the most important components of an embedded device. The CPU is responsible for performing arithmetic, executing programs which include logic, interacting with memory, storage and managing inputs and outputs. Modern processors include a cache which is a faster form of memory that will store data from memory which gets used most often, in order to speed up processing. The CPU will generally be much faster than the memory which is in turn much faster than the storage.

Some processors are packaged as a “system on a chip” or SoC, this includes the system memory with the processor, integrated graphics hardware as well as some non-volatile secondary flash storage. An SoC design would simplify the design for this project by reducing the number of components which need to be included on our printed circuit board. The advantage of not using an SoC is that we can meet each of our requirements more precisely without including hardware that we will not need.

The important metrics of a processor are its frequency, architecture, core count, cache capacity and configuration, thermal design power (TDP), coprocessors included and features supported. Many modern processors include dedicated graphics hardware, floating point arithmetic units, analog to digital conversion, and audio/video codecs and encoding.

ARM7 is a family of low power 32-bit RISC microprocessors released from 1993 to 2001. Intended for microcontroller use, these devices are no longer recommended for new integrated circuit designs. (p) A more modern approach would be to use an ARM Cortex-M processor. ARM Cortex-M is a family of microprocessors intended for microcontrollers and based on a 32-bit RISC architecture.

4.5.2 ARM7

The first processor that we researched for this project was the AT91SAM7SE512B. The reason this part was attractive was because it is affordable, and at 55 MHz 32 bit processor it should be more than powerful enough for our application. Other attractive features of this device are EBI/EMI implementation, I2C, SPI, four independent 16-bit PWM controllers, three 16-bit timers, an RTT, SSC, UART/USART and USB support.

This arm7 SoC also provides pulse width modulation which may be required for our light source. This is a surface mount device available in either a 128 or 144 pin package. There are 512 KB of flash storage which can be used to store our program and 32 KB of RAM which may be a limitation for our project, depending on what the user interface becomes.

The direction we are going for the user interface is to use an app which will allow a smartphone to pair with our device over Bluetooth and then doing most of the processing on the smartphone. This gives us the ability to use lower power hardware. The AT91SAM7SE512B operates with an input from 1.65 to 3.6 Volts and draws 80 mA peak power supply current, for a maximum power draw of 288 mW.

4.5.4 ARM Cortex-M

The ARM Cortex-M family of processors is designed to be a low cost, low power processor for microcontrollers. ARM Cortex-M processors are based on a 32-bit RISC ARM instruction set architecture (ISA). One ARM Cortex-M processor that we think is an excellent candidate for inclusion in our senior design project is the FS32K144, which can be purchased for \$5.00 manufactured by NXP USA Inc. The FS32K144 is powered by an ARM Cortex-M4F core running at 80 or 112 MHz depending on the configuration.

The FS32K144 comes equipped with an IEEE-754 single precision FPU for processing floating point data as well as a Cryptographic Services Engine which may be useful if encryption is required for the communications of this device. Cycle Redundancy Check (CRC) is also present on this chip for error detection to ensure our data is uncorrupted. The FS32K144 has an integrated digital signal processor (DSP) and 7 separate clocks. 5 power management states are available to allow this system to consume less power depending on which features, peripherals and processing power are currently needed.

2 MB of flash memory with error correcting memory (ECC) are available for program storage on the FS32K144. 2 12-bit analog to digital converters (ADC) are built in to this SoC. For communication protocols, the FS32K144 supports up to 3 modules connected over UART, 3 low power SPI modules, up to 2 low power I2C modules, a 10/100 Mbps

ethernet with IEEE1588 (precision time protocol) support. The FS32K144 will accept voltage from 2.7-5.5 Volts and draw between 29.8 μ A and 61.3 mA depending on which features are currently enabled and in use. This provides a maximum power consumption of 337.17 mW.

Another important factor to consider for the cost of the project is the cost of a development board. While the FS32K144 would be a fitting product for use in the CFS and can be had for less than \$5.00 per piece, the development board that we would be using to prototype for this processor can not be had for less than \$65.00. The STM32F407VE is a 32-Bit ARM M-4 processor which can be acquired for \$4.41 or less and is more than powerful enough for our project and has the GPIO we will need for parallel communication with our sensor, UART capabilities for interfacing with our Bluetooth module. The development board which we will be needing in order to prototype with this processor is available for \$9.00 or less which removes a large burden that would otherwise strain our budget.

Below is Table 6, comparing processors by features supported and cost. Since each processor included has enough computing power by clockrate, that is not included in the table. Memory will be an important benchmark for the device we choose because it limits the resolution of data that we can process and send. Since we have decided to use an image sensor with a built in ADC to simplify our design, we are no longer considering ADC implementation in a processor. Because of the favorability of the STM32F407VE, we have chosen to include this processor into our project.

Table 6. Processor table of comparison

Processor	Power Consumed	RAM	Component Cost	Development Board cost
AT91SAM7SE512B	300 mW	32 KB	\$10.00	N/A
FS32K144	337.17 mW	64 KB	\$5.00	\$65.00
STM32F407VE	58.5 mW	192+4 KB	\$4.41	\$9.00

4.5.5 Power Delivery

To be useful, a power supply must be able to provide power at a constant specified voltage, regardless of the load and the power being drawn from it. Every design is going to have limitations and compromises, there will be a very slight drop in voltage as current being drawn increases, the number of components being used and the complexity of the power supply all need to be balanced.

There are two obvious approaches to powering an electronic device, we can use power from a 120 VAC outlet or we can use battery power. The advantage of powering the CFS with the plugin approach is that the device has a theoretically unlimited runtime and never needs to be charged. Disadvantages are that the device must always be plugged in and receiving power from the electrical grid in order to function. The advantage of using battery power is that the CFS will operate for a time even if the power grid is not functioning and allows the device to be portable and analyze samples in the field.

The utility of a portable chlorophyll fluorescence spectrometer is an attractive feature, for this reason we have elected to power our device with a battery. The output voltage needs to remain within an acceptable range even as the battery's voltage decreases with discharge. When the battery is discharged, the battery needs to be disconnected because being discharged completely is damaging to the battery.

In order for every component of our device to operate as designed, each must be supplied with the necessary power within the rated voltage, usually 3.3 or 5 Volts. When a battery is used to provide power for a device, the voltage is going to attenuate based on the charge level of the battery. Because electronic components are sensitive to fluctuations in voltage, our design must account for inconsistent sources.

There are various tools available to aid the electrical engineer in designing a power supply circuit. One such tool is Texas Instruments WEBENCH Power Designer. Webench is a web-based utility that will aid in design by providing a circuit based on input parameters which is tunable, including recommendations for components. Emphasis can be placed on optimizing cost, efficiency or footprint. Alternatively, a balanced approach can be used which will compromise between the three.

Webench supports designing for a DC or AC supply. For the CFS, we have decided to provide power from a lithium-ion cell. For this reason, we will develop our designs using the DC/DC Power Design environment. There are components designed just for regulating power at these voltages such as the 7805 linear regulator, typically packaged as a 3 pin component. The 7805 has an input voltage pin, a common (ground) pin as well as an output voltage pin. A boost converter or other form of switching regulator can be used to convert 3.7 DC Volts provided by a lithium ion battery to 5 Volts ("Boost Converter Operation".

LT1070 Design Manual, Carl Nelson & Jim Williams). The 7805 can provide up to 1.5 Amps at 5 Volts (7.5 Watts) as long as sufficient heat dissipation is allowed and the input voltage is in the range of 7 and 25 volts. This integrated circuit utilizes a network of transistors and resistors as shown in Figure 12 with voltage reference Zener diodes, switching to adjust the resistance in order to provide the correct voltage for a range of current being drawn.

Another approach to voltage regulation is a switching regulator. A switching regulator is a device which uses pulse width modulation to produce an output which is lower than its input. The output voltage is going to be equal to the magnitude of the peak output voltage multiplied by the duty cycle. The limitation of this technology is that the input must be higher than the desired output, or a different type regulator is required. An example of a discrete component used for a switching regulator is the LM2576 Step down voltage regulator.

This device is capable of delivering 3 Amps of power and can be adjustable. The LM 2576 comes as a 3.3, 5, 12, or 15 Volt regulator, as well as an adjustable version. The LM2576 offers fault protection built in as well as a fixed frequency oscillator. The advantage of an

LM2576 over a linear regulator is higher efficiency. This translates into less power consumption as well as less heat production in our device. The efficiency of the switching regulator is highly dependent on the input voltage as well as the output voltage. The greater differential present between input and output voltage, the lower the efficiency of the switching regulator.

For the CFS, we will be required to increase the voltage from the 3.7 Volts of our lithium ion cell to the 5 Volts, 3.3 Volts and 4.6 Volts required by our electronics. In order to do this a boost converter can be used. A boost converter is a type of switching regulator which is used to produce a DC output which is greater than its DC input. The simplest boost converter that can be made contains a single transistor and diode, used with an energy storage component. The energy storage component can be a capacitor, an inductor or a combination of both.

The transistor can be a MOSFET or a bipolar junction transistor and operates as a switch, charging the energy storage device in the closed state and then discharging the energy storage device in series with the source voltage and the load when the switch is in the open position. As the device is rapidly switched on and off, the energy storage device does not fully discharge, and the supply current is sufficient to meet the demands of the load.

Using a capacitor in parallel with the load helps to maintain the required voltage across the load in both switching states. The higher the capacitance and the higher the equivalent load resistance, the lower the voltage ripple will be. The equation governing the discharge of a capacitor is $V = V_{Max} * e^{-t/RC}$ where V is the output voltage, V_{Max} is the peak voltage, t is the time in seconds, R is the load resistance measured in ohms, and C is the capacitance value of the capacitor in parallel with the load, measured in Farads.

There are commercially available boost-buck converters which can provide what we need for the power supply in this device, however by integrating this part onto our printed circuit board with the battery cell charging and voltage regulation circuit, we can reduce the volume of the device. By implementing every part of the power supply, charging circuit, battery, sensors, Bluetooth module, and light source we can include all the electronics on the device onto a single PCB.

The first step in designing a power supply for an electronic device is determining the power and voltages required. The total power required for our system is going to be the sum of the power required for each individual component, as shown in Table 7. Estimate of power consumption. Since we have not yet determined the components we will use with certainty, I will look at all the options we are currently considering for a single component and consider the power requirement that is larger. This does not account for all losses that will be present on the device, however it will function as a minimum value and rough estimate of the power that this device will need.

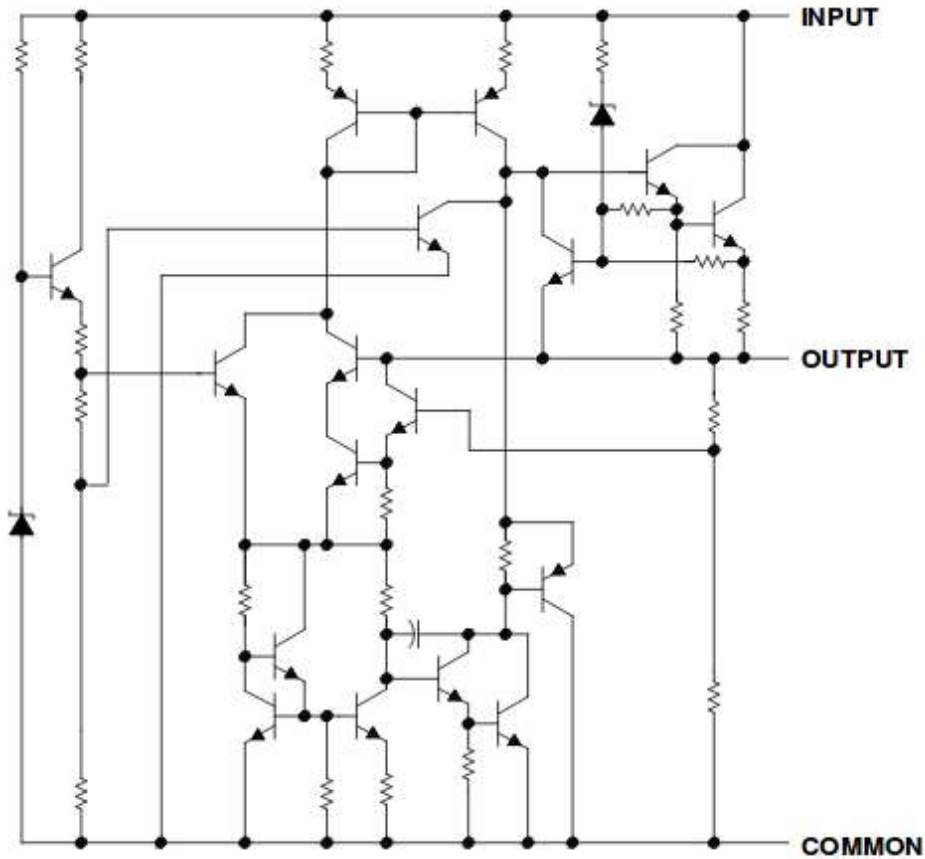


Figure 12. Internal Functioning of a 7805 linear regulator

Sources of power loss can be found due to the internal resistance of the battery, and losses in the power supply itself, resistances in the printed circuit board, soldered connections and so on, all producing heat. However, not every component will be functioning continuously. The radio antenna will not always be activated, the processor has low power modes which will be used whenever the requirements for the processor allow, the light source and sensor will only be active when taking a measurement and not run continuously.

Table 7. Estimate of power consumption

CPU [STM32F407VET]	1.95 V 30mA (Assuming 30MHz operation)
Laser Diode [MZH8340550D-AL01A]	3.00 V 160 mA
CMOS Sensor [AR0130]	1.8 V 82 mA + 2.8 V 40 mA
Bluetooth Module [RN4020]	1.95 V 16 mA
Total	829.3 mW

Calculating the power draw for a component can be done when a datasheet lists nominal values for voltage and current. To do this we use Equation 4. For the MLX75306, the datasheet specifies 7 mA during operation. Multiplied by the power supply voltage of 3.3 V, this yields a power draw of 23.1 mW.

Similarly, for the TSL3301CL, 17 mA is specified in the data sheet for the supply current during operation. Multiplied by the power supply voltage of 5 V, this component will draw 85 mW of power during operation. The TSL1401CL draws 4.5 mA from the power supply at a nominal 5 V, consuming 22.5 mW. The TSL3301CL requires the most power, 85 mW maximum so we will use that figure for our design.

$$P(\text{Watts}) = I(\text{Amps}) \times V(\text{Volts})$$

Equation 4. Calculating Power from Current and Voltage

The FS32K144, which is an ARM Cortex-M processor which we are considering requires between 2.7-5.5 Volts and draws between 29.8 μ A and 61.3 mA depending on which features are currently enabled and in use as well as the clock frequency. This provides a maximum power consumption of 337.17 mW. The ARM7 processor we are looking at is the AT91SAM7SE512B which draws a peak of 80 mA at a maximum supply voltage of 3.6 Volts resulting in a maximum power consumption of 288 mW. Because the FS32K144 has a higher power consumption we will use this figure for our calculations.

The light source we are currently considering is the NDVA416T 45mW violet laser diode. Despite being a 45mW laser, the NDVA416T does not consume 45mW of electrical power. The actual power requirement will be higher due to losses. The NDVA416T draws 75 mA at 4.6 V, consuming 345mW.

The components which we will be using are the STM32F407VET ARM processor, the MZH8340550D-AL01A laser diode, the AR0130 CMOS sensor and the RN4020 Bluetooth module. The device will be powered with the Samsung 25R single cell lithium ion battery. For our battery charging circuit, we have decided to use the AP5056. Using TI Webench, 4 voltage regulation integrated circuits were found which would be most suitable for use in this project to meet these loads given the single cell lithium ion battery. The 4 ICs we will be using are the TPS62231DRY, the TLV71328PDBV, the TPS62233DRY and the TPS799195. The TPS62231DRY was selected to provide 82 mA at 1.8 Volts which is required for the AR0130 CMOS sensor. The TLV71328PDBV was selected to provide the 40 mA at 2.8 Volts for the AR0130 sensor. The TPS62233DRY was selected to provide 160 mA at 3.0 Volts which is required for our MZH8340550D-AL01A laser diode. The TPS799195 was selected to provide 30 mA for the STM32F407VET ARM processor as well as 16 mA for our RN4020 Bluetooth module, each at 1.95 Volts.

4.5.6 Battery

The battery is an important component for any portable electronic device. Battery weight, capacity, maximum power output, and longevity must be taken into consideration. The choice of one of several competing battery technologies will have a large impact on the final form of the senior design project. A lead acid battery would be low cost and therefore helpful for keeping the budget as low as possible. However, lead acid batteries are heavier and have lower energy densities than some competing technologies, resulting in a more cumbersome final product.

A lithium battery has higher energy density and thus a lower weight for a given energy capacity and power capacity, however this comes at a higher cost. For this project, the weight savings absolutely justifies using a lithium battery to power our instrument. The capacity we require is enough to sustain the maximum power draw of our device for a continuous 6 hours of operation. To find the desired capacity of our battery, we use Equation 5 which tells us the relation between power and energy. Rearranging for energy, we get energy is equal to the maximum power draw multiplied by the duration of discharge.

$$P(\text{Watts}) = \frac{\text{Energy}(\text{Joules})}{\text{Time}(\text{Seconds})}$$

Equation 5. Calculating Power from Energy and Time

Computing Energy capacity for power equal to 0.83 Watts times 21,600 seconds which comes from our 6 hour battery life constraint results in a battery capacity of 17.9 kJ or 4.98 Wh which is equal to 1,350 mAh at 3.7 Volts. Another important operating parameter for a battery is the maximum current supplied. There are many batteries available which meet or exceed these requirements such as the Panasonic NCR 18650B which has a capacity of 3400 mAh, delivers 3.7 Volts and can supply up to 4.65 Amps.

The Panasonic battery can be found online for around \$5.00. An alternative would be the Samusung 25R which is also a 18650 size battery and operates at 3.6 Volts. The Samsung 25R has a capacity of 2500 mAh and can supply 20 Amps. The Samsung 25R is available online for around \$4.00. Both batteries meet our technical requirements and are low cost enough to not have a profound impact on our budget. Both of these batteries are compact enough that they can be soldered to our printed circuit board resulting in further space savings. When designing a circuit involving a lithium battery, special care must be taken not to damage the battery. We have decided to use the Samsung battery because it balances performance, cost and footprint favorably.

4.5.7 Battery Charging Circuit

If not designed correctly, a lithium battery can become very dangerous, getting hot and even catching fire. A lithium ion battery cell can safely be charged up to 4.1-4.2 Volts but never higher. A lithium ion battery cell can also not be discharged below 2.5 Volts and operating a battery at the extreme thresholds reduces the battery's service lifetime. A lithium ion battery will also have a maximum discharge current rating, and this is very important because a battery can fail destructively if this is exceeded. If the load current is too high then the battery should be isolated from the circuit. Dedicated integrated circuits exist specifically to ensure that lithium batteries operate safely and correctly. One such integrated circuit is the Texas Instruments bq2970 voltage and current protection integrated circuit for single cell lithium-ion and lithium-polymer batteries.

The bq2970 uses MOSFET transistors to remove the battery cell from the circuit when the charge parameters are no longer within the safe range. As shown in Figure 13, the transistor labelled CHG has a diode bridging the source with the drain. The effect of this is to shut

off the charging if the voltage applied is too high, preventing the maximum charging current from being exceeded. The lithium cell can still be discharged even if the CHG circuit is disabled.

The DSG diode will shut off the DSG NMOS in exactly the same way if the voltage of the lithium ion cell becomes too low or if the discharge current is too high. The ion cell can still be charged even when the DSG circuit is disabled. Lithium cells can share a protection circuit if they are connected in parallel. The bq2970 is a very low cost component and can be purchased for \$0.55 per piece. The Hipera AP5056 battery charge management circuit is an 8 pin device that provides 1 Amp of charging current, has a 4.2 Volt charging voltage and a 2.9 Volt trickle charging threshold.

The Chipera AP5056 is a constant voltage and constant current linear battery charge management circuit. This 8 pin device provides 1 Amp of charging current, has a 4.2 Volt charging voltage and a 2.9 Volt trickle charging threshold. The AP5056 is designed specifically to incorporate charging via USB cable. If we decide to implement data transfer over USB as well, that would make this component a good candidate to charge the battery at the same time with the same cable.

The AP5056 is fully programmable, is capable of taking input from an NTC temperature sensor to open the circuit in the event that the battery gets too hot. Connecting the temperature input pin to ground will cause the management circuit to function normally without taking temperature into account. Ensuring the battery stays within a safe temperature range is important not only for prolonging the life of the battery but also for safety. A battery which gets too hot potentially becomes very dangerous.

Simplified Schematic

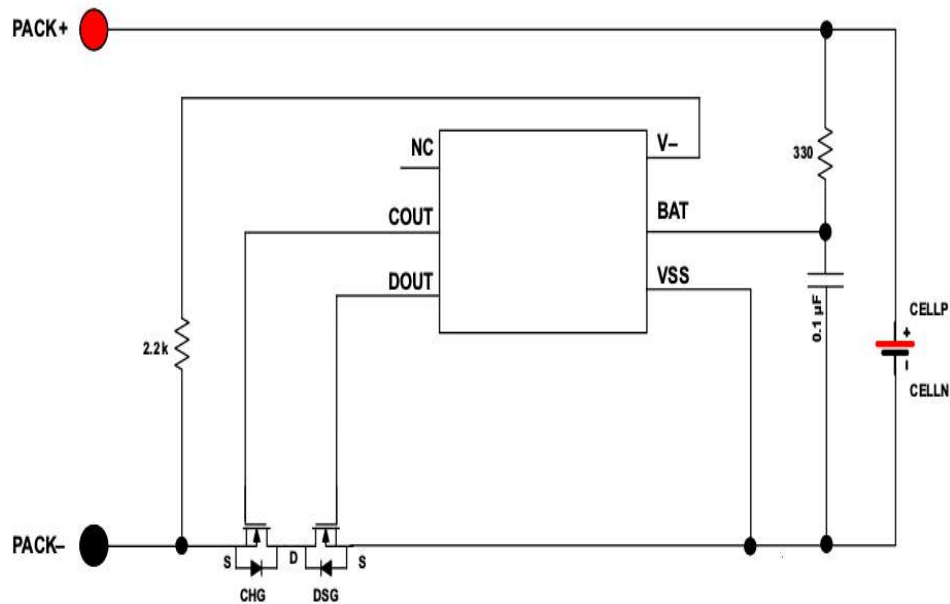


Figure 13. Simplified schematic for the bq2970

4.6 User Interface

The User Interface is a pivotal part of any product design, due to how deeply entangled the user interface and user experience are with the cost, ease of use, and durability of a product. When deciding how our customers will interact and experience our product, we considered both on-board and off-board interface methods and prioritized analyzing how each option would affect the usability and portability of our product. The level of complexity for each user interface method was also taken account throughout our analysis.

4.6.1 Smartphone Application (Wireless)

The advantage of using a wireless communication paired with a smartphone is that it reduces the amount of hardware required. A relatively cheap Bluetooth module would eliminate the need for SD storage or wired communication. The drawback to this approach is that it requires the user to have a smartphone and it requires us to write an app to interface with the device. Research on the wireless communication protocols and hardware modules considered for this user interface method are included in sections 4.7 and 4.8 of this paper.

4.6.2 Desktop Application (Wired)

It is possible to connect our device to a PC over USB. This could reduce the overall cost of product and be simpler to implement, but it has its disadvantages as well. The drawback to this approach is the device either becomes stationary (not portable at all) or requires the integration of storage for the data to be recorded. This would probably be implemented as a microSD card connected over I²C, or possibly SPI or UART.

4.6.3 On-Board Touch Screen

An onboard touch screen has the advantage of one device for both user input and data output. The touchscreen can be a simple and intuitive way to interact with electronics. The main drawback we saw with an on-board touch screen is that it would increase the price of our product and be a large single point of failure. If the on-board touch screen ever malfunctioned, the device would be rendered totally unusable and would require an expensive and possibly destructive repair process. This is a big drawback because large touch screens are commonly fragile and can crack easily or become water damaged; given that our device is likely to be used outdoors, on-board touchscreen malfunctions are something that we can expect to be common or our device if we were to go with this user interface method.

Furthermore, an on-board touch screen would greatly increase the power consumption of our device, which would complicate the design of our power source circuit and reduce the battery life of our device. Because of these reasons, we felt that an on-board touch screen was more of a hindrance to the overall usability of our product, and we have decided to not research it further.

4.6.4 On-Board Display with Mechanical Buttons

Due to the large amount of touchscreen-specific issues identified with the onboard touch screen user interface method that was researched, our team decided to research a physical screen with mechanical buttons as an alternative method of providing an onboard user interface. When compared to a large touch screen, this user interface has many benefits such as being less expensive to replace, and not being as susceptible to water damage.

Although it has some benefits, having an onboard screen with mechanical buttons still has some of the drawbacks that we found with the onboard touch screen option. The main drawbacks of this user interface method are increased power consumption, increased cost, and increased software development and hardware design complexity. Having all the processing done onboard the device would also require a much stronger microcontroller, raising the cost of the device even more. Due to these issues, our team decided to not have an onboard user interface method at all.

4.6.5 User Interface Comparison and Final Selection

After finishing initial research for possible user interface styles, the team decided that we would not be implementing any on-board user interface. This was due to the fact that an on-board user interface would increase the cost of our device and would increase the complexity of the chassis and software design. Although we had decided to stick to an off-board user interface early on in our research phase, we still needed to decide whether we would use wireless or wired communication between the off-board client device and our measurement device.

We want our device to be portable, so we opted to make mobile phones the main supported client for our device, which led us to choosing a wireless user interface as the main user interface method. We also plan on supporting wired communication for a wired off-board user interface; This interface will serve mainly as a backup user interface for debugging and in the case that the wireless communication is no longer working and will be designed with desktop and laptop computers in mind.

Table 8. User Interface Method Comparison

User Interface	Cost	Notes
On-board Touch Screen	High	Not chosen due to cost, durability, and implementation complexity
On-board Screen + Buttons	Medium	Not chosen due to cost and implementation complexity
Off-board – Wireless	Low	Will be used as main user interface method
Off-board – Wired	Low	Will be used as a backup user interface method, due to its reliability

4.7 Wireless Communication

In this section, we analyze different wireless communication methods that may be used to provide a wireless off-board user interface for our product. Wireless communication will allow for a convenient way to transmit and receive data between the user and the device. When analyzing different wireless communication technologies, we took note of how each method affected the cost and ease of use of our product. Specifically, we compared the maximum range, device compatibility, latency, power consumption, data rate, and implementation complexity of each of the technologies.

4.7.1 Bluetooth Classic

The first wireless communication technology that was assessed was Bluetooth, which is a wireless communication technology designed for secure device-to-device communications, mainly geared towards devices that are near each other. In this section, we outline our research related specifically to Bluetooth Classic, which is a term referring to the classic operating mode of the current Bluetooth standard. A summary of our technical findings can be found in Table 9.

Table 9. Traditional Bluetooth Specifications

Specification	Value	Notes/Pertinency
Range	30 m	Comparatively low, but sufficient for use in our product
Device Compatibility	High	Compatible with almost all mobile devices
Latency	~100 ms	Comparatively high, but sufficient for use in our product.
Power Consumption	Low	
Data Rate	2-3 Mbps	Comparatively high, more than enough the data our product will transfer
Implementation Complexity	Low	Easily available software libraries and sample code

Bluetooth seems to excel in almost all the technical specifications that we were judging wireless communication standards by. The specifications in which Bluetooth stands out the most area power consumption, device compatibility, and implementation complexity. Bluetooth was designed primarily for low power consumption, which is necessary to provide our users with a product that can survive on battery power for a long enough time for them to perform many analyses.

Due to Bluetooth being the industry standard for short range low power device communication for the last few years, there is a large amount of resources available for the development of applications based on Bluetooth communication; this increased availability for development examples and research greatly reduces the implementation complexity for

this protocol. The ubiquity of Bluetooth in industry today also increases the number of devices that will have Bluetooth modules built in, which increases the compatibility of our product with products that our customers may already own.

Although Bluetooth excelled in most of the categories researched, there were some worrying results. When compared to the other wireless technologies considered, Bluetooth had by far the greatest average latency; while latency is not the most important specification we will be taking into account, we still want to ensure that our customers can get their analysis data to their devices as quickly as possible to improve the user experience.

4.7.2 Bluetooth Low Energy

Since the release of Bluetooth 4.0 in 2010, Bluetooth has had two versions: Bluetooth Classic, and Bluetooth Low Energy. While researching Bluetooth Classic, we came across Bluetooth Low Energy and decided to research it as another possible wireless communication technology that we could use to send data between our device and the customer devices if we implemented an off-board user interface. A summary of our technical findings can be found in Table 10. Bluetooth Low Energy Specifications.

Bluetooth Low Energy shares many of the core features of Bluetooth Classic. Like Bluetooth Classic, Bluetooth Low Energy, or BLE, is a wireless communication technology designed for secure device-to-device communication at short ranges. While it shares many similarities to Bluetooth Classic, BLE is designed specifically for low power sensors and phone accessories which do not require continuous connection. Bluetooth Low Energy has many of the same benefits as Bluetooth Classic regarding the specifications we were analyzing, and even has improved performance on some. BLE has much lower power consumption than Bluetooth Classic and all the other wireless communication technologies analyzed, usually anywhere from 1%-50% of the power consumption of Bluetooth Classic.

Table 10. Bluetooth Low Energy Specifications

Specification	Value	Notes/Pertinency
Range	50 m	Comparatively medium range, more than enough for our product
Device Compatibility	Medium	Compatible with most mobile devices from the last 4 years
Latency	~6 ms	Comparatively medium, sufficient for our product
Power Consumption	Very Low	50% or less of Bluetooth Classic
Data Rate	2 Mbps	Comparatively medium, sufficient for our product
Implementation Complexity	Low	Less software libraries and sample code than Bluetooth Classic, but similar implementation

In addition to lower power consumption, BLE has a higher range than Bluetooth Classic, a similar maximum data rate, and even has greatly reduced latency, which was one of the main concerns we had with Bluetooth Classic. Although our findings were mostly positive, some concerns did arise throughout our research. The main drawback to using BLE would be the reduced compatibility, this is because BLE is not backwards compatible, so it requires the hardware Bluetooth module to support the Bluetooth Low Energy standard.

Since BLE is a newer standard, compared to Bluetooth Classic and some of the other technologies analyzed, less devices have Bluetooth modules which support BLE. This could cause issues for our customers, especially in the case that we only provide Bluetooth connectivity between the off-board user interface (application), and the actual product.

4.7.3 Wi-Fi

Wi-Fi is the common name for the set of standards defining wireless network communication. Our team briefly researched Wi-Fi to see if it would be a good fit for the wireless communication that may be required between our device and an off-board user interface device. A summary of our technical findings can be found in Table 11.

Table 11. Wi-Fi Specifications

Specification	Value	Notes/Pertinency
Range	100 m	Comparatively high, more than enough for our product
Device Compatibility	High	Compatible with almost all mobile devices and laptop computers
Latency	1.5 ms	Comparatively low, more than enough for our product
Power Consumption	High	Can use up to 40 times more power than Bluetooth Classic
Data Rate	~1 Gbps	Comparatively very high, more than enough for our product
Implementation Complexity	High	Highly complex communication protocol to implement

While Wi-Fi is widely used for wireless communication, our research led us to believe that it will not be a good fit for our project due to their being many drawbacks to this technology that greatly outweigh the few benefits it has. The main benefits of Wi-Fi include extremely fast data transfer speeds, especially compared with the other wireless communication technologies, as well as more range and lower latency.

These benefits are outweighed by the drawbacks which include much higher power usage than the other wireless communication technologies, and a much higher implementation complexity. For our project, range and data transfer speeds are not as important as power consumption and implementation complexity, so we have decided not to consider Wi-Fi communication as a final candidate for our wireless communication technology.

4.7.3 ZigBee Wireless Technology

ZigBee is a wireless technology developed to address the needs of low-power wireless Internet of Things networks which have become more common in the recent years. Our team briefly researched ZigBee to see if it would be a good fit for the wireless communication that may be required between our device and an off-board user interface device. A summary of our technical findings can be found in Table 12.

The main reason ZigBee was researched was due to the fact that ZigBee was designed with low-cost, low-power IoT networks in mind, but upon further research it was found that it would not be a good fit for our project because our product does not fully match the intended use-case of this communication technology. ZigBee excels at providing connectivity for networks of multiple interconnected sensors and devices, due to their custom “digiMesh” technology; digiMesh is allows for the implementation of mesh networks without single points of failures.

Table 12. ZigBee Specifications

Specification	Value	Notes/Pertinency
Range	~300 m	Comparatively high, more than enough
Device Compatibility	Low	Not compatible with many mobile phones
Latency	20 ms	Comparatively medium, meets standards
Power Consumption	Low	Similar power consumption to BLE
Data Rate	250 Kbps	Comparatively low, but may be enough
Implementation Complexity	High	Not as many guides or software examples due to being a newer protocol

Our product will not require a mesh network, given the fact that there will only be two products involved in the wireless communication at any given time, which would be the CFS and the customer’s mobile device or computer. Because we will be unable to take advantage of the digiMesh technology, ZigBee has little benefits over the other wireless technologies that were analyzed. On top of having few benefits, ZigBee also has some drawbacks such as lower compatibility, due to mobile phones commonly not having ZigBee compatible modules, higher implementation complexity due to our members not having experience with the ZigBee protocol, and a lower average data rate.

4.7.4 Wireless Communication Comparison and Final Selection

Throughout our research we found that, out of the wireless communication technologies analyzed, Bluetooth stood out due to its overall low power consumption, low implementation difficulty, and high device compatibility. This left us needing to decide between Bluetooth Low Energy and Bluetooth Classic; after analyzing the two communication technologies further, the team decided to choose Bluetooth Low Energy for this product.

The main deciding factor was the significant reduction in power consumption for Bluetooth Low Energy. Although Bluetooth Low Energy is compatible with slightly less devices, there are still enough mobile phones which support Bluetooth Low Energy to make it a viable choice. Table 13 below shows the comparisons between various wireless communication technologies which were researched and compared.

Table 13. Wireless Communication Comparison

Technology	Power Consumption	Client Compatibility	Implementation Complexity
Bluetooth Classic	Low	High	Low
Bluetooth Low Energy	Very Low	Medium	Medium
Wi-Fi	High	High	High
ZigBee	Very Low	Very Low	High

4.8 Wired Communication

In this section, we analyze different wired communication methods that may be used in our product, both within our circuit for communication between sensors and the microcontroller, and between the product and an external user interface device. Choosing the right communication protocols for the communication within the circuit is essential to increasing the efficiency of the circuit and reducing the PCB design complexity. Wired communication technologies are also important because having wired communication as a method for an off-board user interface device to communicate with our measurement device will allow for a convenient way to transmit and receive data between the user and the measurement device.

To narrow our search, we only analyzed serial communication technologies for our project. Serial communication is any wired communication that transmits single bits at a time, as opposed to parallel communication technologies which send multiple bits at the same time. Parallel and serial technologies each have their benefits, but we felt that serial technologies best suited our project so that we could minimize the amount of wires to minimize the complexity of our PCB design.

When analyzing the different serial communication technologies, we took note of how each method could be leveraged in our project. Because of the many different places where wired communication can be used within our project, our research was more focused on finding the strengths of each technology and where it would best fit within our project, instead of trying to find a single communication technology that solved every problem. When analyzing the strengths and weaknesses of each technology, we took note of the use cases in which the technology is most commonly used, as well as the technology's latency, data-rate, overall compatibility, and cost.

4.8.1 UART

UART, or Universal Asynchronous Reception and Transmission, is a serial communication protocol. As seen in Figure 14, UART only requires the use of 3 wires for communication: Tx (transmit), Rx (receive), and Ground. Unlike SPI and I2C, the other serial communication protocols we researched, UART communication does not require a shared clock signal. This is because in UART communication both the receiver and the transmitter have their own clock signals that are synchronized based on the configuration of the device.

The fact that no shared clock is required makes UART a great option for transmitting data between two devices, which is why this is one of the common uses for the UART protocol. For this reason, we will be using the UART protocol to transmit data between our measurement device and an off-board user interface device, to provide for a wired communication alternative to our main wireless off-board user interface.

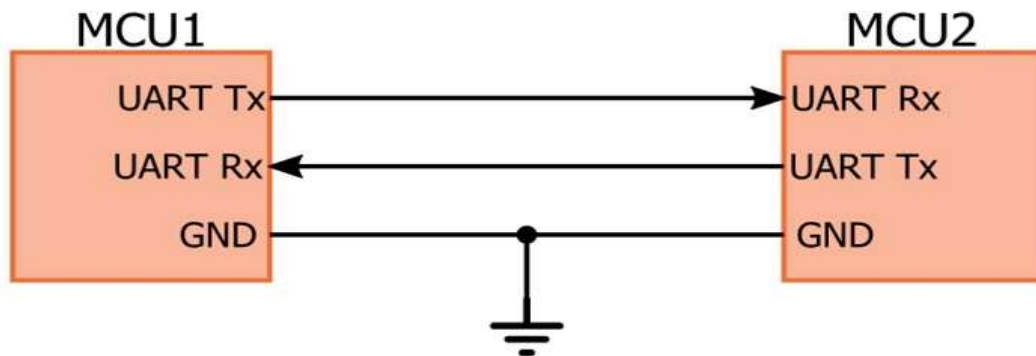


Figure 14. UART Device Configuration
Reprinted with permission from EETech Media, LLC [EET.UART].

We will be using UART over USB, also known as Serial over USB, for this communication. UART over USB was also chosen due to the experience that some of the team members had with the technology. Figure 15 shows an example of how the operating system of the user interface device could communicate with the measurement device via Serial over USB by using a Communication Class Driver.

4.8.2 I2C

I2C, or inter-integrated circuit, is a serial communication protocol which is designed specifically for microcontrollers. As seen in Figure 16, I2C only uses 2 wires for communication and uses a shared bus with master and slave devices, allowing you to connect up to 128 different devices to communicate with each other over the same set of busses. The two wires used in I2C communication are the SDA line (data), and the SCL line (clock). Like SPI, I2C is a synchronous communication protocol which is why a shared clock line is required between the devices.

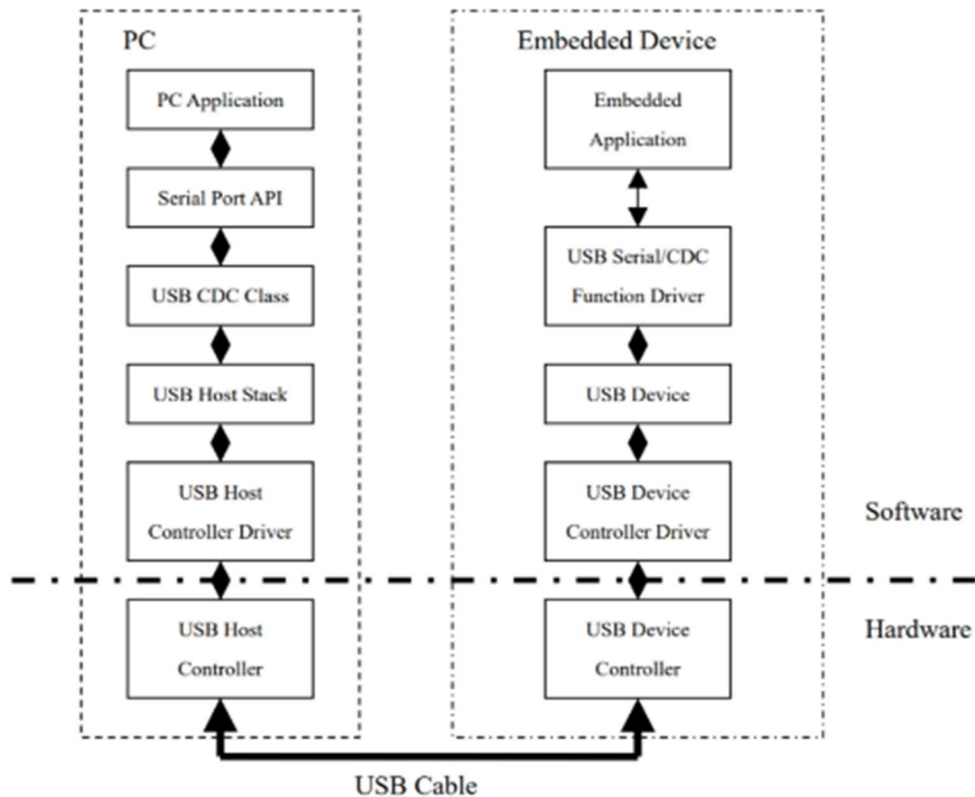


Figure 15. Serial over USB Communication

Reprinted with permission from Micro Digital [MD.WUUES].

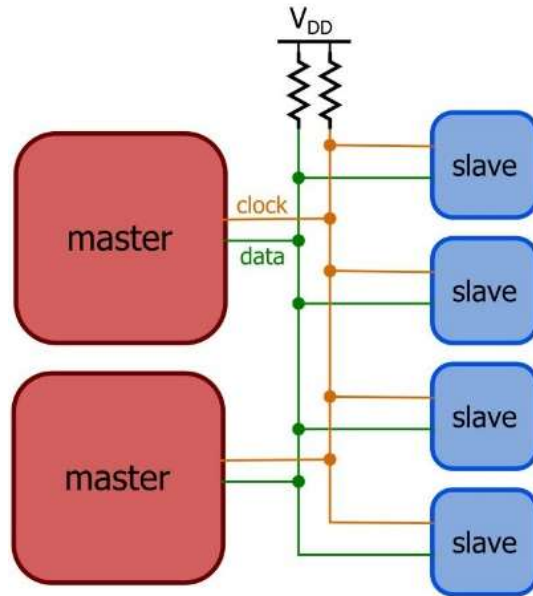


Figure 16. I2C Device Configuration

Reprinted with permission from EETech Media, LLC [EET.I2C].

The fact that there is only one data line means that I2C is only half-duplex, unlike UART which is full duplex, which means that when using I2C only one device can transmit data at a time on the I2C bus. To be able to handle that many devices on a single data line, I2C uses a master-slave architecture where there can be many masters and many slaves. In the master-slave architecture, the master devices get to control all reads and writes on the wire; this makes it so that I2C can use a bus topology while avoiding the chaos of having multiple devices trying to communicate at the same time.

One of the main benefits of I2C is the ability to maintain a low signal count even with many devices on the wire, due to the fact that it only requires 2 signals compared to SPI which requires more. Another big benefit of I2C is the option for multiple masters, but this benefit is not one that we would take advantage of, as we do not see a need for multiple masters in our design.

While the need for less signals and wires would simplify our PCB design, this benefit is countered by the need for pull-up resistors. These resistors consume space on the PCB and complicate the layout, as well as increase the power dissipation in our circuit. Another drawback to using I2C is that firmware development for I2C communication is usually more complex than UART or SPI. The largest drawback for I2C is that when compared to SPI, the speeds are much lower.

Even though I2C has many drawbacks when compared to SPI, it is very commonly used to configure sensors. This is the case with many of the Bluetooth and Camera sensors we have researched. While we may use SPI to transfer data between our sensors and our MCU, we will likely incorporate I2C into our design for the purpose of sensor configuration.

4.8.3 SPI

SPI, or Serial Peripheral Interface, is a serial communication protocol designed to allow multiple microcontrollers to communicate with each other, much like I2C. As seen in Figure 17 and Figure 18, SPI also uses a shared bus with a master and multiple slave devices, but SPI uses three main wires for communication: the CLK line (for the shared clock signal), the MOSI line (master output line), and the MISO line (master input line). In addition to the three main lines, SPI will also have one extra wire for each slave, used by the master for selecting which slave is being communicated with at a given time.

The shared clock signal means that SPI is a synchronous communication protocol, unlike UART. The fact that there is two data lines means that SPI is full duplex, unlike I2C which is only half-duplex, which means that when using SPI two devices can transmit data at a time. Even though SPI is full duplex, it still uses busses to support multiple devices on the same two data lines. To be able to handle that many devices on the shared lines, SPI uses a master-slave architecture where there can only be one master and many slaves. In the master-slave architecture, the master device gets to control all reads and writes on the wires; this makes it so that SPI can use a bus topology while avoiding the chaos of having multiple devices trying to communicate at the same time.

Master and slave devices can be configured in two possible ways: Multiple-Slave-Select configuration and Daisy-Chain configuration. Examples of both configurations can be found in the figures below. Multiple-Slave-Select configuration is the standard SPI configuration. Even though it requires more data lines than the daisy-chain configuration, after conducting our research we have decided that the Multiple-Slave-Select configuration is the configuration we will use when implementing SPI communication in our device due to the increased simplicity and greater sensor support.

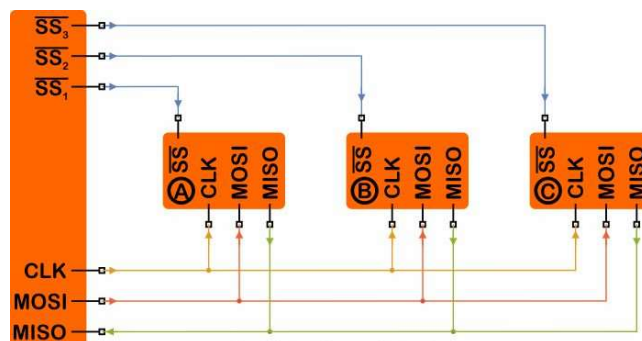


Figure 17. Multiple-Slave-Select SPI Configuration

Reprinted with permission from EETech Media, LLC [EET.SPI].

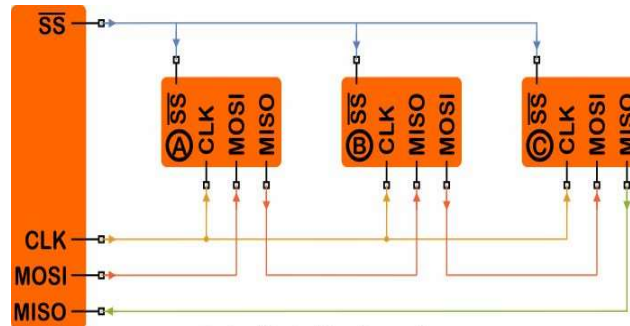


Figure 18. Daisy Chain SPI Configuration

Reprinted with permission from EETech Media, LLC [EET.SPI].

The main benefit of SPI is the data rate; SPI is known to be much faster than I2C on average. This is because the SPI protocol is much simpler which minimizes overhead and the fact that the protocol supports higher clock frequencies. The simplicity of the SPI protocol not only increases the data transfer rate, it also makes firmware development and low-level hardware design for SPI communication much easier.

The main drawback of using SPI is the higher pin-count due to the requirement for each slave to have a separate slave-select signal. SPI also only supports a maximum of four slave devices, which is much smaller than I2C's 128 possible slaves. This reduction in maximum slave amount reduces the number of sensors that you can connect to a single MCU using the SPI protocol. Another slight drawback to SPI is that there is no central SPI standard. Without a central standard, many sensors and devices have slightly different definitions of how SPI communication should be conducted. This increases the amount of research that has to be done when using parts that communicate of SPI.

Throughout our research we found that SPI is much less common than I2C, even though it has many benefits. A common use for SPI in circuits is for data transfers that require higher speeds, such as SD card readers, display modules, and camera modules. This has been the case with many of the SD card readers and camera modules we have researched, and we will implement SPI for use in these cases.

4.8.4 Wired Communication Comparison and Final Selections

Throughout our research we discovered that no wired communication technology is perfect, and that they are each best suited for very specific tasks. For this reason, we have chosen to implement all wired communication technologies that we researched, as they each meet a certain need that we have for our project. Table 14 below shows what we will be using each wired communication technology for.

Table 14. Wired Communication Technology Uses

Wired Communication Technology	Use in Project
UART	Debugging, Wired User Interface
I2C	Component Configuration: Camera Sensor, Bluetooth Module

4.9 Bluetooth Module

In this section, we analyze different Bluetooth modules that may be used to provide our measurement device with the capabilities needed to communicate with a wireless off-board user interface device. Wireless communication will allow for a convenient way to transmit and receive data between the user and the device; these modules have been researched for use in the event that we choose Bluetooth or Bluetooth Low Energy as the wireless communication method for our off-board user interface.

When analyzing the different modules, we took note of how each method affected the cost, development complexity, and ease of use of our product. Specifically, we compared the maximum range, device compatibility, Bluetooth version, latency, power consumption, maximum data rate, size, and implementation complexity of each of the modules.

4.9.1 HC-05

The HC-05 Bluetooth module is a popular module amongst hobbyists due to its affordability and simplicity; you'll find this module in the majority of Bluetooth compatible beginner Arduino projects. Due to the ubiquity of this module, our team researched it to see if it would be a good fit to provide our measurement device with the wireless communication capabilities that may be required between our device and an off-board user interface device. Table 15 contains a summary of the technical specifications of this device.

As mentioned previously, the main benefits of the HC-05 module are its affordability and low implementation complexity. HC-05 modules can be found online for less than \$10 per part, which would help us maintain a low cost for our device and offset some of the higher than expected costs of the optical equipment. The implementation complexity for this module is so low due to the fact that it is extremely popular amongst the hobbyist community. This means that there are a wide variety of existing projects that include this module, giving us an almost endless source of tips and other good information regarding how to properly integrate this module into a design; the ubiquity of this module also means that there are well-developed software libraries written to interface with the API of this device, making the software development significantly easier.

Table 15. HC-05 Technical Specifications

Specification	Value	Notes/Pertinency
Bluetooth Version	V2.0+EDR	Outdated Bluetooth version, missing key features
Max Data Transfer Rate	3 Mbps	Average among modules researched
Minimum Footprint	12.7mmx27mm	Average among modules analyzed
Sensitivity	-80dBm	Same as the RN42
Transmit Power	+4dBm	Same as the RN42
Supply Voltage	3.3 V	Average among modules researched
Current Draw	N/A	Unavailable
Communication Protocol	UART	ASCII Command Line Interface over UART

The main drawback of this device is the fact that it only supports Bluetooth V2.0. This is the lowest supported version of Bluetooth out of the Bluetooth modules that we researched, which leaves this module at a great disadvantage. When compared to the Bluetooth V2.1 supported by the RN42 module, a comparable module which we analyzed, Bluetooth V2.0 is missing important features such as the Bluetooth Simple Pairing Protocol (SPP). Having a Bluetooth module which supports SPP is important to us because SPP reduces the pairing complexity and would improve the usability and overall user experience for our product and having an easy to use product is important to our team. Another feature missing in Bluetooth V2.0 is Bluetooth Low Energy support. During our research of Wireless Communication technologies, we found that the qualities of Bluetooth Low Energy were in-line with our goals for the project, and we would prefer to have a Bluetooth module which supported this technology, which was introduced in Bluetooth V4.0.

4.9.2 RN42

The RN45 Bluetooth module is an affordable Bluetooth module which is very similar to the HC-05 module. Because this module has been used in many other Senior Design projects, our team researched it to see if it would be a good fit to provide our measurement device with the wireless communication capabilities that may be required between our device and an off-board user interface device. A summary of the technical specifications of this device can be found in Table 16. Throughout our research of this module we found that the RN42 is highly like the HC-05 module, especially in terms of the technical specifications. The main technical difference between the two modules is the fact that the RN42 module supports a higher version of Bluetooth. The RN42 supports Bluetooth V2.1, compared to the HC-05 which only supports Bluetooth V2.0. As mentioned in the previous section, this is important because Bluetooth V2.1 comes with support for the Simple Pairing Protocol, which is a feature we would like to have so that we can provide our customers with the best user experience possible.

Table 16. RN42 Technical Specifications

Specification	Value	Notes/Pertinency
Bluetooth Version	V2.1+EDR	Contains more features than the HC-05, but still does not support BLE
Max Data Transfer Rate	3 Mbps	Average among modules researched
Minimum Footprint	13.4 x 25.8 x 2.4 mm	Average among modules researched
Sensitivity	-80 dbM	Same as HC-05
Transmit Power	+4 dBm	Same as HC-05
Supply Voltage	3 V – 3.6 V	Average among modules researched
Current Draw	2 uA, 3 mA, 30 mA	Comparatively medium
Communication Protocol	UART, PIO, AIO, SPI	ASCII Command line interface over UART

Although it is very similar in terms of technical specifications, the RN42 is missing some of the key benefits that the HC-05 had. The RN42 costs upwards of \$30, almost 3 times as much as the HC-05 module. Although this is still a small amount compared to our overall budget, we did not find that the 300% increase in price is justified, especially because the module has almost the exact same technical specifications as the HC-05. The RN42 also does not share the same ubiquity of the HC-05 module, meaning that there are not as many software libraries that exist for this module. Another drawback of the RN42 is that, although it supports a newer version of Bluetooth than the HC-05, it still does not have support for Bluetooth Low Energy, which was introduced in Bluetooth V4.0.

4.9.3 RN4020

The RN4020 Bluetooth Low Energy RF module is a Bluetooth communication module that supports Bluetooth 4.1 and includes an MCU, digital analog I/O capabilities, an on-board stack, and an ASCII command API. In our initial research, we found that this module is one of the most common modules for Bluetooth Low Energy communication. Therefore, our team researched to see if it would be an adequate measurement device and appropriately interface with wireless communication capabilities.

A summary of the technical specifications of this device can be found in Table 17. This module differs greatly from the two Bluetooth Classic modules that we researched for this portion of our design. Compared to the first two modules researched, the RN4020 has a much smaller footprint, uses a fraction of the power, has a stronger signal, and is more sensitive. While it is not cheaper than the HC-05, the RN4020 is still very affordable, especially when its technical specifications are taken into account. The RN4020 can be found for under \$20, placing it between the HC-05 and the RN42.

Table 17. RN4020 Technical Specifications

Specification	Value	Notes/Pertinency
Bluetooth Version	V4.1+BLE	Supports Bluetooth Low Energy
Max Data Transfer Rate	1 Mbps	Comparatively low, sufficient for our product
Minimum Footprint	11.5 x 19.5 x 2.5 mm	Small compared to other modules researched
Sensitivity	-92.5 dBm	Higher than most modules researched
Transmit Power	+7.5 dBm	Higher than most modules researched
Supply Voltage	3.3 V	Average for modules researched
Current Draw	900 nA, 1.5 mA, 16 mA	Comparatively low, since BLE uses low power consumption
Communication Protocol	UART, PIO, AIO, SPI	ASCII Command line interface over UART

Aside from besting the other modules in most of the technical specifications analyzed, the main advantage that the RN4020 has is that it supports Bluetooth 4.1 and Bluetooth Low Energy. This capability is important because the Bluetooth Low Energy would be the best fit for our project as far as wireless communication technologies go. The only drawbacks that the RN4020 has are the data transfer rate and ease of implementation. These drawbacks are not unique to the RN4020; lower data transfer rate and slightly higher implementation difficulty are characteristics that will come with most Bluetooth Low Energy sensors.

4.9.4 ESP32

ESP32 is a low-cost, low-power chip series with Wi-Fi & dual-mode Bluetooth capabilities built in. In our initial research, we found that this chip is commonly used in amateur Bluetooth Low Energy projects. Because of this, our team researched it to see if it would be a good fit to provide our measurement device with the wireless communication capabilities that may be required between our device and an off-board user interface device. A summary of the technical specifications of this device can be found in Table 18.

Upon further research our team found that, although an ESP32 chip can be used as a separate Bluetooth or Wi-Fi module, the chip is more commonly used as a full microcontroller because of the large amount of capabilities that are built into this chip. ESP32 chips support peripherals such as touch sensors, temperature sensors, CAN 2.0, and more. Because the ESP32 is a full system on a chip, as opposed to a dedicated Bluetooth module, we found that this device would be overkill for this project. Even though this chip is extremely low cost, it would have higher PCB design complexity, and much higher power usage compared to the other modules researched.

Table 18. ESP32 Technical Specifications

Specification	Value	Notes/Pertinency
Bluetooth Version	V4.2+BLE,EDR	Highest supported Bluetooth version of modules researched
Max Data Transfer Rate	4 Mbps	Comparatively high
Minimum Footprint	25.5 mm × 18 mm × 3.1 mm	Average for modules researched
Sensitivity	-97 dBm	Highest among modules researched
Transmit Power	+12 dBm	Highest among modules researched
Supply Voltage	3.3 V	Average for modules researched
Current Draw	100 uA, 30 mA, 100 mA	High for a BLE module due to unnecessary components
Communication Protocol	UART, PCM, SDIO, SPI	ASCII Command line interface over UART

4.9.5 Bluetooth Module Comparison and Final Selection

After analyzing the results of the research, the team decided to choose the RN4020 RF module for our Bluetooth communication. This decision was mainly due to the RN4020's support for Bluetooth Low Energy, its low power consumption, and low cost. Out of the 4 modules analyzed, only the RN4020 and the ESP32 supported Bluetooth Low Energy, which is preferred for this project to keep the battery life as long as possible. Between the RN4020 and the ESP32, the RN4020 had lower power consumption and would be easier to integrate into our PCB design, both were due to the inclusion of many unnecessary modules in the ESP32 board. Table 19 on the next page compares the modules that were researched and highlights the RN4020 as our choice.

Table 19. Bluetooth Module Comparison

Module	HC-05	RN42	RN4020	ESP32
Cost	<\$10	<\$35	<\$20	<\$20
Size	12.7mm x 27mm	13.4 x 25.8 x 2.4 mm	11.5 x 19.5 x 2.5 mm	25.5 mm × 18 mm × 3.1 mm
Power Consumption	Medium	Medium	Very Low	Low
Bluetooth Version Support	V2.0	V2.1	V4.1, BLE	V4.2, BLE+EDR

5. Project Design

This section describes the hardware designs which the project for the chlorophyll fluorescence spectrometer went through in order to achieve its constraints, standards, and research goals.

5.1 Hardware Design

This section describes the hardware design of the chlorophyll fluorescence spectrometer. Previous hardware designs are briefly reviewed so that there is no confusion about the particulars of the final design. This section includes the optics design, the electronics design, and the joining of the two.

5.1.1 Optical Housing Design

A simplified final system design is shown Figure 19.

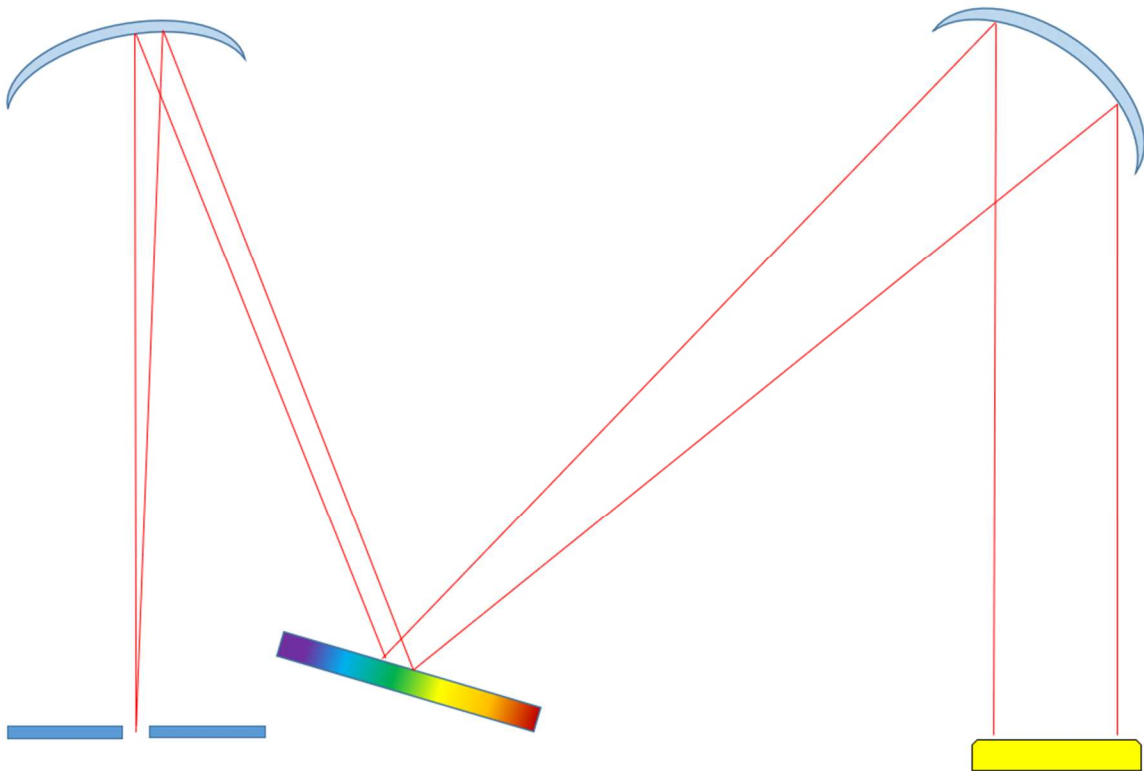


Figure 19. Dimensionless optical system design.

First, the question must be raised about the monochromator: why were only reflective gratings chosen when transmissive gratings would simplify the optical system? The reason a reflective grating was chosen over a transmissive grating is due to the popular blaze angle

for transmissive gratings being at 14.7 degrees, which correlates to a peak wavelength efficiency of 300 nm. Despite thorough searches, few transmissive gratings could be found with a blaze angle closer to 4.3 degrees, and those that had blaze angles around the ideal wavelength were too expensive for the project's budget. From here, transmissive gratings were discarded for reflective gratings.

Originally, the system had a lens in front of the entrance slit, but after discussing with faculty, it was decided that the lens could be safely discarded. This design change saved the team some money and cut down the dimensions of the optical housing.

There are two systems to the optics design: the system before the grating and the system after it. It is prudent to design this system backwards, starting with the sensor array at the end. If it is not done this way and the system is designed from the start forwards, the variables will compound on each other and the system will be much more difficult to solve.

The ideal case for this system was to have the light from the vertical entrance pupil (which will spectrally spread horizontally) be spread across the active horizontal dimension of the image sensor. The system was designed to project the image of the slit onto the sensor such that its spectrum from the grating was in focus. In order to give a margin of error in the design process, we designed the system such that the light from the entrance slit only spread across 90% of the active horizontal dimension. This covered the case where the optics might have spread out the spectrum a little wider than anticipated; this decision prevented the loss of any extra waveband information. According to the ARDR image sensor's data sheet, the active horizontal dimension is 4.83 mm. 90% of this is 4.347 mm, so we designed the system such that the image of the entrance slit was smaller than 4.34 mm in width by the time it reached the image sensor as shown in Figure 20.

The light that hit the diffraction grating had an angular dispersion which de-collimated it from the front half of the optical system. To re-collimate it for the detector, we placed a focusing mirror at a distance equal to the mirror's focal length away from the grating after accounting for astigmatism incurred from using mirrors at non-incident angles. To find this focal length, the angular dispersion of the waveband from the diffraction grating and the angle of the light incident on the grating from the front half of the optical system was calculated.

Consider again Equation 2. The longest λ is 700 nm and the shortest λ is 600 nm. $a = \frac{1 \cdot 10^{-3} \text{ m}}{300} = 3.33 \text{ } \mu\text{m}$, where a is the spacing between the grooves of our grating. The grating that was purchased is blazed for the first order, so $m = 1$. The only variable constraint is the angle of light incident on the grating θ_i , which is a metric that can be manually controlled. For the long end of the waveband, $\frac{m\lambda}{a} = 0.21$. For the short end of the waveband, $\frac{m\lambda}{a} = 0.18$. These numbers will be used in place of their variable fraction counterparts from here on out.

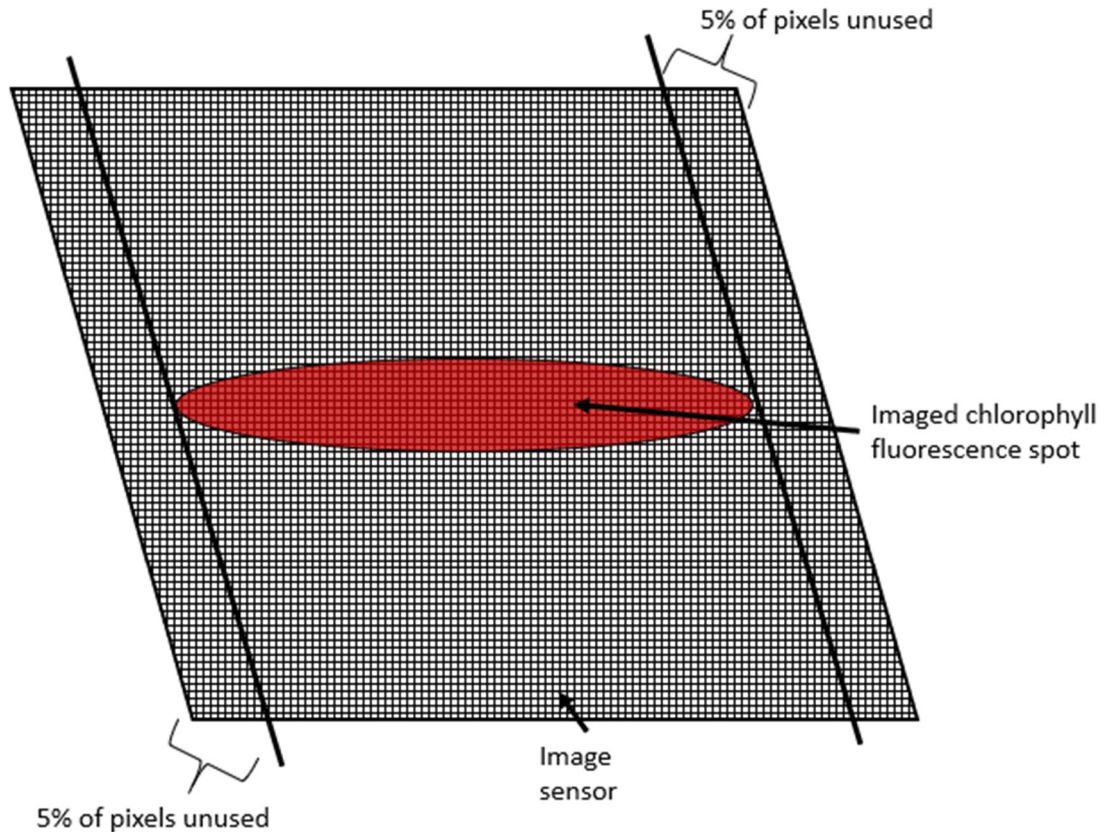


Figure 20. 90% sensor fill using the chlorophyll fluorescence spot.

The grating angular dispersion is the longest wavelength's dispersion minus the shortest wavelength's dispersion, or $\sin^{-1}(0.21 + \sin \theta_i) - \sin^{-1}(0.18 + \sin \theta_i)$. Since θ_i is a manipulatable variable, the above function acted as a tool to produce the angular separation we desired. The plot relationship between incidence angle and grating angular dispersion is shown in Figure 21. There was a cut-off at $\theta_i = 51.84^\circ$, so as long as the grating incidence angle did not exceed this value, the grating angular dispersion remained a real number.

The reason the angular separation is so important is its effect on the effective slit size when the light reaches the image sensor. The tangent relationship gave the exact distance from the grating to the final mirror required for the light to spread to its ideal size, which the mirror then collimated on to the image sensor. Again, the focusing mirror was placed at its focal length's distance from the grating (after accounting for astigmatism) to focus the light at the sensor. This helped us narrow down our mirror choices for the system.

However, it is important to note that the size of the slit imaged through the system will affect the focal length of the focusing mirror. Consider Figure 22. The angular dispersion θ_m is divided between the shortband dispersion at one end of the grating and the longband dispersion at the other.

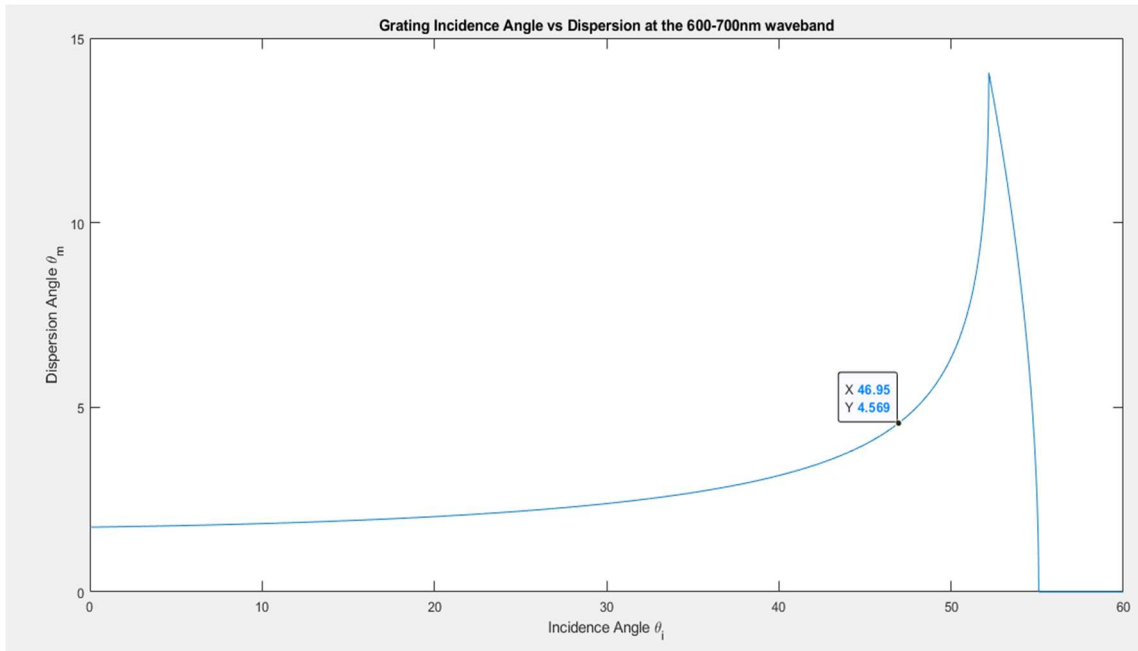


Figure 21. Diffraction grating incidence angle vs angular dispersion at 600-700nm waveband

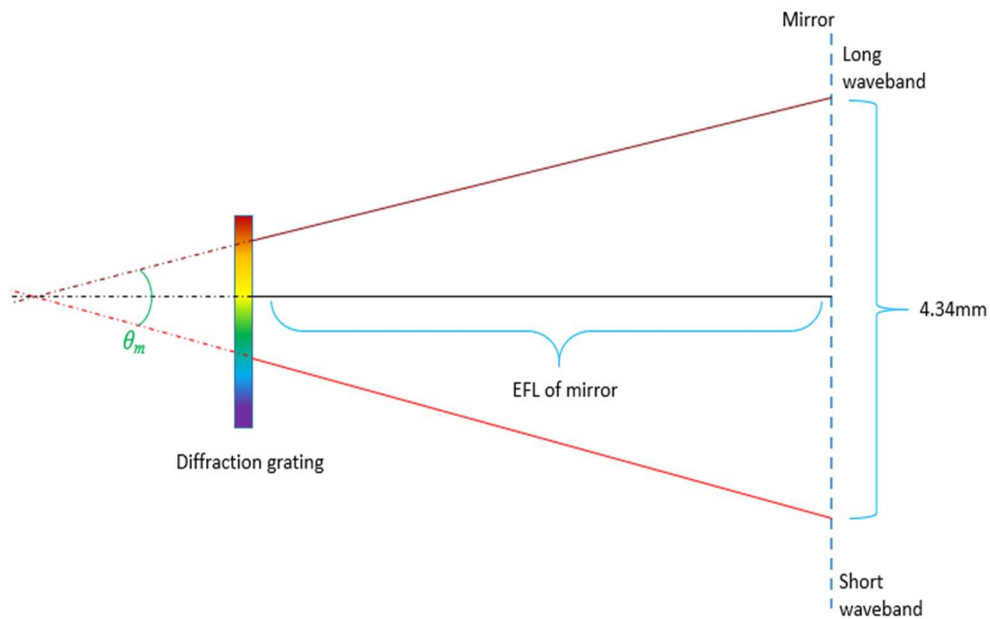


Figure 22. Illustration of the geometric system between the diffraction grating and the focusing mirror (simplified)

Geometric analysis cannot be made from the grating to the mirror since the object to be analyzed would be a rhombus, not a right triangle. By tracing the geometric triangle back to the virtual space behind the grating, a true right triangle is made. The base of this full triangle was solved for using the known trigonometric tangent identity, the angular dispersion θ_m , and the ideal image size of less than 4.34mm. Then, to find the effective

focal length of the mirror, we subtracted the base of the triangle behind the grating from the base of the full triangle.

In equation form, the effective focal length that the focusing mirror should have is shown in Equation 6. This equation can be equalized to any focal length and the controllable parameters can be matched appropriately. A common focal length used in spectrometers is 40mm, and since cheap mirrors usually come in multiples of 25mm, the design team elected to go with a focusing mirror that has a 50mm effective focal length.

$$efl = \frac{4.34 - slit}{2 * \tan\left(\frac{\theta_m}{2}\right)}$$

Equation 6. Effective focal length of focusing mirror using slit size and angular dispersion

Using Equation 6 and a slit size of 200 μ m and aiming for an efl of 50mm, it was found that the angular dispersion $\theta_m = 4.6^\circ$, which corresponds to an incidence angle $\theta_i = 47^\circ$ for the collimating mirror to grating interface. The actual efl of this system, using these angle metrics, was 50.008 mm which creates a focusing error of 0.016%. A focusing error this low is generally ignorable and was ignored going forward.

The incidence angle, a controllable factor required for the hardware design of the system before the diffraction grating, was then known. The system after the grating was thus solved and included a 10% error buffer at the imaging plane just in case calculations were not perfectly accurate or there were optical misalignments.

Now, consider the task of matching the F-number of the two mirrors. The F-number is a unitless ratio of the focal length to the diameter of the aperture. In this case, the aperture of a mirror is its physical diameter. Two considerations were made: the size of the F-number and the effect of that F-number on cost. Generally, as the F-number's absolute magnitude increases (1, 2, 5, 10, 20, etc.), the aperture lets in less light but has a greater depth of field. And, conversely, as the F-number's absolute magnitude decreases (10, 5, 2, 1, 0.75, 0.5, etc.), the aperture lets in more light but loses depth of field.

Since this a spectrometer, we decided that depth of field should not be immensely important in the design process. Gaining as much light as possible to maximize signal, however, was a primary design concern. As such, the F-number of both optics were chosen such that they matched and were relatively low in absolute magnitude. Anywhere from f/1 to f/4 is a safe range, but a specific F-number needed to be chosen. This is where the requirement specifications helped narrow the search.

As F-number decreases in absolute magnitude, the price generally goes up for mirrors since more surface area needs to be prepared for reflectance. f/4 mirrors cost between \$35 to \$50. f/4 mirrors offer large effective system sizes (the size of the distance from the entrance slit to the collimating mirror), but this correlates to an increase in the dimension specification, which was something the team wished to avoid. f/4 mirrors also take in a little less light than their lower magnitude counterparts. f/1 mirrors are very, very expensive, usually

reaching \$150 per mirror or more, heavily constraining the cost requirement. However, their effective system size is generally small. $f/1$ systems also take in the most amount of light, a plus for the chlorophyll fluorescence spectrometer.

In the end, a happy medium at $f/2$ was decided since this F-number offers a great amount of light transmission, generally acceptable price ranges, and reasonable system size. Had we been able to anticipate the issues brought on by COVID-19 as discussed in 6.8, we would have chosen a mirror with greater depth of field and a smaller entrance pupil. Considered focusing mirrors are shown in Table 20. That which was highlighted in green was chosen for integration into the CFS.

Table 20. Mirror prices and other metrics

Part name	Manufacturer	Price	EFL (mm)	Diameter (mm)	F#
CM127-050-P01	ThorLabs	\$39.50	50	12.7	3.937
CM254-050-P01	ThorLabs	\$60.34	50	25.4	1.968
CM508-050-P01	ThorLabs	\$90.63	50	50.8	0.984
10DC100ER.1	Newport	\$141.00	50	25.4	1.968

The collimating mirror's F-number must be matched. There are only a few collimating mirrors that have a small efl at the standardized diameter. As such, it was decided that the same mirror should be used for both focusing and collimating. Thus, the mirror highlighted in green in Table 20 was purchased twice, eliminating any F-number matching concerns and providing no need for extraneous calculations.

The chosen mirrors were coated with silver. According to ThorLabs, their silver-coated mirrors offer an average of 97.5% reflectance in the 450 nm to 2 μ m waveband as opposed to the aluminum-coated mirrors offering only 90% reflectance in the same waveband. Both mirrors cost the same and have the same dimensions, so to minimize loss from reflection, silver-coated mirrors were chosen for the CFS. All optical components were thus selected and a basic outline of the spectroscopy system was made.

5.1.2 Optical Loss Calculations

As light moves from the source to the receiver, it incurs many levels of power loss from propagation, reflection, transmission, and imperfect efficiency at the grating and sensor. A loss calculation is important because it describes how much signal the source loses by the time the light reaches the sensor.

There are five primary optical components: two concave mirrors, one entrance slit, one diffraction grating, and one sensor array. The light also has to propagate from the chlorophyll sample through a cuvette and through the system to reach the sensor. These sources of loss can be calculated using ideal equations, tweaking them slightly to account for real-world variations, and summing them all up at the end.

For the geometric system, propagation losses were considered negligible and were not included in the calculation. The total loss incurred by the fluorescence from when it enters the spectrometer to when it reaches the sensor is included below in Table 21. The numbers used for each calculation is included in Appendix C, Table 35.

Table 21. Table of expected interface losses

	600nm	683nm	700nm
Reflection loss from collimating mirror (dB)	0.1323	0.0877	0.0877
Reflection loss from diffraction grating (dB)	1.3668	2.0066	2.0761
Reflection loss from focusing mirror (dB)	0.1323	0.0877	0.0877
Sensor quantum efficiency loss (dB)	1.0790	1.6115	1.6749
Total Losses (dB)	2.7104	3.7935	3.9264

Considering the table above, in an ideal situation without calculating the losses incurred from fluorescence passing through the slit, the system sees over half the power lost from propagation from slit to sensor. Most of the power loss comes from the diffraction grating since its efficiency curve peaks around 500nm, shown in Figure 23. There is also power loss at the sensor's interface due to its quantum efficiency curve, shown in Figure 24.

To account for these losses, special consideration was made toward power output from the sample and fluorescence isolation. The darker it is inside the optical housing, the lower chance there is of scattered light affecting the signal received at the sensor end, so we designed the system to perfectly isolate the fluorescence effect within the pump housing. The power output from the sample must also be maximized, hence the high drive current for the laser light source.

Unfortunately, loss mitigation was regulated to just these two considerations—that is, they were the only way to prevent the fluorescing light from losing so much power that it appeared as noise at the sensor side. Thankfully, the process to reach peak fluorescence is comparatively slow (about 1 second) and the intensity lasts for a long time, maintaining about 85% max intensity for at least 20 minutes [Qck.Htn].

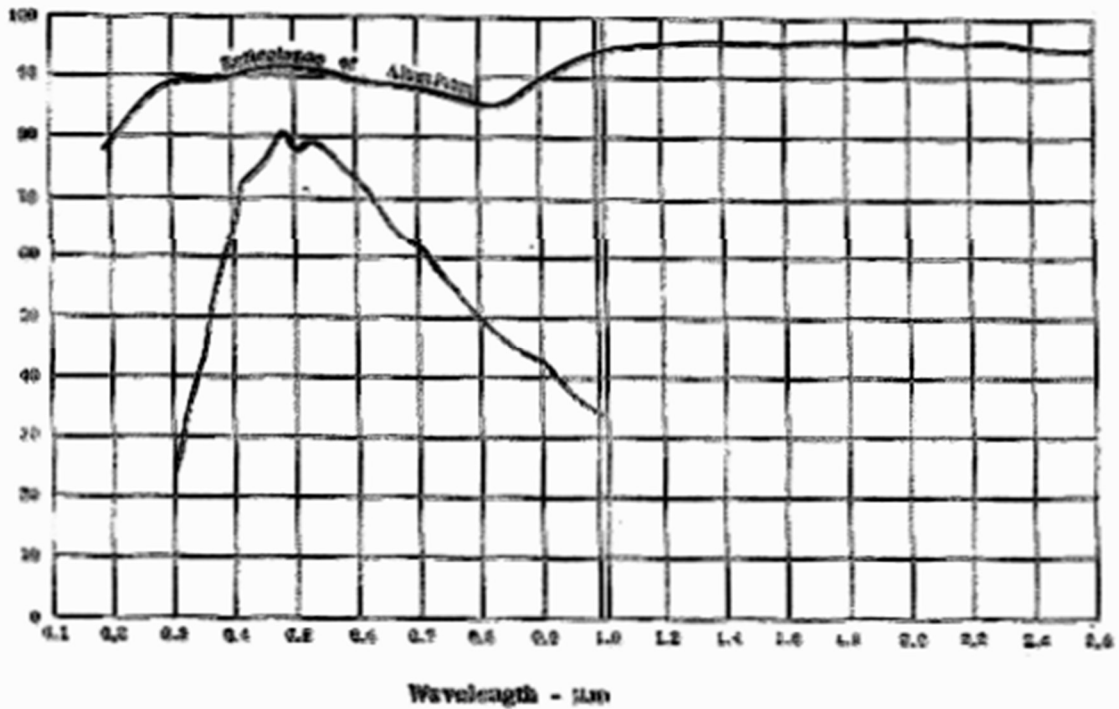


Figure 23. Diffraction grating efficiency curve (source quality)

*Republished from Richardson Gratings' data sheet for 53-*270R gratings.*

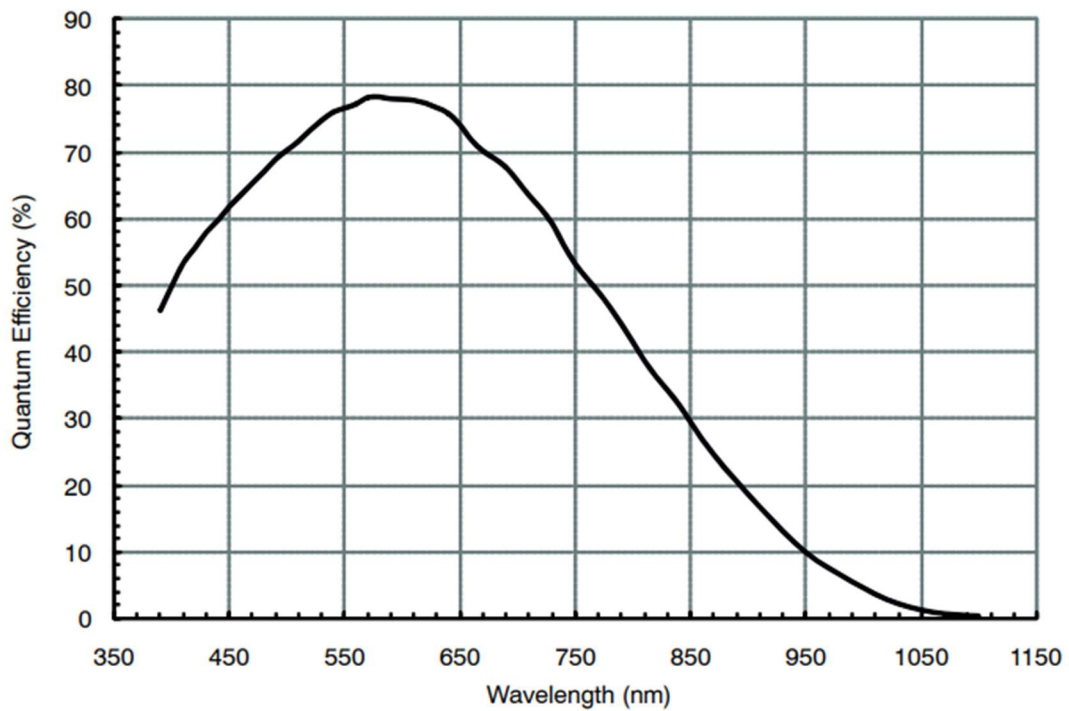


Figure 24. ARDR Monochrome Sensor quantum efficiency curve vs wavelength

Republished from ON Semiconductor's AR0130CS data sheet.

With these loss calculations in mind, we knew that if losses proved too great for the sensor to operate in capture mode where not enough signal was obtained, the sensor's integration time could be increased to a very long timescale to absorb as many photons as possible. This was not implemented in our final design due to the intensity of the received signal, but it was good to know we had the option in case we needed it.

5.1.3 Electronics Design

Texas Instruments WeBench was useful in the design of the power supply for the Chlorophyll Fluorescence Spectrometer. The design parameters used include the range in voltage that the lithium ion cell will fluctuate during operation. This is going to range from 4.2 Volts down to 3.7 Volts. Across this range, each component will continue to be supplied the necessary voltage and current to operate normally. The reason specialized integrated circuits are used is because as the source voltage changes and as the current drawn from each component changes, the output voltages need to stay constant.

From the datasheet for each component, we learn how to connect and configure each regulator. From the datasheet for the TPS62233DRY, we learn that the TPS62233DRY can output up to 500 mA and that the efficiency will vary depending on the current draw. Efficiency is also affected by the input voltage, output voltage and inductor/capacitor values.

The voltage regulation is accomplished with pulse width regulation in a switching circuit at 3 MHz. 4 ICs we will be using are the TPS62231DRY, the TLV71328PDBV, the TPS62233DRY and the TPS799195. The TPS62231DRY was selected to provide 82 mA at 1.8 Volts which is required for the AR0130 CMOS sensor. The TLV71328PDBV was selected to provide the 40 mA at 2.8 Volts for the AR0130 sensor. The TPS62233DRY was selected to provide 160 mA at 3.0 Volts which is required for our MZH8340550D-AL01A laser diode. The TPS799195 was selected to provide 30 mA for the STM32F407VET ARM processor as well as 16 mA for our RN4020 Bluetooth module, each at 1.95 Volts.

To protect the Samsung INR18650-25R single cell lithium ion battery during charging, we are using the AP5056 battery charger. This integrated circuit has the function of safely limiting the charge which can flow to the battery during charging. It will also limit the voltage placed on the battery to 4.2 Volts for safety and longevity of the component. The charge rate is programmable using a resistor on pin 2. From the data sheet we have decided to use a 1 k Ω resistor for a charging rate of 1 Amp since this is a safe charging rate for our lithium cell.

The battery charger has an optional input for a temperature sensor which disconnects the battery any time the temperature exceeds the safe operating limit for the lithium ion cell. The lithium ion cell acts as the input voltage for each of the 4 voltage regulation circuits. Our ARM processor and Bluetooth module share a voltage regulator because they are able to operate at the same voltage and the supply can provide enough current for both.

The charging circuit includes indicator LEDs for the purpose of indicating charge state. The integrated circuit is programmable in the sense that the charging current can be specified by setting a resistor value Figure 25. Shows the implementation of these devices to provide power to each load in the CFS. Figures 37-41 comprise the complete power schematic for our device.

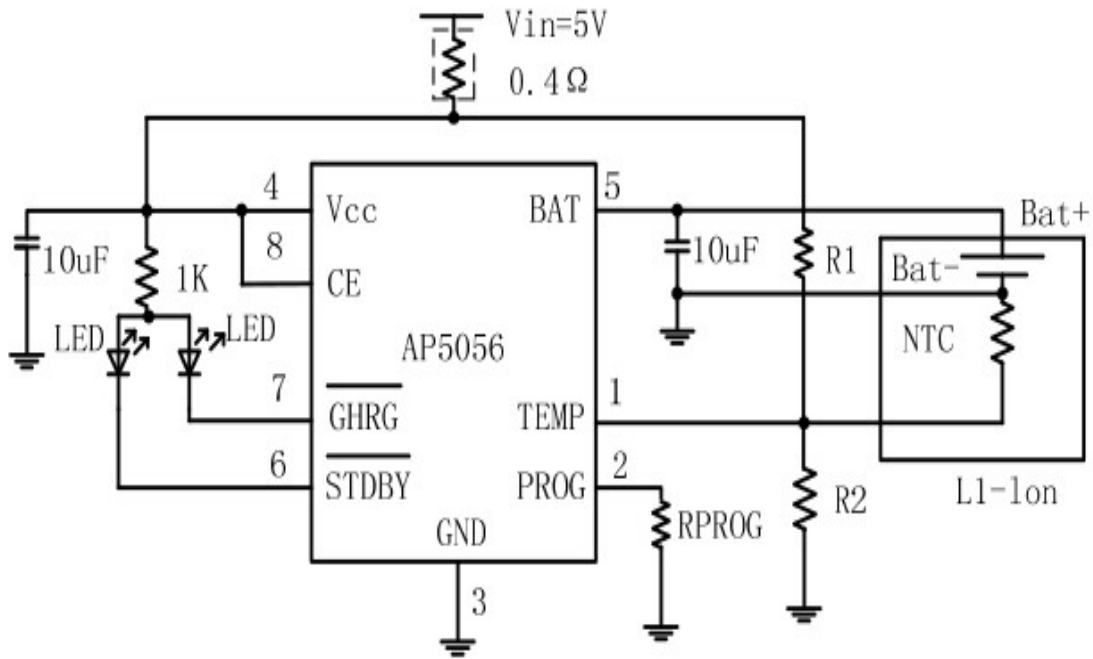


Figure 25. Battery Charging Management Circuit

Made by Luke Preston using AP5056 Datasheet.

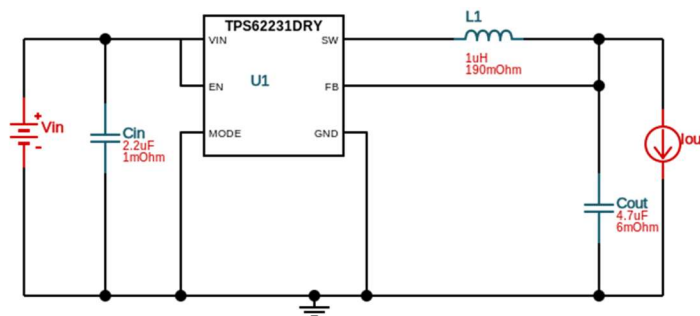


Figure 26. CMOS sensor 1.8 Volt supply

Made by Luke Preston using TI WeBench.

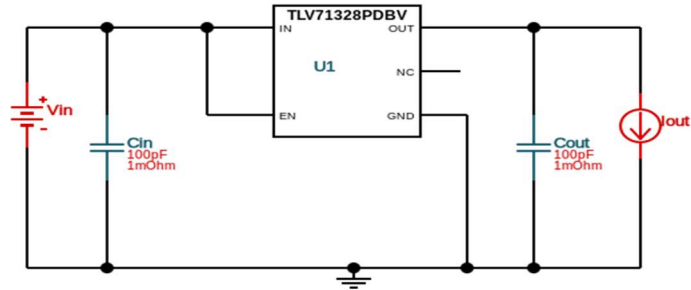


Figure 27. CMOS sensor 2.8 Volt supply
Made by Luke Preston using TI WeBench.

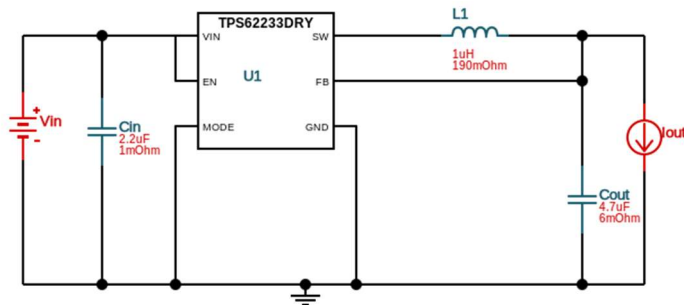


Figure 28. Laser Diode 3.0 Volt Supply
Made by Luke Preston using TI WeBench.

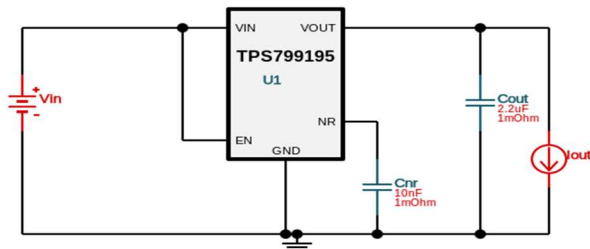


Figure 29. ARM M-Processor and Bluetooth module power supply
Made by Luke Preston using TI WeBench.

The first step in building a PCB is to design a schematic for the device. We have chosen to use Eeschema for this purpose. Below we have integrated each component to one circuit diagram for our design, removing the features which we will not need. An example of a feature which was not needed was the temperature sensor for the lithium ion cell. Because our current draw is going to be so small, the additional circuit for monitoring the temperature is not necessary and was removed.

An important consideration for components with high frequency switching is the impedance. Because transient voltages in a high frequency switching circuit will deviate from their desired values and because the length between PCB traces are sometimes large, using capacitors near the voltage inputs for some of the inputs is necessary in order to isolate the inputs. It is important that the effective series resistance be small on these isolating capacitors in order for them to be effective. The placement of these capacitors is

also important. The closer they are to the input they are buffering the better. When designing the printed circuit board this will be an important consideration. The capacitors may need to be placed on the other side of the PCB to get as close as possible, to minimize the inductance due to the PCB traces.

Figure 41 shows the complete schematic for the Fluorescence spectrometer. The largest component in the circuit is the stm32f407ve processor. This integrated circuit will be located in the center of the board to reduce total trace distance because it has the largest number of connections. There are four integrated circuits dedicated to voltage regulation and one integrated circuit that facilitates charging the lithium ion cell.

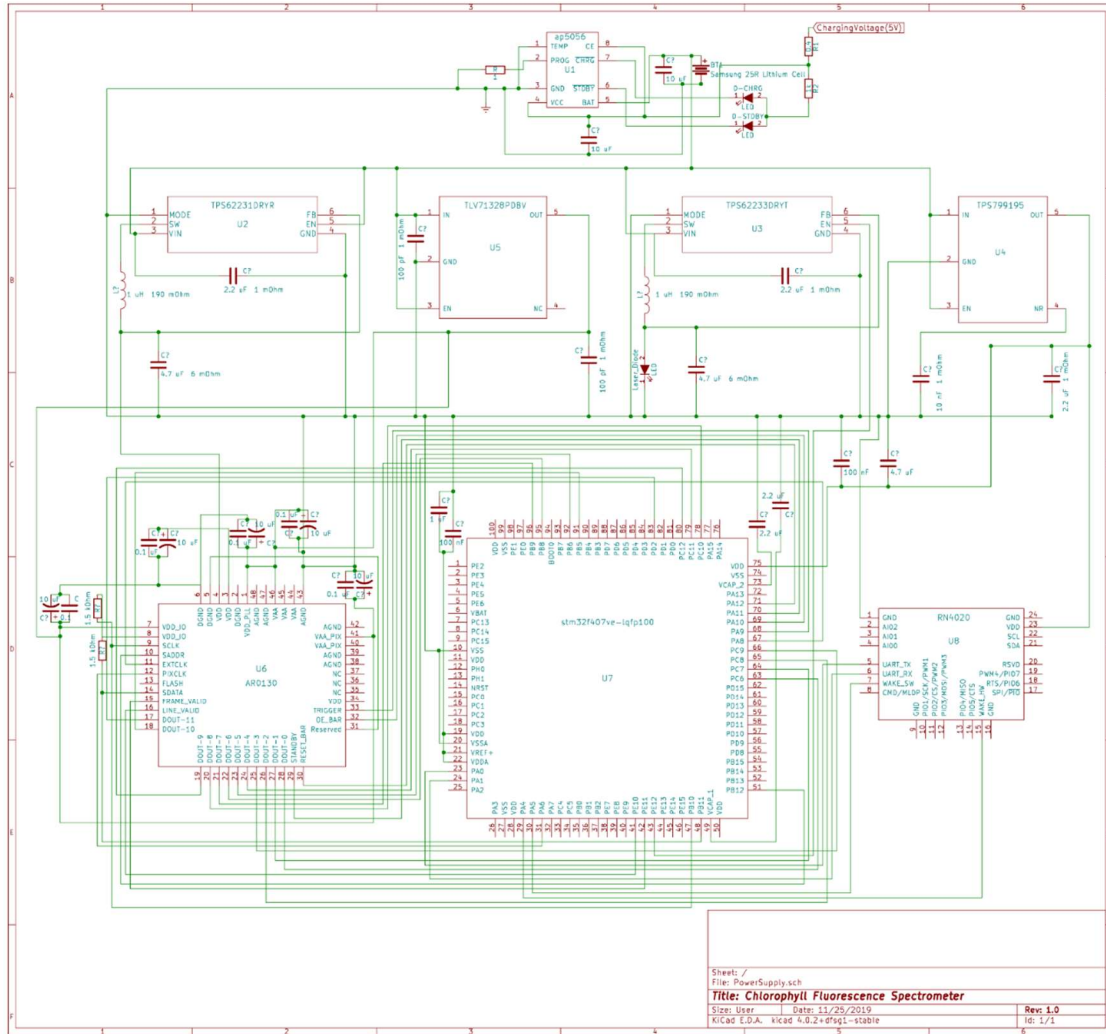
The charging input will be implemented using a MicroUSB connector supplying 5 Volts to the input of the AP5056. The trigger for activating the laser will be controlled by the GPIO pin PE12 which is pin 43 on the LQFP100 package. This is connected to the enable pin of the TPS62233DRY voltage regulator. An earlier concept for this design would have used a MOSFET transistor to control the activation of the MZH8340550D-AL01A 405 mm laser diode. We realized that this complicated the design unnecessarily and would introduce losses as well as power wasted as heat dissipation.

The light source is a two-pin device, only passing power. However, it has its own dedicated voltage regulator and the regulator has an enable pin. The slew rate for our voltage regulator is high enough that the latency is negligible. Our laser will be powered on for one or more seconds to take measurements from our CMOS sensor. The data connections required to connect our processor with the Bluetooth module are shown in **Error! Reference source not found..** Two additional pins will provide power from our voltage regulator at 1.95 Volts and a connection to ground.

Our CMOS sensor interfaces with the ARM processor via a 12-bit parallel connection. In order to control the device, other connections are necessary including the master clock input, pixel clock output, and trigger input. The CMOS sensor requires 5 power connections, with a separate ground for analog and digital connections as a result of the high frequency switching of the component.

Table 22. Bluetooth Module IO Connectors

Description	Bluetooth Module Pin Number	Microcontroller Pin Name	Pin Number (LQFP100)
Generic GPIO (Wake HW)	15	PA4	29
Generic GPIO (Wake SW)	7	PA5	30
UART4_TX	5	PA0	23
UART4_RX	6	PA1	24



Made by Luke Preston using Eeschema

There are two pins to the CPU which will be used for programming the device, SWDIO and SWCLK which are pins 72 and 76 respectively. Another two pins are required for debugging, USART2_TX and USART2_RX which are pins 25 and 26 respectively. These will be implemented on the PCB using 4 pinouts, labelled with the silkscreen.

Figure 30. Circuit schematic for the CFS

The AR0130 requires voltages at 2.8 and 1.8 volts and each supply connection needs to be decoupled using two capacitors in parallel. The maximum allowable effective series resistance for these capacitors in parallel is $2\ \Omega$ as per the AR0130 datasheet. The capacitors should be $0.1\ \mu\text{F}$ and $10\ \mu\text{F}$ in parallel and placed as physically close to the contact on the processor as possible to minimize inductances in the trace and provide a true voltage value. The data and control connections required to connect our processor with the CMOS Sensor module are shown in Table 23.

Using this electronic schematic, the printed circuit will be developed during winter break and refined in the first week or two of senior design two. The plan for our group is to design the printed circuit board using our schematic, laying out the physical location and footprint of each component and connection, and then send the designs to an external supplier who will fabricate the boards for us. We will be ordering two or three boards as an assurance in case we have a manufacturing defect and need to start over. The cost of the board is an important factor, but not nearly as important as the time it would take for us to order and receive another part.

We will be populating the boards ourselves using 0805 components when possible. The reason for this selection is that 0805 components are very easy to solder by hand and will not result in soldering defects. The circuit board will be a two layer design, which allows our circuit board to be more compact than it would be if we only placed components on one side of the board. Limiting our design to two layers simplifies design and fabrication, keeping the cost of the CFS low. As discussed in the research portion of this document, we will be using KiCad Pcbnew and PCB footprint editor to complete the design of our printed circuit board. KiCad has the ability to export a design as a series of GERBER files, an industry standard which we can send to our board manufacturer.

These GERBER files will instruct the board manufacturer on how the board is to be constructed, including the necessary information about all contacts, connections, vias, and traces. Two files will be used to describe the copper top and bottom, which map out the topology of all the conductor traces and solder contacts on the printed circuit board. Another two files will be used to specify the top and bottom solder mask, which is a nonconductive polymer layer used to prevent short circuits. The solder mask is usually green but can be any other color as well.

Additionally, two files will be used to communicate the top and bottom silkscreen. The silkscreen is the layer which is used to label and mark the printed circuit board. Reference designators are applied to components and a logo may also be added. The silkscreen is generally white ink, but other colors are possible. Finally, one GERBER file will be used for the drill legend. Drilled holes are used for mounting the board rigidly to the housing of the device as well as placing electrical connections from one layer of the board to another, which are called a vias. Drilled holes are expensive and vias do not provide as good an electrical connection as a copper trace, so the use of drilled holes on our printed circuit board should be minimized.

Table 23. CMOS Sensor IO Connections

Description	CMOS Sensor Pin Number	Microcontroller Pin Name	Pin Number (LQFP100)
Master Clock (MC01)	11	PA8	67
I2C_SDA	14	PB11	48
I2C_SCL	9	PB10	47

Generic GPIO (SADDR)	10	PB12	51
Generic GPIO (TRIGGER)	33	PA9	68
Generic GPIO (OE BAR)	32	PA10	69
Generic GPIO (STANDBY)	29	PA11	70
Generic GPIO (RESET BAR)	30	PA12	71
Generic GPIO (LINE VALID)	16	PE10	41
Generic GPIO (FRAME VALID)	15	PE11	42
DCMI_D0	28	PC6	63
DCMI_D1	27	PC7	64
DCMI_D2	26	PC8	65
DCMI_D3	25	PC9	66
DCMI_D4	24	PC11	79
DCMI_D5	23	PB6	92
DCMI_D6	22	PB8	95
DCMI_D7	21	PB9	96
DCMI_D8	20	PC10	78
DCMI_D9	19	PC12	80
DCMI_D10	18	PB5	91
DCMI_D11	17	PD2	83
DCMI_PIXCLK	12	PA6	31

The printed circuit board implements our circuit schematic across two separate PCBs connected by a 26 pin ribbon cable connector. The boards are ordered as a single unit joined by a perforated edge. You can see the PCB design below in Figure 31. This configuration allowed us to keep the cost for the boards down. The main PCB integrates the microcontroller, Bluetooth module, laser module power supply, battery charging circuit, the lithium battery cell, the debugging and programming pins, power on switch and reset button. The smaller PCB integrates only the AR0130 CMOS sensor and the corresponding voltage regulation circuitry. The CMOS sensor PCB also has all surface mount components besides the sensor itself on the same side of the PCB. This was done to allow the board to be mounted flush to wall of the CFS.

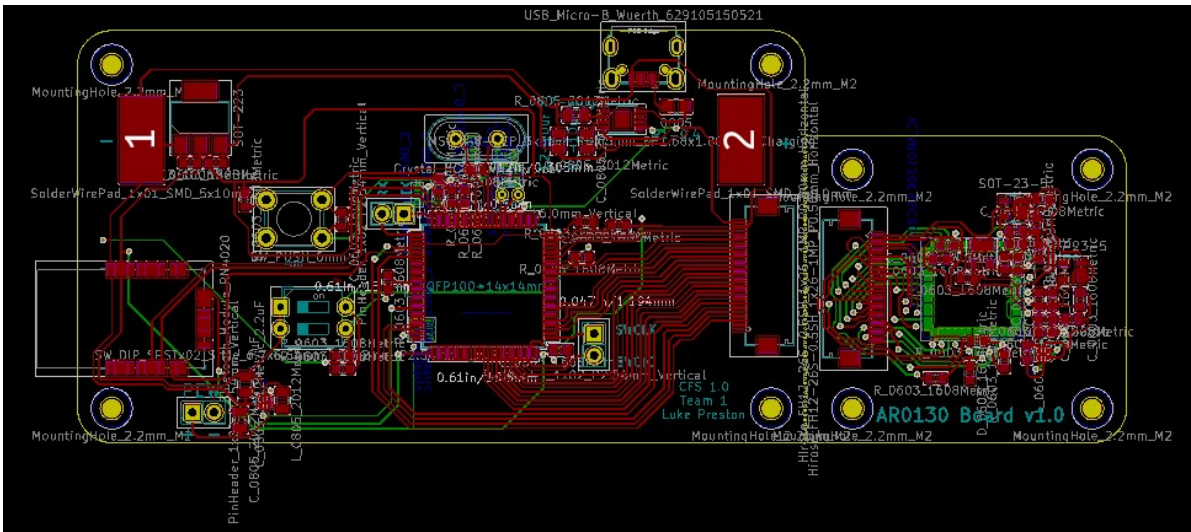


Figure 31. PCB Schematic

5.1.4 Laser Housing Design

The laser housing in our device contains the elements which allow our chlorophyll to fluoresce and emit light at the desired range of wavelengths. This includes the laser module, a quartz cuvette, and an optical slit. The housing was planned to be manufactured so it could hold the laser and cuvette in place while allowing enough light to pass through the slit and into the main optical housing. A layout of the laser housing and its dimensions can be seen in Figure 32.

5.1.5 Housing Design

The completed housing design is shown in Figure 33. There were several options available for building the housing unit for the chlorophyll fluorescence spectrometer, such as metal, plastics, and wood. A light metal like aluminum or variants tempered with other metals is ideal in most cases, but since the CFS has wireless capabilities, building the casing out of metal was not advisable. Wood has a significant chance of damaging the sensitive optics as it will splinter and rot over time. For these reasons, black acrylic was chosen as the material for the device. Special care was taken to not have light leak through from the outside of the enclosure and interfere with the optical instruments. The casing was planned to be totally sealed on all sides. There are four internal walls to isolate the pump source, the fluorescing sample, and the spectroscopy instruments from stray light; see the black outlines in Figure 33.

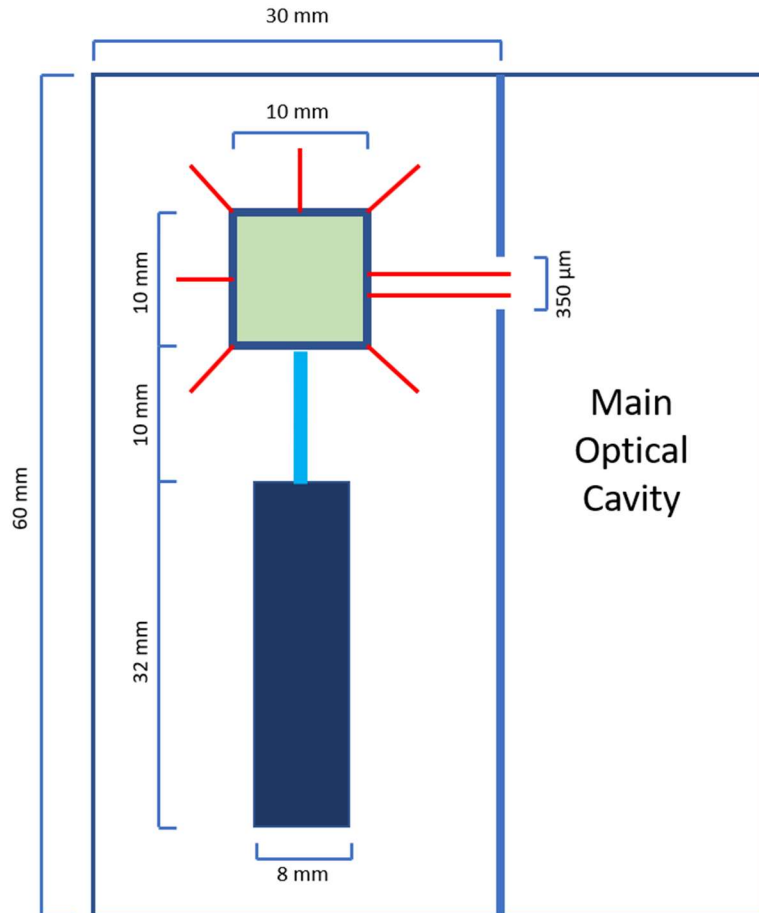


Figure 32. Dimensions of pump housing
Made by Robert Bernson.

It was critically important, as discussed in 5.1.2 Optical Loss Calculations, that the sensor could read as much light as possible strictly from the fluorescence of the sample while excluding all other background noise. Thus, firstly, the sample and light source were enclosed in their own section to ensure no extra light is scattered into the entrance slit. The chlorophyll samples were excited only by the laser pump and the maximum amount of light left the sample and reached the slit. Eliminating all background noise at the source prevented noise from propagating through the spectroscopic system and ruining signal at the sensor. The material used in this case design was black acrylic.

Secondly, the spectroscopy section was enclosed in its own walls with the dimensions shown in Figure 33. This was the most sensitive part of the CFS and was designed to be “light-tight”, preventing stray light from entering the spectroscopy housing and interfering with the signal. The material used for this housing was black acrylic. The optical components are held in place using parts custom-machined from black acrylic.

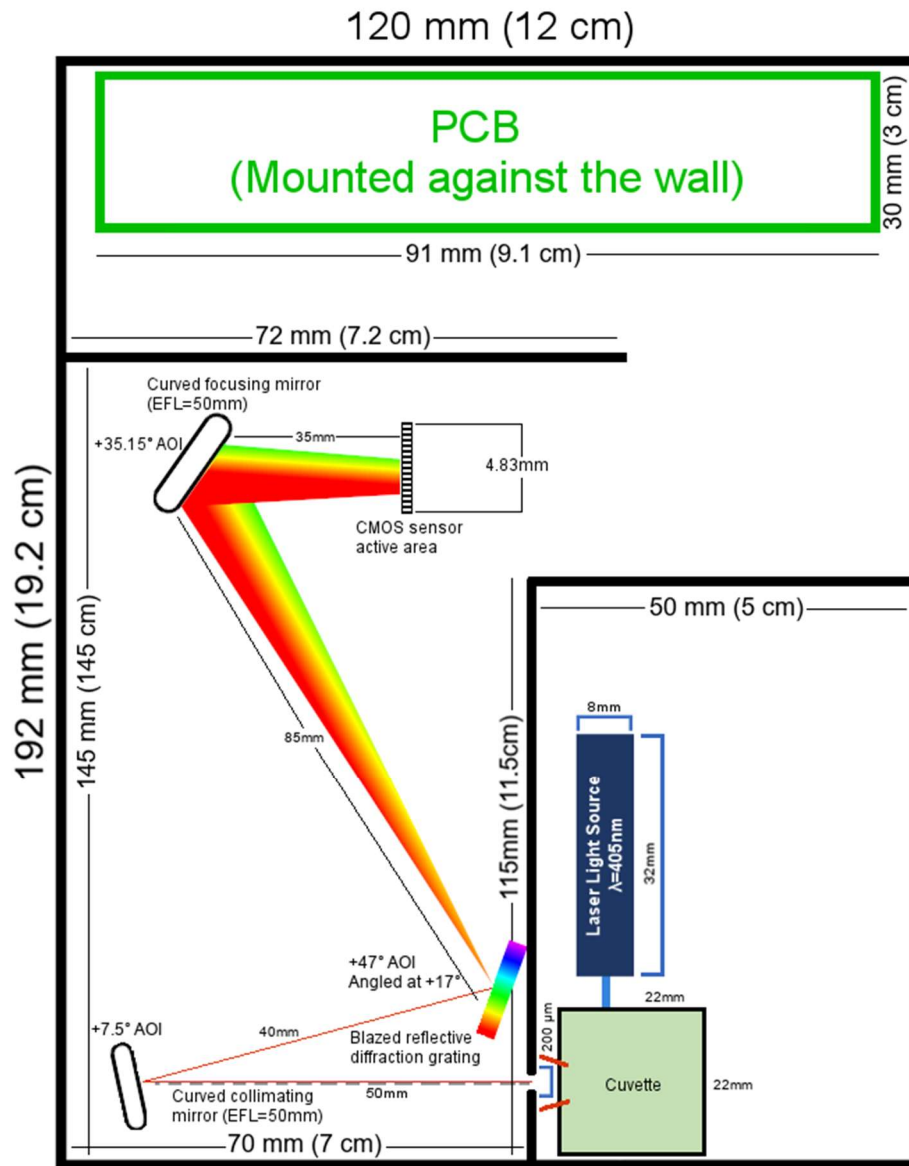


Figure 33. Complete housing design with dimensions, angles, and labels

Made by Samuel Knight

Thirdly, the CFS itself was designed to be housed in a case that allowed the device to be easily transported, stored, and used in stable areas. The case had the dimensions shown in Figure 33 and was made entirely from black acrylic. The reason this material was chosen over metal is due to metal's electromagnetic properties. While plastics in general have a lower elastic modulus, impact strength, and tensile strength than metals, they have a much lower electric interference. It was important that the optics and electronics interact with the mobile phone for the user to receive information. Metals would cause a Faraday Cage effect and ground all wireless signals trying to enter or leave the device.

A brief discussion can be had about how the housing design meets the engineering requirement specifications, specifically the dimension requirement of being volumetrically less than 4000 cm³. With the length and width given in Figure 33, the area of the device is 0.0230m². In order to reach the volumetric requirement, the device will have to be shorter than 17.4 centimeters, a goal which was easily achieved during building. The housing design above satisfied the dimensions requirement. The successes and failures of the housing design are discussed in more detail in 6.8 .

5.2 Software Design

In the following subsections we will present the details of our software design process and final overall software design. The software design for this product was extremely important, due to the fact that we plan for our software is one of the features that makes our CFS stand out among other similar products. The software in our product empowers the user to effortlessly receive the results of the measurements on their mobile device and allow them to view the results of the analysis in multiple different easy to understand views.

To increase the efficiency of our software design, we divided our design process into two separate design processes: Embedded software design and Mobile software design. This separation was caused by the large differences between the two pieces of software, which we are treating as two separate programs; these differences include different programming languages, runtime environments, and constraints. We will go into more detail about each of these software design processes in the following sections.

In Figure 34 on the next page you can see overall use-case diagram for our CFS. This diagram shows at a high-level how users can interact with the CFS software, and how the embedded and mobile programs will interact with each other. Use case diagrams are a form of UML diagram which overview the usage requirements for the system at a high level. In the diagram you will see the different actors and systems that are at play throughout the use of our app, as well as the sequences of actions that are possible while using the CFS software.

5.2.1 Embedded Software Design

The embedded software design for this project consists of the software design for the firmware that will be running on the CFS measurement device. The firmware we developed is executed on the Cortex-M4 32-bit microcontroller, which uses the ARM architecture. Because the software is running on an ARM CPU, we decided to use the C programming language for the development of this software. The C programming language was chosen because it is lightweight and will allow us to manage our memory use, which will be required due to the low amount of memory available to us on the microcontroller. It has also been chosen because there are many compilers that will compile C code into ARM machine code. The development was done using the System Workbench for STM32 integrated development environment (IDE).

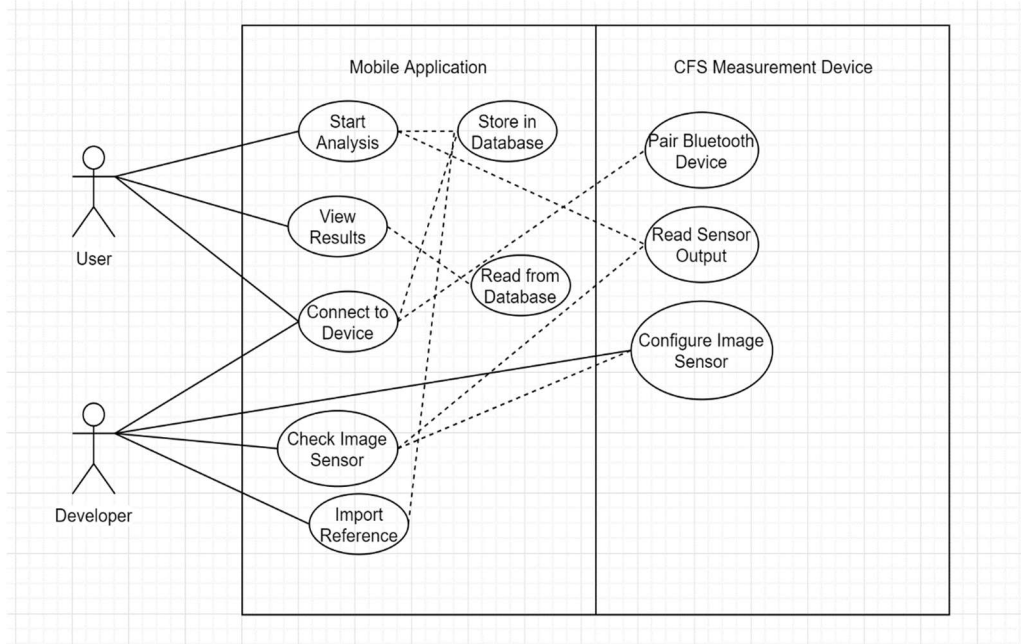


Figure 34. Use Case Diagram

5.2.1 Embedded Software Design

The embedded software design for this project consists of the software design for the firmware that will be running on the CFS measurement device. The firmware we developed is executed on the Cortex-M4 32-bit microcontroller, which uses the ARM architecture. Because the software is running on an ARM CPU, we decided to use the C programming language for the development of this software. The C programming language was chosen because it is lightweight and will allow us to manage our memory use, which will be required due to the low amount of memory available to us on the microcontroller. It has also been chosen because there are many compilers that will compile C code into ARM machine code. The development was done using the System Workbench for STM32 integrated development environment (IDE).

The firmware controls the coordinating communication between the sensors on the physical device and ensuring that the sensor data during analysis is sent to the mobile application for further processing and visualization. The main sensors that our software interacts with on the device is the image sensor, which captures the light from the fluorescence of the chlorophyll, and the Bluetooth module, which sends the sensor data to the mobile application. The firmware is also tasked with properly configuring the sensor modules before analysis. More information about the processes that will be used to control the sensors can be found in the following sections.

5.2.1.1 Block Diagram

In Figure 35, you will find a high-level diagram which illustrates the overall design of the embedded portion of our software design. This control flow diagram shows the main control-flow and logic for our program.

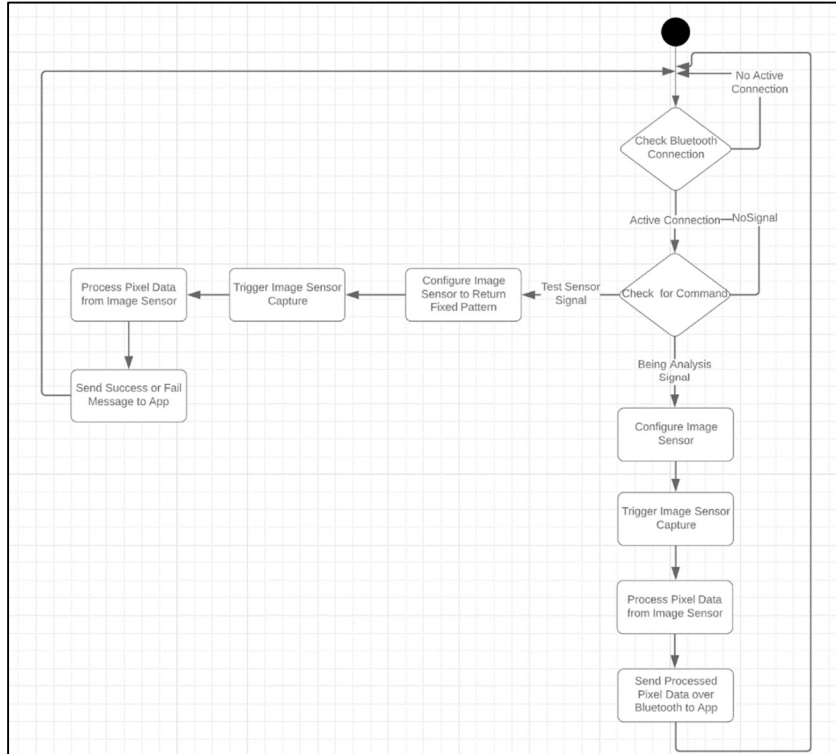


Figure 35. Embedded Software Block Diagram

5.2.1.2 Image Sensor Interaction

The image sensor is the most important module in the CFS measurement device. This sensor measures the amount of light hitting each individual pixel on the sensor, and reports that data to the Microcontroller. We are using this sensor in capture mode instead of video mode, which made the development process easier. Interaction with the image sensor was achieved via 2 separate digital connections.

To configure the image sensor, we used an I2C connection which allowed us to choose an arbitrary register on the module to write to, and then write our data into that register. By writing specific data into the correct registers, we were able to configure every aspect of the image sensor to ensure that we are properly capturing the information we need. To achieve this, we used a pre-written I2C library to facilitate the core I2C functionality, and then wrote code using that library to send the correct values to the necessary registers to configure the device. The generation of the register contents was done using bitwise operations in the C programming language.

Unlike the sensor configuration, the pixel data is not transmitted over an I2C connection. The sensor sends the raw pixel data over a parallel data connection line, which we connected to the microcontroller. Because the image sensor only sends one pixel at a time over the parallel line, and because the data is sent as raw pixel data, we needed to write our own algorithm to read and process the data. This algorithm consists of a large loop that repeatedly reads the incoming pixel data and stores it for later processing, continuing until it has read the pixel data for all pixels in the image sensor.

Because we have a limited amount of RAM memory, we are not able to store all pixels in memory at the same time; to get around this, we decided that we only needed to store the accumulation of all pixels in each column instead of the individual value of each pixel. This means that in our algorithm, once a pixel comes in the value of that pixel will be added to the current value of the addition of all of the pixels with that same X-axis, which are stored in an array. With this method, we will only need to store one array with an integer for each column, which is much less than storing an integer for each pixel. Once all pixels have been iterated over, we then send this data over Bluetooth to the mobile application for further processing.

One challenge we experienced when developing the embedded software was synchronizing the parallel data transfer between the sensor and the microcontroller. The Image sensor utilizes multiple synchronization signals to signify when valid pixels are being transmitted. One constraint when ensuring proper synchronization is that our main clock and pixel clock will need to be completely out of phase with each other, so that we may capture the value of the pixels from the parallel line during the rising edge of the pixel clock, which will be synchronized with the falling edge of the main clock. A more detailed timing diagram of the IO timing can be found in Figure 36. The first synchronization signal provided by the image sensor is a pixel clock, which is generated based on an external clock that is provided to the sensor from the microcontroller. The pixel clock is used to keep track of the timing used to output pixels. The other signals provided by the sensor is the LINE_VALID and FRAME_VALID signals. When both signals are high, then the pixels being outputted are valid. Invalid pixels are used for horizontal and vertical data padding. When doing our initial development, we attempted to handle the data transfer synchronization ourselves in software using general purpose GPIO pins and signal interrupts; we were unsuccessful with this strategy and later found that our microcontroller had specific pins capable of taking in DCMI synchronization signals to receive pixel data from an image sensor.

In order to take advantage of the microcontroller's built-in DCMI support, the data transfer had to be performed through the Direct Memory Access module. Because of this, the pixels were no longer received as a stream, but as a block of data that is moved into an array by the DMA module. Because of this, all of the data from a capture had to fit into memory at once. To get around this issue, we used the VSTART and VSTOP registers to capture 10 rows of pixels at a time into memory, add the pixel values into the accumulation array, and then initiate the next capture of 10 rows. This process was repeated 12 times so that we could capture all 1280 rows in our accumulation array.

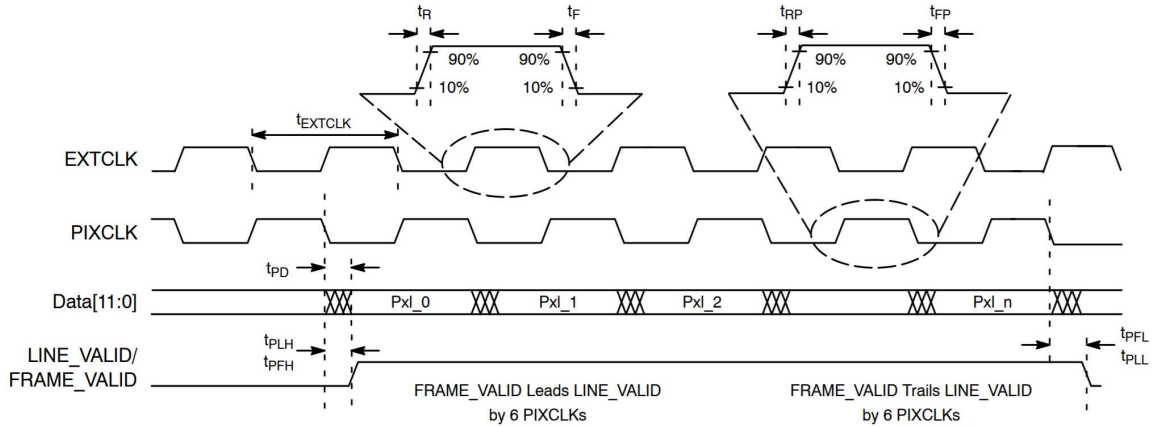


Figure 36. Timing Diagram for Reading Pixel Data

Used with permission from SCILLC dba ON Semiconductor. [ONS.ARO130].

5.2.1.3 Bluetooth Sensor Interaction

The Bluetooth module we are using on the CFS measurement device is the RN4020 RF module. This module is controlled via ASCII commands over a UART connection. To interface with the module, we used a pre-written UART library and built our own RN4020 library. The RN4020 library abstracts away the communication of the device using the UART library and allows us to use high-level functions such as “writeData” and “readData”, which maximizes code reuse and reliability. The functions that we had to write were not too complex, as we are only be using the basic features of the Bluetooth module. Our software is in charge of accepting connections, keeping track of the connection state, receiving signals, and sending data.

The signals that we receive on the Bluetooth module are put into a C programming language switch statement to decide what function corresponds with that incoming signal, and what action to take. Once this has been decided, the action will be taken, and the result will be sent to the requesting device over Bluetooth; this data transmission is also handled by the embedded software. Throughout our software design, we also worked to maximize the amount of time that the device spends in sleep mode, to capitalize on the low power capabilities of the Bluetooth module we are using. To configure sleeps and wakes, we are using UART interrupts to sense when data needs to be transmitted or received.

To be able to transfer all of our data between the mobile application and the embedded software via Bluetooth Low Energy, we created a custom Generic Attribute Profile (GATT) service on the Bluetooth Low Energy module. This GATT service is created with a specific unique identifier, so that the mobile application can differentiate the CFS service from other built-in services the Bluetooth module may offer. Within the custom CFS service, we have defined two custom GATT characteristics. One characteristic is used by the embedded software to send data to the application, and the other channel is used for commands and responses to be sent between the mobile application and the embedded software.

The data channel is configured to be read-only, with notifications on; this makes it so that only the embedded software can write values to the data characteristic, which is used to transfer the analysis results back to the mobile application once the application requests that an analysis be executed. The data channel also utilizes the “notify” feature of Bluetooth Low Energy, which makes it so that the Bluetooth sensor will notify the mobile application whenever new data is written to the characteristic by the embedded software; this is important because it removes the need for polling when receiving data, which wastes cycles and power. The command channel is configured to allow read and writes, since this characteristic is used as a bi-directional channel for the application and embedded software to use to send commands back and forth. Specifically, this characteristic can be used by the application to request a new analysis and can be used by the embedded software to notify the application of the current status of an ongoing analysis.

5.2.2 Mobile Application Software Design

The CFS’ Mobile Application serves as the main user interface for the device. This software consists of a mobile application which configures the CFS to prepare it for sample analysis, as well as initiates any analyses and receives the sensor data resulting from that analysis. The mobile application is tasked with storing all analysis results and providing the end-user with the results in a multitude of graphics and result summaries which ensure that the results of the analysis are both simple enough for a layman to get value out of the results, but also detailed enough for expert analysis.

Throughout the initial design process for the mobile application, the team decided to limit the target operating system for the mobile application to Android. This choice was made due to Android being easier to develop for and test on, due to Apple having more restrictions on application development and publishing for iOS. More specifically, our mobile application requires Android API 21 or greater, due to the improved Bluetooth Low Energy support that was added in this API version. Android Studio was used as the interactive development environment to write and debug the code for the mobile application. A summary of technical design choices for the mobile application can be found in Table 24 below, and more detailed explanations of the software design can be found in the subsections that follow.

Table 24. Mobile Application Design Choice Summary

Design Choice	Final Selection
Supported Operating System(s)	Android
Earliest Supported Android API	API level 21
Local Database Technology	SQLite3
User Interface Framework	Java

5.2.2.1 Block Diagram

In Figure 37 below, you will find a high-level diagram which illustrates the overall design of the Mobile Application portion of our software design. This control flow diagram shows the main control-flow and logic for our program and is what we used as guidance when developing the software.

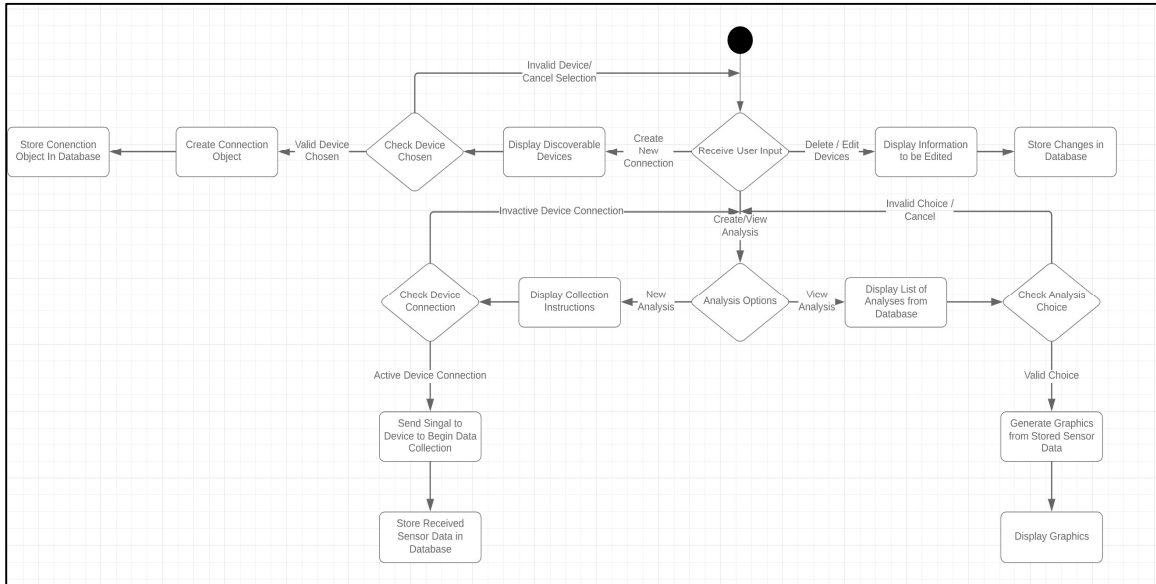


Figure 37. Mobile Application Block Diagram

5.2.2.2 Bluetooth Communication Design

Bluetooth Low Energy support was added to Android in Android version 4.3 (API level 18). This version of android included built-in platform support for BLE, providing APIs that developers can use to facilitate Bluetooth Low Energy communication as long as the phone has a Bluetooth module that supports BLE. The APIs provided by Google allow developers to easily discover devices, discover services, and transmit and receive information with other BLE devices in range of the mobile phone. In this section we will describe how our design leverages this API to allow for the transfer of sensor data between the embedded software and the mobile application.

Our mobile application requires the use of the “BLUETOOTH” and “BLUETOOTH_ADMIN” android permissions to ensure that it can both manage the Bluetooth connections on the device, including discovering and creating connections with new devices, and transmit and receive data. BLE devices can be defined as either central or peripheral devices; in this case the Mobile Application is defined as a central device, because it is tasked with scanning, while the measurement device is advertising. The Mobile Application is also a BLE “Client” device, because it will be receiving data from the measurement device, which acts as the “Server”.

Bluetooth Communication in the app is initiated by the user, who through the GUI can select an option telling the application that they want to pair their device with a nearby CFS device. During this stage the Mobile Application will search for devices that are advertising themselves with a certain device type defined in their metadata and will display these devices to the user so that they can choose which device they would like to pair with. Once a user chooses the CFS device they would like to pair with, the user will be prompted to input information about that CFS device. All the information about CFS devices and their connection status is stored in the local database.

After a successful Bluetooth connection is made, the mobile application allows the user to initiate a sample analysis, which will then send a message over the Bluetooth channel to the CFS device to begin measuring. Measurement data is sent from the CFS to the mobile application via a Bluetooth Low Energy “Generic Attribute Profile (GATT)” characteristic. The sensor data that is received via GATT messages is stored in the local database and associated with a collection time.

5.2.2.3 Local Database Design

The mobile application uses a database stored locally on the phone to store data related to the application. This database contains a structured set of data that allows the application to efficiently store and retrieve relevant information. The structured and relational properties of the database allow the application to not only store the data, but also store the relationships between different pieces of data and retrieve that data based on the relationships in an efficient way.

For our application, we have chosen SQLite3 as our database management system. We chose SQLite3 because it is lightweight and does not require an extra program to be running on the mobile device. SQLite databases are stored in a single file, so they are portable, meaning they will work on any mobile device as long as we are able to store files, and require a low amount of resource, which reduces overhead.

The SQLite database will mainly be used to store 2 types of data: CFS device data and analysis data. The CFS device information that is stored is information about the different CFS devices that the mobile application has connected to in the past, along with metadata about each device. The metadata that is stored includes a nickname for the CFS device, the embedded software version that the CFS device is running, the hardware ID for that device, and the last time that the Bluetooth connection with that device was alive. The analysis data includes the results that are read from the image sensor on the CFS device for a given analysis. The analysis data that stored includes both reference analyses and user-generated analyses. Reference data will be used to compare the health of the users’ plants to known healthy or unhealthy plants.

Because the data we are storing has three main types, we have decided to use 3 tables in our Database. There is one table for user analyses results, one for reference analyses, and one table for CFS device connections. Because we are using a relational database, the three

tables are related to each other using foreign keys where necessary. Our database design is detailed in the Entity Relationship Diagram in Figure 38.

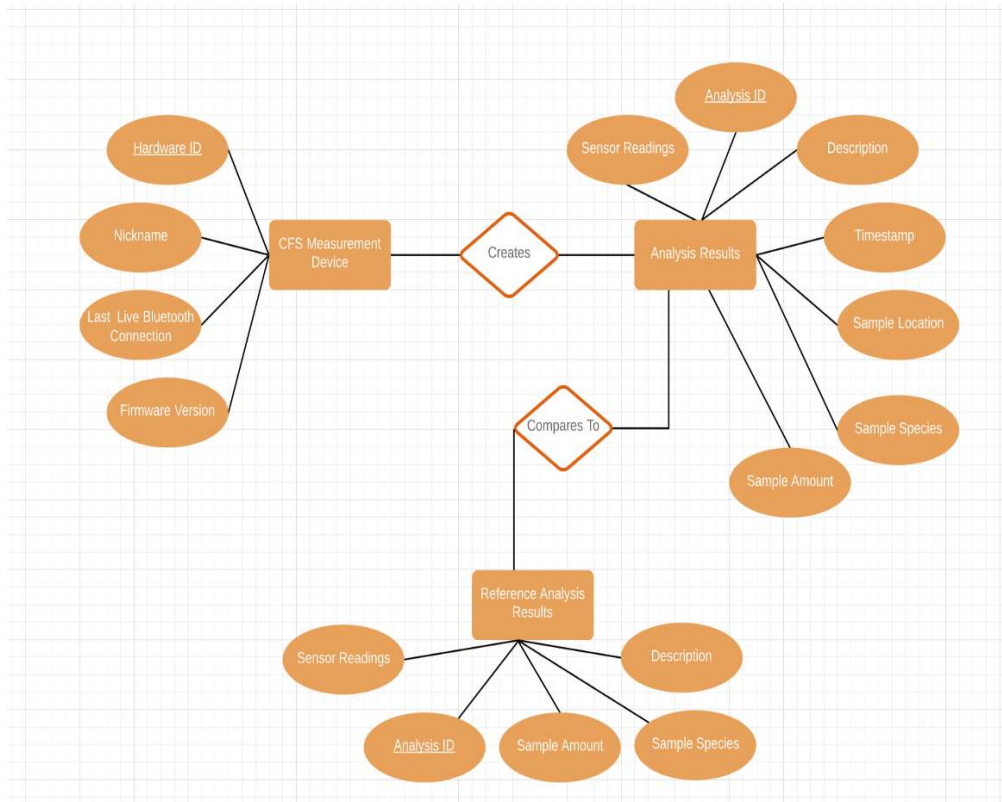


Figure 38. Entity Relationship Diagram for Application Database

5.2.2.4 Graphical User Interface Design

The majority of the software developed for the mobile application was be for the Graphical User Interface of the application. Because the mobile application will be the primary way for users to interface with the CFS device, we have put a lot of time into ensuring that the GUI for the application is well-designed and easy to use. We have chosen to use Android Studio for the overall development of the application, including the graphical user interface development.

When developing an android application, there are many user interface frameworks that are available. For the CFS mobile application, we chose to use the Java programming language and framework; this choice will make the development for the GUI portion of the application easier, because of our familiarity with Java over Kotlin.

When designing what the GUI for the application was going to look like, we followed the Android Material Design specification. This specification is a comprehensive guide from Google for designing visual, motion, and interaction aspects of an Android application. By closely following the Material Design best practices, we will ensure that our application looks and feels like other android applications; this increases the ease of use for the mobile application, as well as makes it look more appealing to our users.

A common issue that we have seen many other developers run into when designing a graphical user interface is that many people do the software development and visual development simultaneously, which can lead to conflicting design choices and may require a lot of re-development. For this reason, our GUI design process consisted of us sketching out all of the views and actions that will be necessary for our application before we began working on any of the software. In Figure 39. Initial GUI Design Sketch, you will find our initial sketches for the graphical user interface of the CFS mobile application.

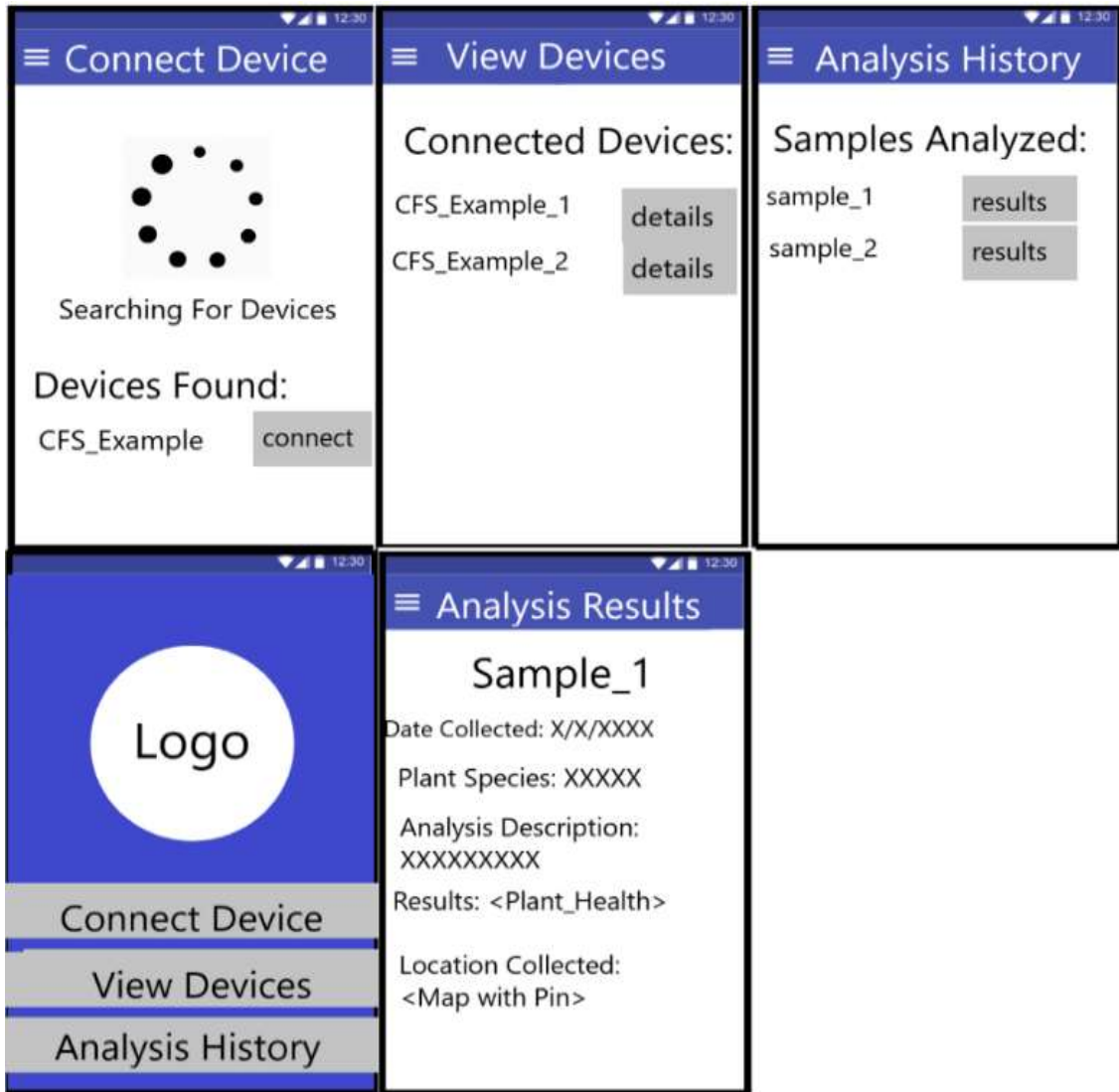


Figure 39. Initial GUI Design Sketch

Due to time constraints and a lack of experience with user interface design and development, our team had a difficult time developing the user interface throughout the development phase of the project. Although the final product did not implement all of the features that we had planned for, we were able to develop an intuitive user interface that allows the user to interact with the CFS measurement device. Screenshots of our final user interface can be seen in Figure 40 below. In this figure, you can see a user searching for devices, viewing analysis options, choosing a stored analysis to view, viewing analysis results, and comparing analysis results to a reference sample.

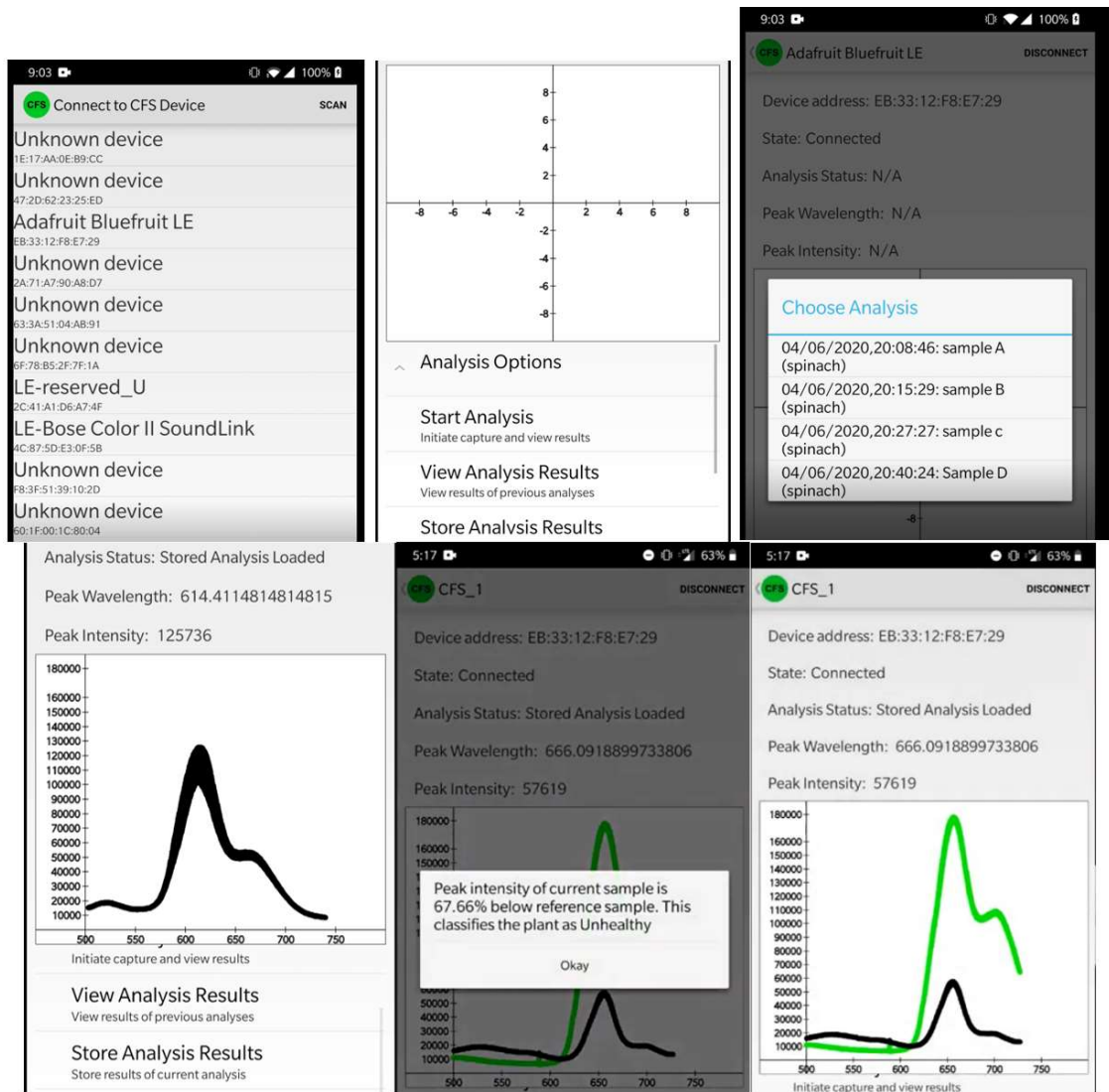


Figure 40. Final Graphical User Interface

5.3 Bill of Materials

Table 25 shows the bill of materials for the final hardware design. The bill of materials' Total Price column includes the price of shipping.

Table 25. Bill of materials

Component	Manufacturer	Description of Purpose	Quantity	Price per unit	Total Price
MZH8340550D-AL01A	Zhuhai MZLASER Technology Company LTD	Pump light source	2	\$9.00	\$40.38
Quartz cuvettes	Scientific Lab Solution	Chlorophyll sample container	2	--	\$20.00
CM254-025-P01	ThorLabs	Collimating/Focusing mirrors	2	\$60.34	\$120.68
33066FL01-270R	Newport Corporation	Reflective diffraction grating	1	\$89.00	\$89.00
ARDR CMOS Monochromatic Sensor	ON Semiconductor	Imaging sensor	4	\$8.38	\$34.68
OPT3002DNPT	Texas Instruments	Testing power sensor	20	-	\$23.23
PCB	Oshpark LLC	Component Integration	3	-	\$46.00
STM32F407VET	STMicroelectronics	CPU	2	\$4.41	\$8.82
STM32F407VET6	STMicroelectronics	Development Board	1	\$8.79	\$8.79
RN4020	Microchip	Bluetooth module	1	\$15.40	\$29.85
AP5056	Wuxi Chipown Microelectronics	Battery Charging	2	\$0.11	\$0.22
INR18650-25R	Samsung SDI Co.	Energy Storage	2	\$3.65	\$7.30
TPS62231DRY	Texas Instruments Inc.	Voltage Regulation	1	\$1.23	\$1.23
TLV71328PDBV	Texas Instruments Inc.	Power Supply	1	\$0.20	\$0.20
TPS62233DRY	Texas Instruments Inc.	Power Supply	1	\$1.32	\$1.32
TPS799195	Texas Instruments Inc.	Voltage Regulation	1	\$0.58	\$0.58
Total					\$432.28

5.4 Design Summary

The design of the chlorophyll fluorescence spectrometer required the interdisciplinary cooperation of computer, photonics, and electrical engineering. The constraints were largely defined by design decisions relating to the optics of the system. Decisions branched from the choice of sensor and light source, to the choice for processor and Bluetooth module based on the computing, data analysis and connectivity required. The methods for meeting our requirement specifications included some compromises, including the size and weight with battery life, processing power and power consumption. At every stage of the design process, cost was a factor. Communication was required between the designers in order to guarantee that each component of the CFS would function as required.

6. Building and Testing

This section describes the timeline of parts acquisition, the build phase, and the testing phase of all component parts researched in section 4. Project Research to complete section 5. Project Design. Included herein is the introduction to the testing phase, individual component testing, build stages, integration testing, and a discussion on the successes and failures incurred during these stages.

6.1 Introduction

One of the team's goals was to acquire and test all major parts before the end of Senior Design 1. Throughout this section, the part acquisition stage for our major parts can be seen as well as our testing procedures, progress, and results. Testing for our CFS was split into two main phases: the individual module testing phase and the integration stage.

The individual module testing phase was conducted to achieve the following goals for each module tested:

- Ensure the module is in functioning order
- Ensure that we know how to properly use the module
- Ensure that the module produces the expected data in a format that we know how to work with
- Ensure the module is compatible with our MCU
- Confirm power draw of module
- Find any issues with the module that were not found during the research phase of this project

After the individual modules were fully tested, we began the integration stage. This phase will be conducted to achieve the following goals:

- Ensure that all our components are compatible with each other
- Fully integrate all major components with our development board so that we can have a base circuit to build our schematic and PCB design from
- Test power delivery and power consumption
- Test accuracy of the optics design

6.2 Status Summary

As of 11/21/2019, we had received all major components needed for individual module testing and the integration stages. Our team completed the individual module testing stage of the project on 11/25/2019 and completed final integration testing on 04/06/2020.

6.3 Part Acquisition

The following table contains a timeline for the acquisition and testing of the major components of our project for the individual module testing phase.

Table 26. Part Acquisition Timeline

Part Name	Description	Date Ordered	Date Received	Testing Date
MZH8340550D-AL01A	Light Source	11/05/2019	11/15/2019	11/25/2019
33066FL01-270R	Reflective Diffraction Grating	11/07/2019	11/15/2019	11/24/2019
STM32F407VET6	Development Board	11/05/2019	11/10/2019	11/21/2019
ARDR CMOS Monochromatic Sensor	Imaging Sensor	11/05/2019	11/11/2019	11/25/2019
OPT3002DNPT	Ambient Light Sensor	11/05/2019	11/08/2019	--
RN4020	Bluetooth Module	11/07/2019	11/11/2019	11/21/2019

6.4 Hardware Component Testing

This section contains the testing procedures and results for the major components of the CFS. This section does not detail the efforts of any multidisciplinary collaborative efforts. This section is only for testing each individual component to ensure its operability as a standalone device. Once the component was tested and was proven to work, the component was marked as greenlit for the integration testing phase.

6.4.1 RN4020 – Bluetooth Module Testing

On 11/11/2019 our team received the RN4020 Bluetooth module and began planning out our testing procedures for this module. This section contains the testing procedures and the testing results for this module. A photo of the received module can be found in Figure 41.



Figure 41. RN4020 Bluetooth Module

The testing for this module consisted of two tests. The first test made sure that the module is functioning properly in general. The second test ensured that the module connected to our MCU. Before conducting any tests, we had to solder leads onto Bluetooth module so that it could be connected to other devices on a breadboard. For our first test, we wanted to ensure that the module was able to turn on, accept commands, and broadcast a signal properly.

To achieve this, we connected the device directly to a computer via a USB to UART adapter and configured the device using the device's UART command API. Using the UART command API we configured the device to be broadcasting using the name "RN4020_Test", and then used a mobile application on a phone to search for Bluetooth Low Energy devices that were broadcasting to see if we could see a device broadcasting with the proper name. This test was successful, as seen in Figure 42, which shows that the device is working properly and has the ability to broadcast a signal. An image of the device being tested on a breadboard can be found in Figure 42.

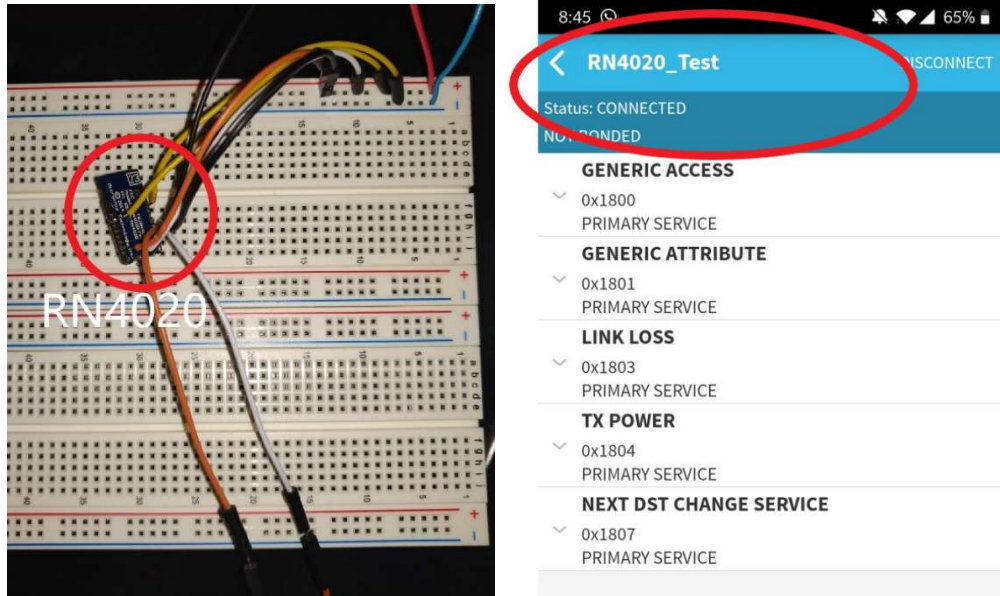


Figure 42. RN4020 Individual Module Testing

For our second test, we needed to make sure that the Bluetooth module could send and receive data from the MCU, as well as be configured automatically via the MCU. To achieve this, we used the STM32CubeMx and Keil IDE software to generate C code that would have the MCU automatically configure the Bluetooth module to broadcast a signal using the name "MCU_Conn_Test". When we initially tried to test this, we ran into an issue where the module would not start broadcasting a signal after the microcontroller was turned on.

After debugging we discovered that this was due to the MCU sending the configuration commands too early before the Bluetooth module was ready to accept commands. To fix this, we implemented a check in our code that waited to receive a signal from the Bluetooth module before sending the configuration commands. This also worked to test to see if the

MCU was properly receiving data from the Bluetooth module. After adding this check to the code, we used a mobile phone application to look for a Bluetooth Low Energy symbol with the proper name. This test was also successful, as seen in Figure 43, which shows that the device was able to send and receive commands to and from the MCU. An image of the device being tested on a breadboard can be found in Figure 43.

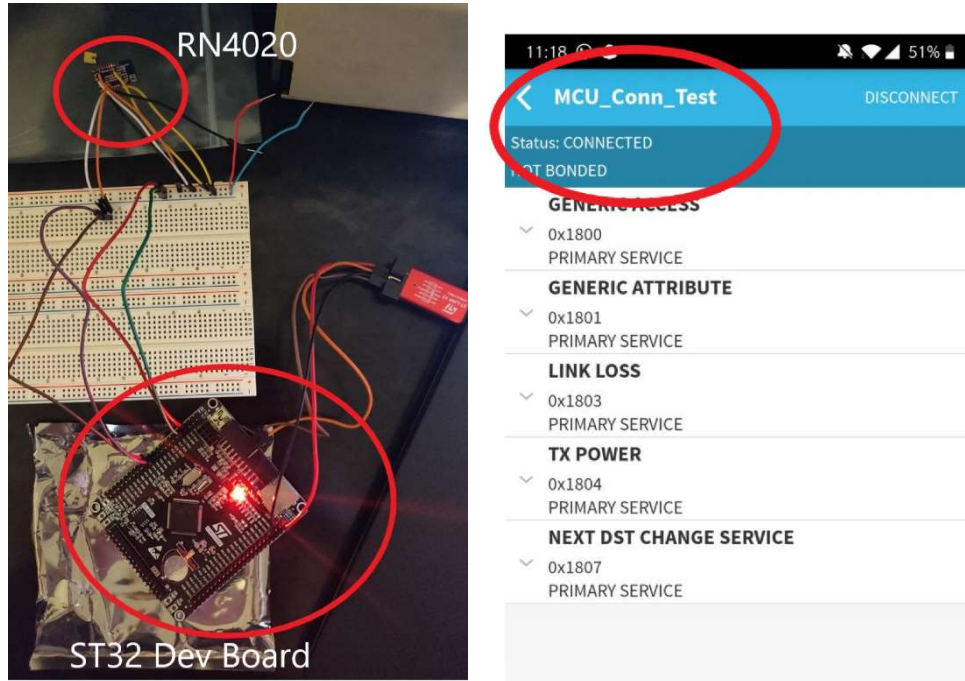


Figure 43. RN4020 Integration Testing

After completing these tests in full, we were able to confirm that the device is indeed working properly, that it can connect to our MCU, and that we can send and receive data between the MCU and the module. A summary of the results of these tests can be found in Table 27.

Table 27. RN4020 Testing Results

Test	Result
MCU Connectivity	Successful
Module Properly Functioning	Successful
Confirm Expected Data Output	Successful

6.4.2 AR0130CS – CMOS Monochromatic Sensor Testing

The AR0130CS CMOS monochromatic sensor (for short, the ARDR) was received on 11/11/2019. This section contains the testing procedures used for this module. A photo of the received module can be found in Figure 44.

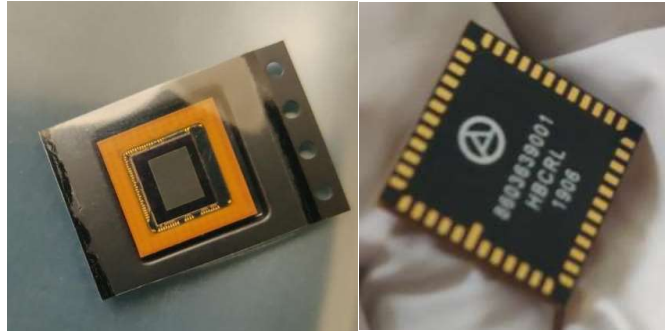


Figure 44. AR0130CS Monochromatic Sensor

The testing for this module consisted of one test to make sure that the module is functioning properly, that it will connect to our MCU, that we can properly write to the configuration registers to the module from our development board, and that we can properly parse the raw pixel data that the module is sending back to us. To test all of this, we soldered leads onto sensor module and connect it to our Development board using a breadboard. When doing breadboard testing of this module, we used a multichannel DC power supply to provide the different power inputs that the sensor needs. We also used .1uF and 10uF decoupling capacitors on each power source for the safety of the module. An image of the sensor connected to our MCU can be seen in Figure 45.

For the first half of the test, we made sure that the sensor can communicate with the MCU over I2C. The I2C channel is only used by the sensor for configuration purposes, and we used this to confirm that the sensor is properly functioning, that the sensor can connect to our MCU, that we are properly powering the sensor, and that our software can write to the configuration registers. This test was completed on 11/25/2019 and was successful.

After connecting the sensor to our MCU we were able to read an example configuration register and print the value to a debug console connected to the device via UART. After confirming that the configuration value read matched the default configuration for the device, we changed the configuration via the I2C connection and then read the register value again. After printing the configuration value to the debug console the second time, we confirmed that this value matched the new configuration value that we had written. The fact that these tests were successful shows that the sensor is working properly and can interact with our MCU and software.

During the previously described I2C configuration testing process, one of the solder joints on the sensor broke. This was an expected issue due to how small the pads on the sensor are, making soldering leads onto the sensor very hard. Due to the timing of this issue, it delayed our second stage of testing for this device, which was supposed to test not only the configuration of the device, but reading the pixel data from the device. After we re-soldered the lead onto the sensor, we planned to continue testing the device to see if we can properly get pixel data out of the sensor. To do this, we connected the MCU to the parallel data output bus of the image sensor and see if we can parse the pixel output from the sensor. To ensure that we are properly reading and receiving the raw pixel data, we configured the image sensor using the I2C connection to display a “test pattern”. When configured in this

manner, the sensor pixels will always return the configured pattern, which we can compare against the pixel data that we are receiving to ensure that we are reading the expected pattern. When conducting this second test, we found that the sensor was no longer functioning properly, and after using a multimeter and oscilloscope to test the sensor we determined that the leads that were soldered onto the sensor had caused a short and damaged the sensor. Because of the difficulty of soldering leads onto a surface mount part, we decided to not finish testing of this individual sensor, and conduct all testing for this sensor during our integration testing phase once the PCB arrived so that we could mount the sensor onto the PCB and connect it to the microcontroller that way. The results of all of our testing can be found in Table 28.

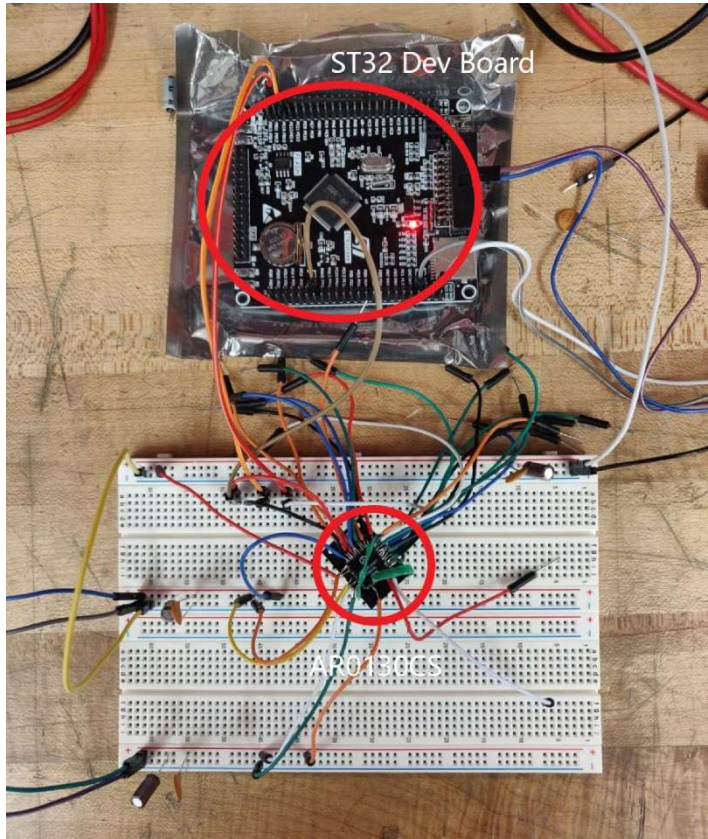


Figure 45. Monochromatic Sensor Configuration Testing
 Table 28. Monochromatic Sensor Testing Results

Test	Result
MCU Connectivity	Successful
Software Interaction	Successful
Module Properly Functioning	Successful
Confirm Expected Data Output	Successful

6.4.3 STM32F407VET6 – Development Board Testing

The STM32F407VET6 development board arrived on 11/10/2019 and planning for the testing procedures of this device has been completed. This section contains the testing procedures the testing results for this device. An image of the received development board can be found in Figure 46.



Figure 46. STM32 Development Board

The testing for this module consisted of one test that made sure that the board was functioning properly, that we could properly write software to the MCU using our integrated development environment, and that we could properly view the results of our software. To test all of this, we generated, compiled, and deployed C code using the STM32CubeMX and Keil IDE software. Once deployed to the development board, this code caused the board to send a string of data over a UART channel. Once the code has been deployed, we connected a computer to the UART channel to ensure that we can receive the string that the board was sending, which confirmed that the MCU was working properly, and that we can successfully write code to the MCU.

The testing for this module was completed on 11/21/2019. We had a few unexpected complications come up during our testing of this module, but after getting all complications ironed out, we were able to get a successful result from the test described in this section. The complications that were encountered mainly stemmed from the team's lack of experience with an STM development board; our team only had experience working with MSP430 development boards and we expected this board to function similarly to the MSP430 boards, which was not the case.

The first complication came when trying to flash our compiled code to the device. With other development board we had used in the past, it was possible to flash the board using a USB connection to the board, and due to the fact that the STM32 board we were using had a USB connection we expected it to be possible to use this USB connection to flash

the device. When we began testing, we realized that the USB connection could not be used for flashing the device, and we would need a separate “STM-LINK” device to be able to write code to the device, this process can be seen in Figure 47. This complication delayed our testing schedule due to having to wait for the STM-LINK device to arrive to be able to test all modules.

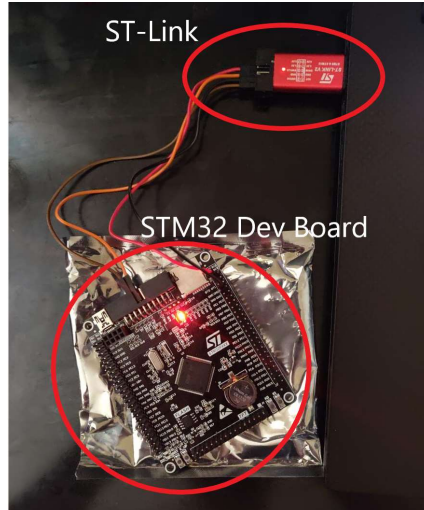


Figure 47. Flashing Development Board

The other complication we encountered was similar to the first; much like in the first complication, we expected to be able to use the USB connection on the board for our UART communication due to being able to do that with other boards we had used in the past. This was not the case, and we also needed to buy a separate USB to UART adapter to be able to receive UART signals from the board, further delaying the testing process. As soon as our UART and STM-LINK devices arrived we were able to conduct the test as described earlier. After we deployed the code to the device and connected the device to a computer via a USB to UART connection, we were able to receive the expected string and confirm that the device was working as expected. Figure 48 shows the development board connected to a laptop via a USB to UART adapter for the purposes of this test.

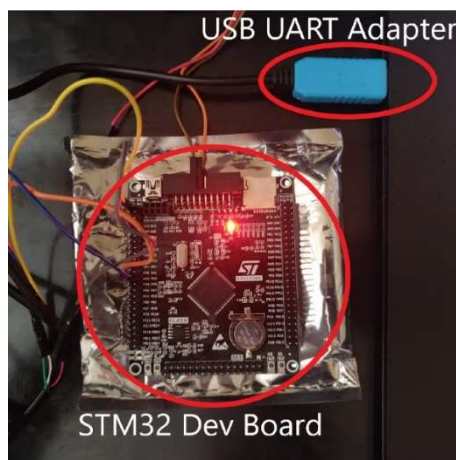


Figure 48. Testing Development Board

Table 29. Development Board Testing Results

Test	Result
IDE Connectivity	Successful
Software Deployment	Successful
Board Properly Functioning	Successful

6.4.4 Newport 33066FL01-270R Diffraction Grating Testing

The Newport Corporation’s diffraction grating 33066FL01-270R was received on 11/14/2019. Table 30 shows the sources which the diffraction grating was tested against. The grating produced ideal rainbow spectra for the two different white light sources and effectively diffracted the laser source in Figure 49, satisfying the testing procedure.

Table 30. Diffraction grating spec test

Source	Waveband	Status
Uncollimated white LED (phone flashlight)	400 – 700 nm	Successful
MZH8340550D-AL01A laser light source	405 nm	Successful
60W non-dimmable soft white LED bulb	400 – 700 nm	Successful



Figure 49. Laser spectrum testing in a dark room

6.4.5 Laser Source Testing

The laser module used for the CFS was ordered from Zhuhai MZLASER Technology Co., Ltd in Guangdong, China. Two laser modules were ordered in case there was any electrical malfunctions during testing which could render one of the modules unusable. The lasers were received on 11/15/2019 and Table 31 displays the laser specifications which were tested for accuracy on 11/25/2019.

Table 31. Tested Specifications for Laser Module

Specification	Company Listed	Manually Tested
Peak Wavelength	405 nm	405 nm @ 23°C
Optical Power	40-45 mW	44.4 mW @ 33.5 cm
Beam Spot Diameter	6 mm @ 10 m	4.4 mm @ 33.5 cm

For testing, the laser module was connected to a Keithley 2231A-30-3 triple channel DC power supply with a DC operating voltage of 2.8 V. The beam spot diameter was measured using a micrometer on a white screen. The peak wavelength and the optical power were determined using a gentec- ϵ Maestro 234907 power meter. All the devices were set up on a Thorlabs optical bench and the beam spot diameter at 33.5 cm can be seen in Figure 50

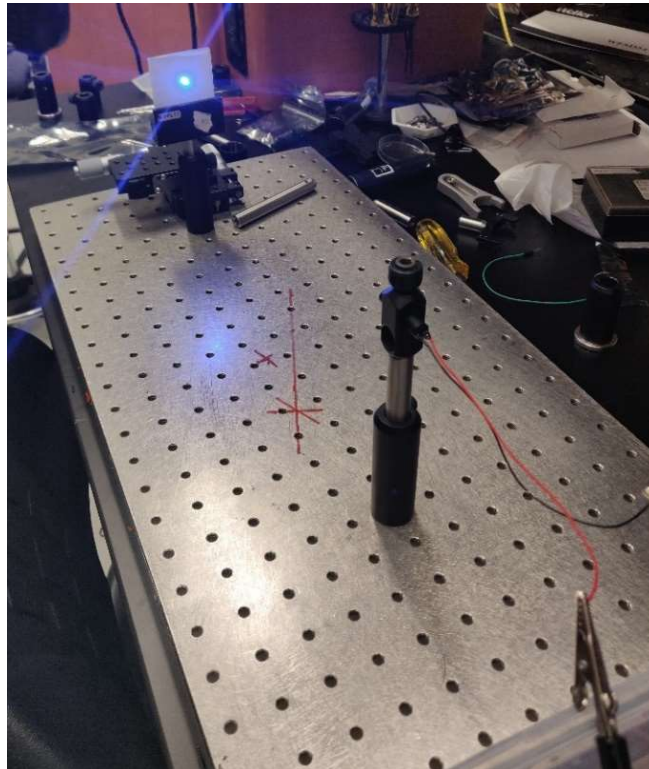


Figure 50. Setup for Measuring Laser Beam Spot Size

6.4.6 Fluorescence Spectrum Testing

In early February 2020, we began testing the optical system designed in 5.1.1 Optical Housing Design. The first step for optical system testing was to ensure that the geometric optics system design effectively imaged fluorescent light from the slit to the sensor interface as planned. Before fluorescence spectrum testing started, the device base and the four internal walls were fabricated with a milling machine. Optical posts and holders were fabricated with a lathe.

To start, the grating was tested to prove that light could be effectively diffracted near the slit. This served to prove that the grating would split the light into its component wavelengths. In Figure 51, what can be seen is an image of multiple slits. What is shown is the zeroth through third modes of the slit's reflection from the grating's interface. This picture proved that the grating could, at a small distance from the slit, diffract the light into set orders.



Figure 51. Grating diffracting fluorescent light from the slit

In order to ensure the optical system was set up correctly, the laser was pointed through the system. Since the diffraction grating is wavelength-dependent, it was expected that the optics would not be perfectly calibrated for the red light coming out of the slit. This was fixed later by manually adjusting the angle of the grating. The system calibration with the laser is shown in Figure 52.



Figure 52. Laser light through the system and reflecting off the screen (two figures)

This proved that the optics were aligned properly. Next, the inner wall was set up with the chlorophyll sample pressed up against the view hole. Initially, the slit was covering the hole to closely match testing procedure to finished product, but after adjusting the optics, no light was able to be seen on the screen. The power output from the slit was measured with a Gentec-EO MAESTRO power meter and was found to be 200 nW at the slit's interface. To get more power out of the sample for testing purposes, a longpass glass filter with 50% transmission at 600 nm was secured. The output through the longpass filter is shown in Figure 53 and can be contrasted with Figure 52Figure 51 to see the power difference.



Figure 53. Fluorescent light at the collimating mirror interface through the longpass filter

This increased amount of light allowed the optical system to be manually aligned. In Figure 54, the light can be seen propagating through the longpass filter setup and is seen reflecting off the focusing mirror into the camera.

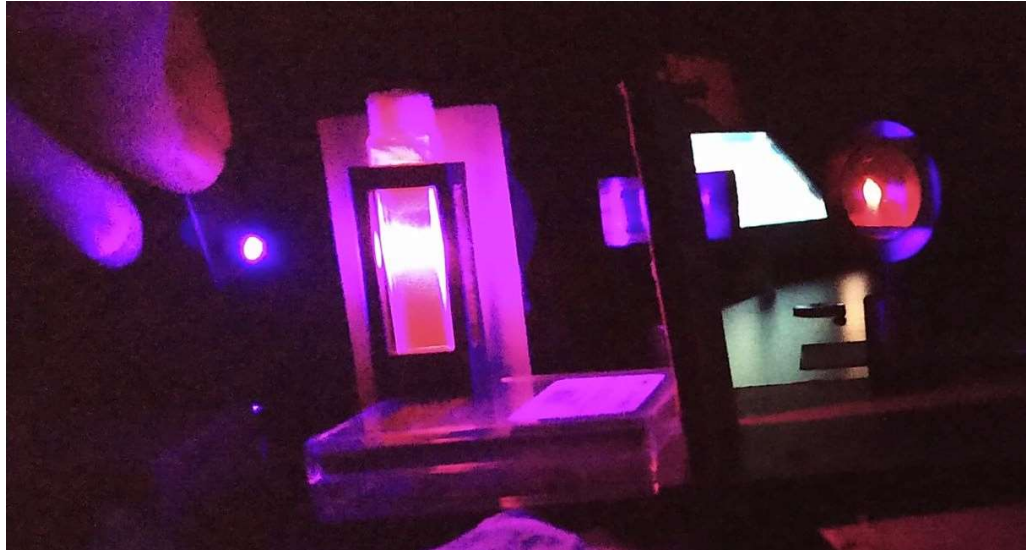


Figure 54. Longpass filter setup with light coming out of the focusing mirror

To complete fluorescence testing, a screen was put at the location of the sensor interface. Again using the longpass filter setup, the fluorescence was imaged through the optics and on to the screen. A small red line was seen on the screen, verifying that our system produced a visible spectrum with a longpass filter. The next step was full integration testing with the ARDR sensor chosen from 4.4.3 Sensor Comparisons.

6.5 Software Testing

This section describes the testing procedures that were used throughout the entire software development process to ensure that the software is functioning properly on our hardware and is free of any major bugs. This section includes procedures for testing both the embedded software and the mobile application.

6.5.1 Development Board Emulation

When developing embedded software, it is often difficult to fully test the code that is being written due to a lack of debugging capabilities on the embedded device, which reduces the visibility that you have on the code as it is running. To circumvent this restriction, we used an emulator to run and debug our embedded software before deploying it to our microcontroller.

One large limitation of this testing method is that it did not allow us to test any of the code that requires interaction with our sensors, as that cannot be emulated. This testing was mainly be useful for ensuring that the code compiles and runs correctly, and that there were no major bugs. When conducting this testing, we used the Qemu emulator to run and debug our code. To debugging our code, we specified breakpoints where we paused the execution of the code and made sure that the variables in memory at that time are what they should have been. We also used debugging features to set breakpoints before crucial parts of the

code that need to be tested and step through those sections of code one instruction at a time. This gave us insight into how exactly the code was executing on our microcontroller; this increased understanding of how our code will execute made debugging issues on the physical microcontroller much easier. For debugging issues with sensor interaction, we took advantage of the ST-LINKs debugging feature to be able to stop and step through code executing on the actual microcontroller through the System Workbench for STM32 integrated development environment.

6.5.2 Physical Measurements

Even though we used an emulated environment to test our embedded software, this environment did not allow us to test the effects that our software will have on the physical MCU and how this will affect our external sensor modules. Testing that the physical effects reflect what is expected by the developer is important to avoid damaging the microcontroller or even our external modules. The main limitation of this testing method is that it required expensive equipment, such as an oscilloscope, which were not always available to our team. Because of this limitation, we did not conduct physical measurement tests as often as the emulation tests for our embedded software.

The physical testing for our software required separate equipment; the main pieces of equipment that we used were Oscilloscopes and Multimeters. The oscilloscopes were used to measure waveforms generated by specific pins on the development board to ensure that our software is generating the waveforms at the correct frequency. Specifically, we used this to test the external clock signal that our MCU provided our image sensor with. To test this, we ran our software that generated the proper clock signal and used an oscilloscope to measure the frequency of the clock signal and ensure that it was in the proper range needed by the image sensor. We also used an oscilloscope to observe I2C and UART communication between the MCU and our external modules, to ensure the communication reflects what is expected based on what the software should be doing. We also used multimeters to check the GPIO pins that are used by our software after running the software to ensure that the software was setting every GPIO pin to the expected value.

6.5.3 Mobile Application Automated Testing

When developing the mobile application, we needed to constantly test the software to ensure that the changes being made did not break previously added functionality or introduce bugs. Because this testing needed to be conducted often, we used an automated testing suite named Junit5 to achieve this testing. Junit 5 allowed us to write automated tests that ran every time any changes were made before the code was compiled. The main drawback for this testing method was the amount of time needed when initially setting up the tests to learn the testing framework and create the automated tests.

While the unit tests that we mentioned in the previous section allowed us to test the core logic of the application, we still needed to test the user interface to ensure the buttons and functionality on the user interface worked as expected. To automate user interface testing, we attempted to use another framework named Espresso. Espresso is similar to Junit in the sense that we needed to spend time initially to learn the framework and create our test

cases, but once they are created, they will automatically run and update us whenever the mobile application has lost functionality. Due to the difficulty of the framework and time constraints, we were unable to implement Espresso user interface testing, and had to manually test the mobile application.

6.6 Building the Device

This section details the construction of the physical housing for the CFS. Work for this section was carried out in the CREOL machine shop using a milling machine and a bandsaw. Holders and posts for the optical components were also machined in the CREOL machine shop.

6.6.1 CFS Base and Walls

The CFS was designed to be shaped like a box, since rectangles are easy to store, transport, and handle. This shape satisfied our Ease of Use goal. Our design for the 3-D version of the CFS went through a few iterations, but the basic shape remained the same and can be seen in Figure 55. In this format, the CFS was designed to have interlocking slots so that the device could be fitted together like a puzzle box. There were four main internal walls to separate the three main sections of the device: the PCB/electronics area (back left), the pump source area (back right), and the spectroscopy area (forward center). The internal wall at center left with the window in it was designed to hold our sensor and was planned to be secured with M2 machine screws through clearance holes and tightened with nuts.

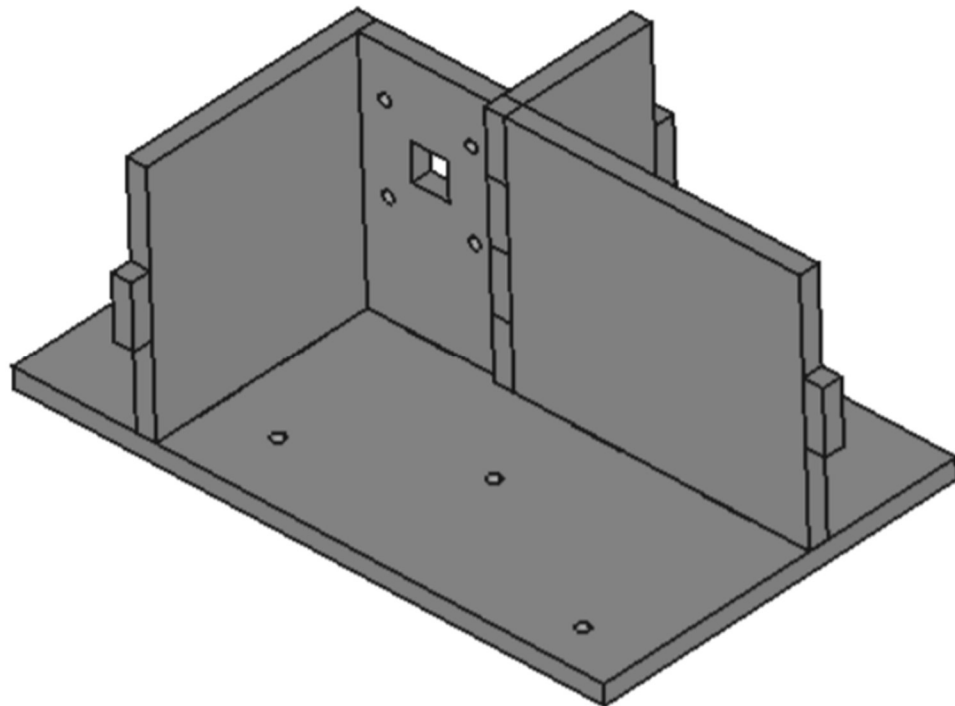


Figure 55. 3-D CFS design with slots

Something else that is not shown in Figure 55 is the entrance hole for the light in the rightmost inner wall. This was machined out later by hand in the machine shop. Its location was determined by finding the center of the collimating mirror and moving to that same position on the rightmost inner wall. The entrance hole was milled out such that an entrance slit could be fixed in place over it, covering the excess light while allowing the fluorescence into the system.

After consulting with faculty in CREOL, it was decided that puzzle box slots for the walls and baseboard were too difficult to implement. The puzzle box slots were discarded in favor of screwing the internal walls into the baseboard. The original slot design for the walls can be seen in Figure 56, but for the final design, we replaced each rectangular puzzle box slot with a screw hole in the center. From left to right, clockwise, the sectioned areas are the spectroscopy section, the PCB/electronics section, and the pump source section.

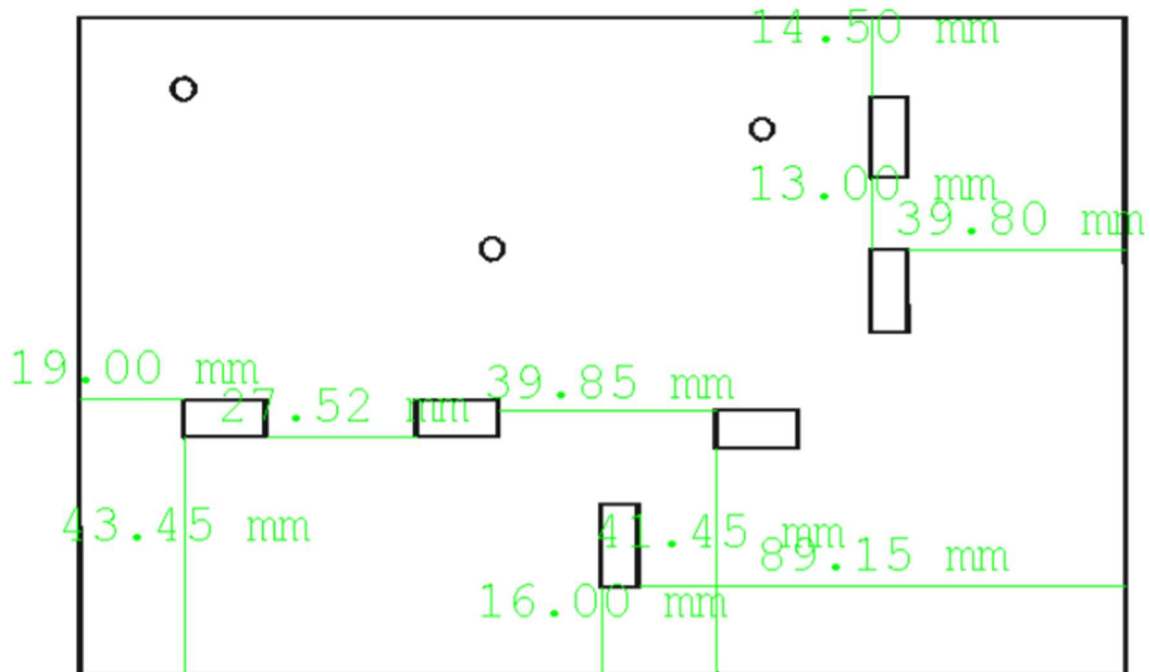


Figure 56. CFS baseboard housing design

The walls were designed to fit the height of the posts and holders that were designed before the housing was finished. The posts and holders combined were a little less than 80mm in height each, so each wall was designed to be 80mm tall with varying lengths. Each wall was cut from the same piece of quarter-inch black acrylic, so each wall shared two dimensions: height and thickness. The only thing that varied was length.

The holes machined for the spectroscopy section were not all used in the final project. The grating hole (middle) was not used for the final setup seen in Figure 33 since it was discovered that the position of the grating led to signal clipping and intense astigmatism at the focusing mirror. This is covered in more detail in 6.8 Building and Testing Discussion.

6.6.2 Posts, Mounts, and Holders

In order to keep the optics in place, we decided to machine posts and holders for the spectroscopy section that would keep the mirrors and grating in place and prevent the system from de-calibrating. To create the holders, the diameter of the mirrors and the grating were measured and holders of those sizes were made in the machine shop using the lathe and the milling machine. Then, optical posts were machined such that the center of each optic was exactly 5cm from the baseboard. The posts and holders plus the mounted optics can be seen in Figure 57.



Figure 57. Empty posts and holders (left); optics mounted in holders (right)

The optics were held in place in their holders using thumb screws which could be tightened using an Allen wrench. The posts held the holders in place by screwing into the base, though the base for the grating's holder was too thin to thread and it was decided that the base should be secured to the post using glue. The posts were then all fitted with custom machined mounts which had screws in their bases that enabled them to be fixed into the accompanying screw holes in the baseboard. To prevent the optics from turning accidentally, thumb twist screws were implemented into the side of the mounts. These enabled the users to fix the optics in place. The one drawback of using this type of setup is that if a casual user gets into the optical system of the device, they can seriously damage the optics or decouple the system to the point where the device is unusable.

6.7 Integration Testing

This section details the integration testing phase of the CFS. Here is where the main interdisciplinary work between computer, electrical, and photonic engineers took place as the CFS was tested for interoperability. Due to the COVID-19 shutdown at UCF in the Spring 2020 semester, integration testing was conducted with demo equipment. The CFS also had to be isolated in a dark room to prevent stray light from entering the system due to problems discussed in 6.8 Building and Testing Discussion.

6.7.1 Pixel Calibration

Before any spectrums could be verified, the pixels had to be calibrated for the location of peak fluorescence. Originally, the spectrum's x-axis in the computer application showed only the pixel number at which a signal was received as seen at the left in Figure 58. To remedy this, two sources with known wavelengths had to be used to adjust the pixel spacing and the pixel start and end.

We used a laser light show module that had two lasers of peak wavelengths 532nm and 650nm. We shined the green laser onto the slit and noted the peak pixel value of the spectrum produced by the CFS; call this pixel value β . We then shined the red laser onto the slit and noted that source's peak pixel value; call this pixel value γ .

Since the difference between the known wavelengths was 118nm, we were able to find the wavelength per pixel that our sensor was resolving at by doing $\frac{118}{\gamma-\beta}$, which was 0.185 nm/pixel. By using this known resolution, we changed the x-axis of our computer spectrum from pixels to nanometers since we had a formula to change the units. Finally, to shift the x-axis forward such that the peak green pixel β corresponded to 532 and the peak red pixel γ corresponded to 650, we graphed the green peak to find out how many nanometers away from 532 the green peak was at that moment (for example, if the green peak was at 100nm, then the whole graph was shifted forward by 432). Once this was accomplished, the red peak was graphed to make sure that it corresponded to 650nm, and when this was verified, the sensor was ready for fluorescence testing. Our calibration sources after calibration are shown in Figure 59 and Figure 60.

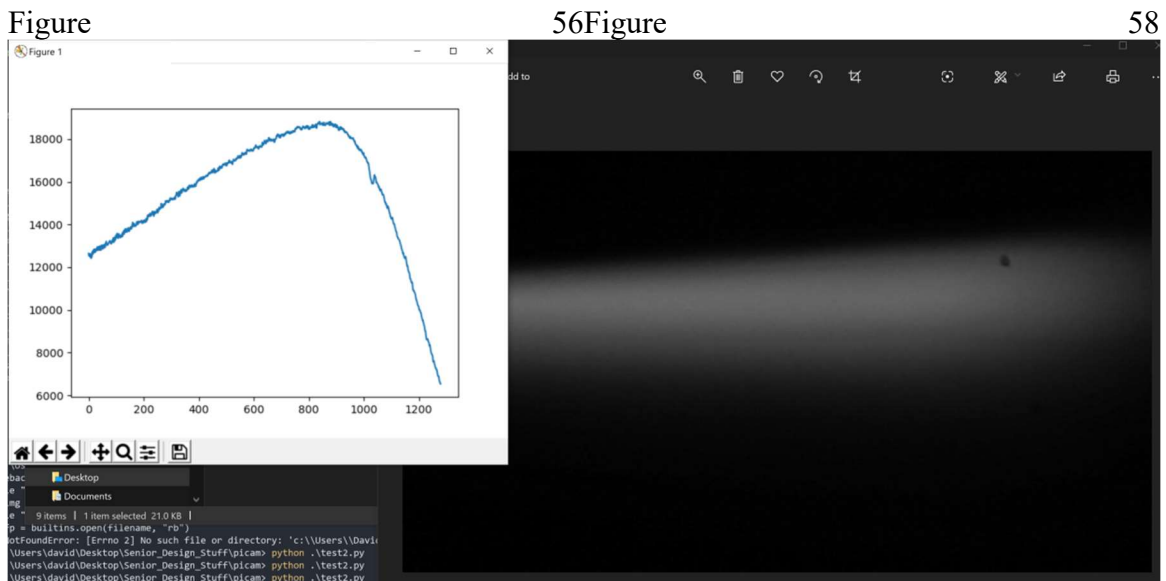


Figure 58. Example of a spectrum before pixel calibration (with imagery)

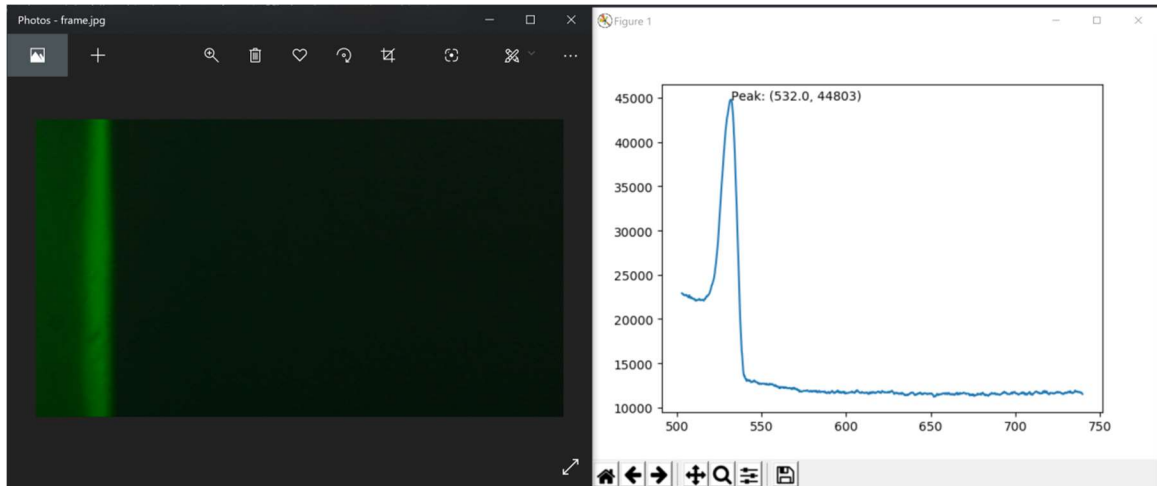


Figure 59. Green laser spectrum after pixel calibration

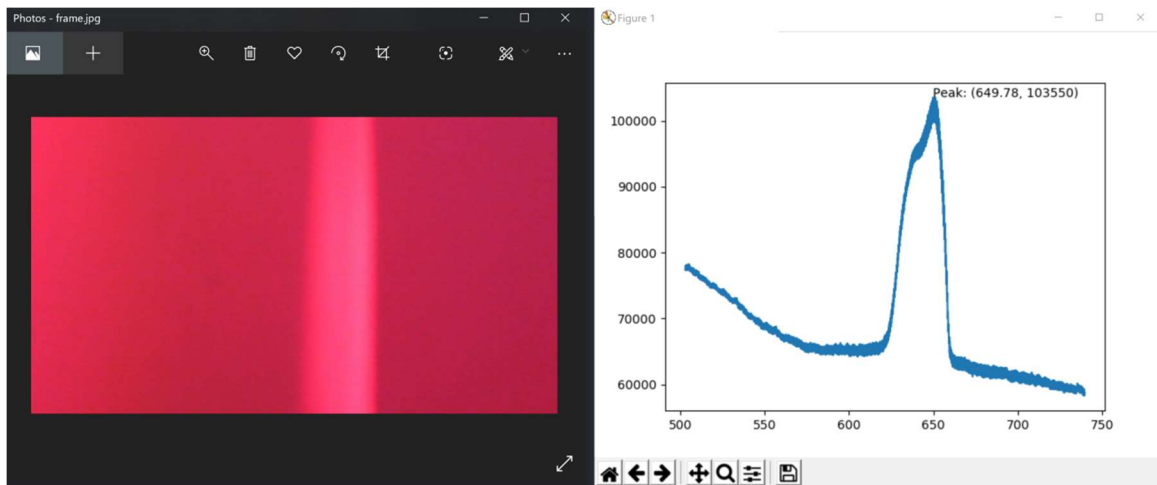


Figure 60. Red laser spectrum after pixel calibration

6.7.2 Camera Imagery and Spectrums

To ensure that the CFS was receiving light from the chlorophyll sample as it fluoresced, the sensor was hooked up to a computer and the default Camera app from the Microsoft Windows operating system was turned on. The light was turned off in the room and the laser was activated. Figure 61 was the live imagery seen from the Camera app and the spectrum produced from our software program after processing a captured still.

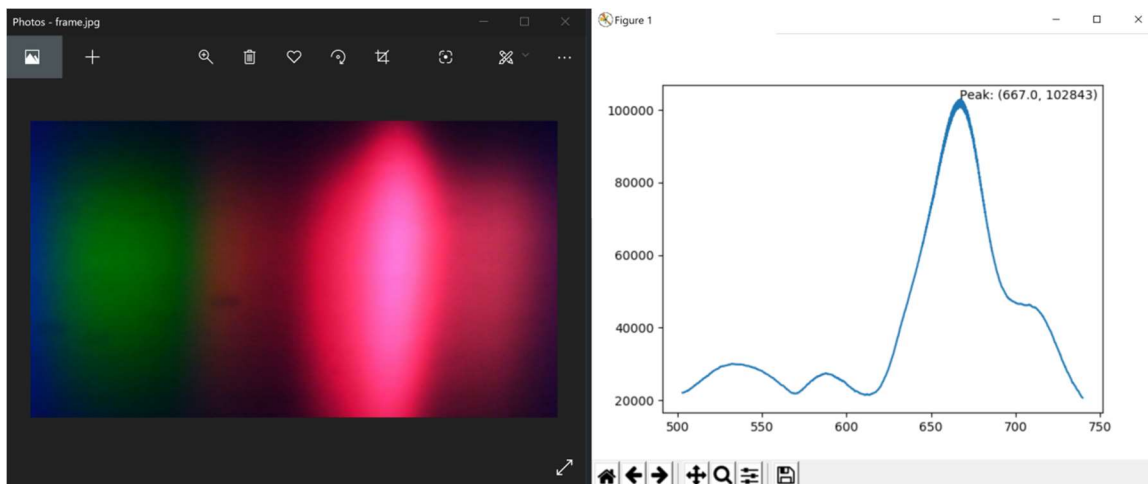


Figure 61. Fluorescence spectrum from Windows Camera app

The green coloring at the left of the picture along with some of the blue was a result of scattering from the laser. This scattering occurred because the sample used in Figure 61 was not prepared in a laboratory environment, leading to a slightly less pure sample. Our sample had a peak wavelength of emission at 667nm which matched with results from scientific papers. [Pond] [Ice] [Braz] With our fluorescence spectrum confirmed on the computer side, the final step was to test with the mobile application.

6.7.3 CFS Mobile Application Spectrums

To ensure that the mobile application software could integrate with the CFS device, the following tests were performed using the mobile application. To be able to transmit the analysis data via Bluetooth to the mobile application without our PCB, the USB-enabled AR0130CS module was connected to a Raspberry Pi. The Raspberry Pi was running a modified version of our embedded software which used a Bluetooth Low Energy module which communicated with the Pi over UART via a breadboard connection. The mobile app was started on a group member's phone and the analysis began. Each test took approximately 40 to 45 seconds to run from the time "Start Analysis" was pressed to when a spectrum appeared on the screen.

First, we checked to make sure our CFS was still calibrated. We ran a test with the green laser source and the red laser source. We received the following images from our tests which showed peak wavelengths of 531.5nm and 651.65nm for the green and red lasers, respectively, seen below in Figure 62. The error in wavelength for the red of 1.65nm corresponds to the red laser light peak shifting to the right by approximately 9 pixels. It was within a safe margin of error, so we elected not to recalibrate the CFS.

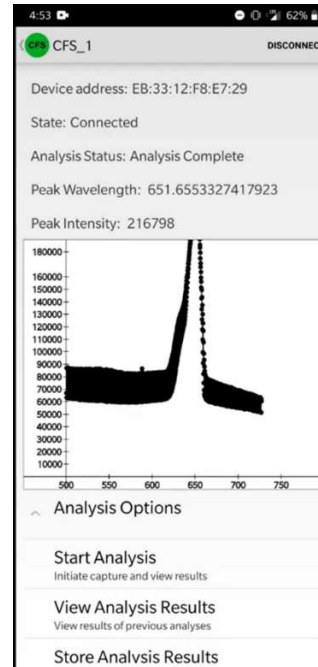
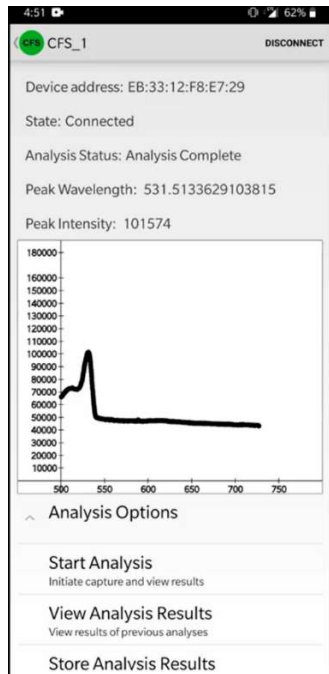


Figure 62. Green laser source (left), red laser source (right)

Next, we tested two chlorophyll samples. One sample was made a few weeks before the testing procedure commenced. The other sample was made the day of the testing procedure. Their fluorescence spectrums are shown in Figure 63. Their comparisons using the in-app comparison feature is shown in Figure 64.

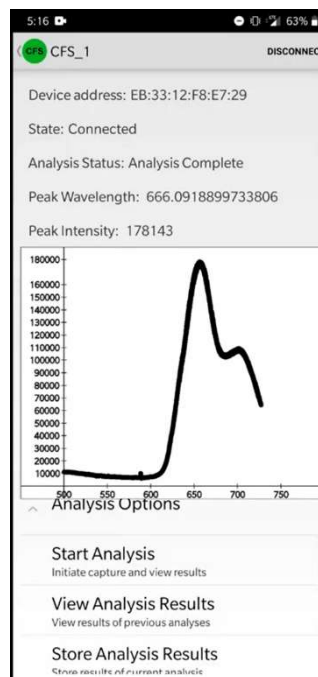
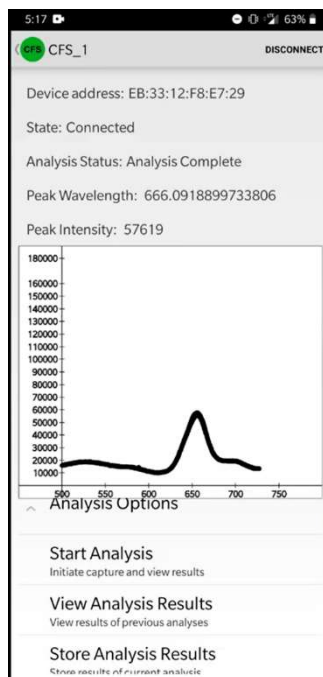


Figure 63. Chlorophyll fluorescence tests: old sample (left), new sample (right)

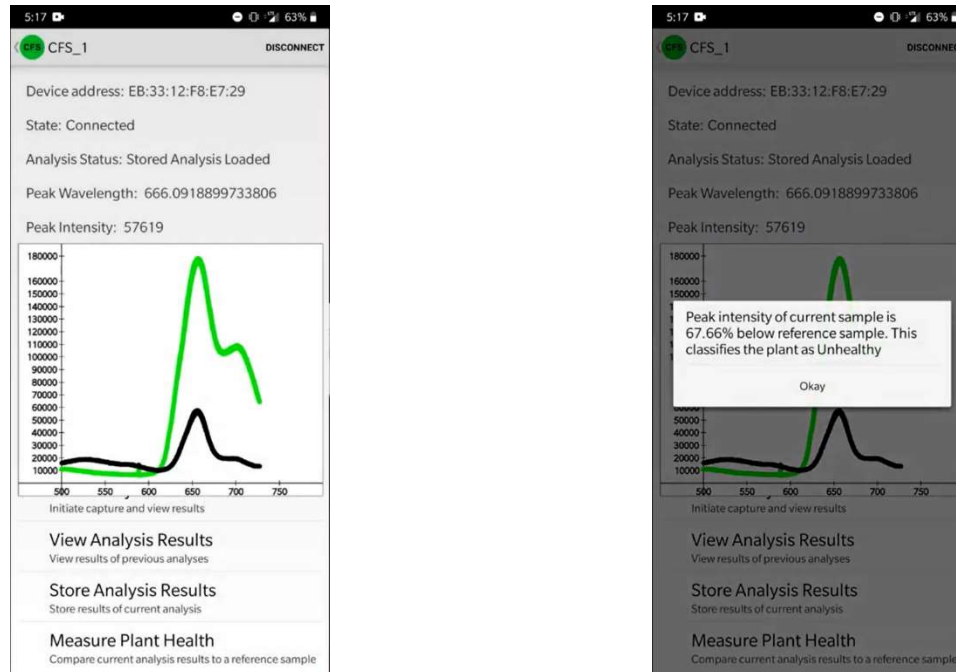


Figure 64. Chlorophyll fluorescence comparisons: graph only (left), qualitative (right)

We used the following metric for fluorescence comparisons. If a tested sample's intensity is between 0% and 20% of that of a reference sample, the test sample is healthy. If the intensity is between 20% and 40%, the test sample is fairly healthy. If the intensity is less than 40%, the test sample is unhealthy.

6.8 Building and Testing Discussion

A few difficulties occurred during the building and testing phase of the CFS which hindered the project's performance. Most chiefly, the COVID-19 shutdown occurred in the latter half of the Spring 2020 semester and prevented the CFS from reaching the completion stage in its housing development. This meant that the CFS could only operate in a completely dark room, which was not the expected area of operation for this device and which violated the Ease of Use project goal.

The COVID-19 shutdown also prevented a second PCB from being ordered for integration into the device. While this did not hinder the CFS's performance, it is worth noting that the PCB had been planned to be updated but this was not able to be accomplished. During PCB troubleshooting, the Bluetooth module was damaged as it was being desoldered. A solder contact which we were using became dislodged and we were not able to repair this. As a consequence of COVID-19, we were unable to order this part as it would not arrive in time.

We had to switch to using a version of our image sensor that was already mounted on a board with USB connectivity and sold as a webcam module because we were unable to use our PCB for testing. This is due to no affordable testing boards available for the image sensor, and it was difficult to solder leads onto such a small surface mount part. This change

also required us to use a Raspberry Pi instead of our STM32 development board for our final demonstration and testing, due to the development board not being able to communicate with the image sensor over USB.

During testing, it was discovered that the original optical configuration in the spectroscopy section was leading to intense astigmatism at the focusing mirror and was causing signal clipping at the grating. Since the grating and the collimating mirror were nearly perpendicular to each other, the light coming off the grating was spreading much wider than expected, leading to signal loss at the focusing mirror. In order to remedy this, the grating was repositioned such that its interface was close to normal with the collimating mirror. These differences can be seen in the following: the old configuration in Figure 56 and the new/final configuration in Figure 33.

7. Operating Procedures

This section of the paper details the standard operating procedures of the CFS as used by a normal end user. This section also serves as the user manual for the mobile app.

7.1 Sample Preparation

In order to test a sample, a sample must first be made. Follow these steps to make a sample from the plant that needs to be tested.

1. Pick a leaf from the species of plant the user would like to analyze.
2. Grind up the leaves into smaller pieces with a length less than 1cm. A spice grinder works well for this step.
3. Add approximately 1 gram of the ground-up leaf into 150mL of acetone.
4. Stir the solution for approximately 1 minute.
5. Pour the solution through a coffee filter into another liquid holder such as a beaker or measuring cup.
6. Pour the filtered solution into the cuvette.
7. Place cuvette inside the cuvette mount and place the cuvette mount into the CFS.

7.2 Mobile Application

Follow these steps to operate the CFS after the sample has been placed inside of the device.



Figure 65. CFS Application Icon

1. Open the “CFS” application on your mobile device. The Icon of the application will look like the icon shown in Figure 65.

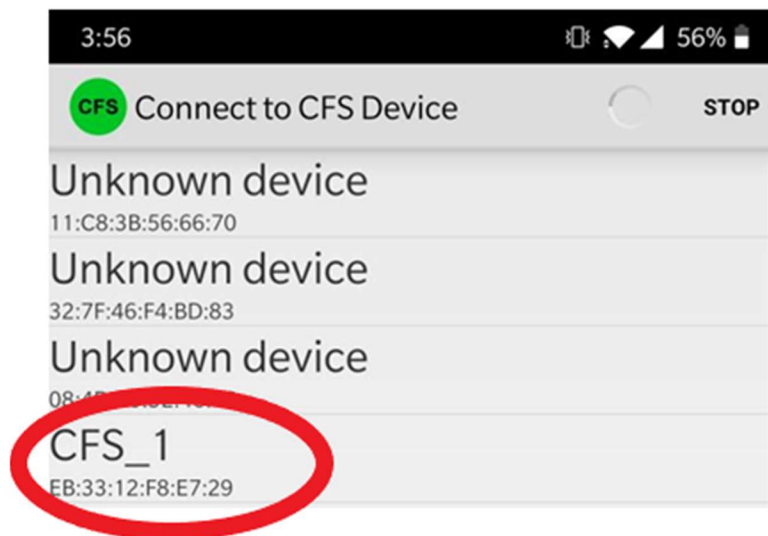


Figure 66. Selecting Device in CFS Application

- On this initial screen, you will see a list of Bluetooth Low Energy devices in your proximity. Search for your CFS device in the list and click on it once you have found it. CFS devices will broadcast their name as “CFS_X” where X is the serial number of the device. An example can be seen in Figure 66. If you do not see any devices with “CFS” in their name, ensure the measurement device is powered on.

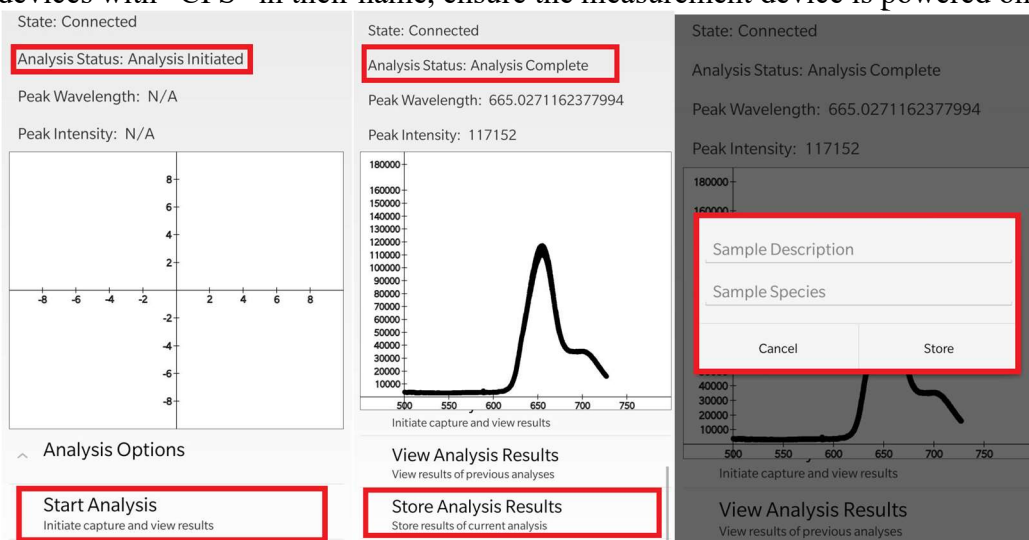


Figure 67. Conducting Analysis Via CFS Application

- Once you have clicked on the name of your CFS device, you will be taken to the analysis menu for the device. If you would like to begin a new analysis, expand the Analysis Options menu at the bottom of the screen and press “Start Analysis”. The current status of your analysis will be displayed at the top of the screen under “Analysis Status”. Once your analysis is complete, you can store the analysis by using the “Store Analysis Results” button at the bottom of the screen and entering the requested information. This process can be seen in Figure 67.

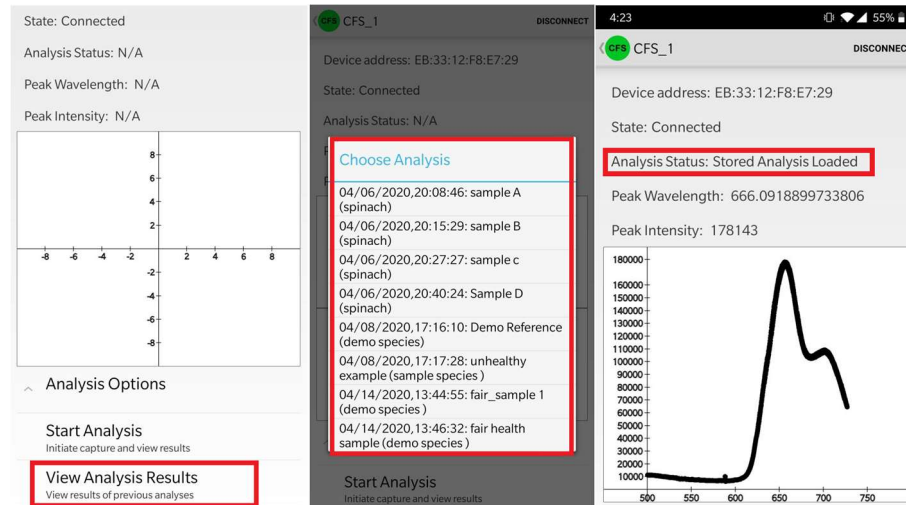


Figure 68. Viewing Stored Results in the CFS Application

- If you would like to view stored analysis results, expand the “Analysis Options” menu at the bottom of the screen and press “View Analysis Results”, then select the results you would like to see in the pop-up menu. This process can be seen in Figure 68.

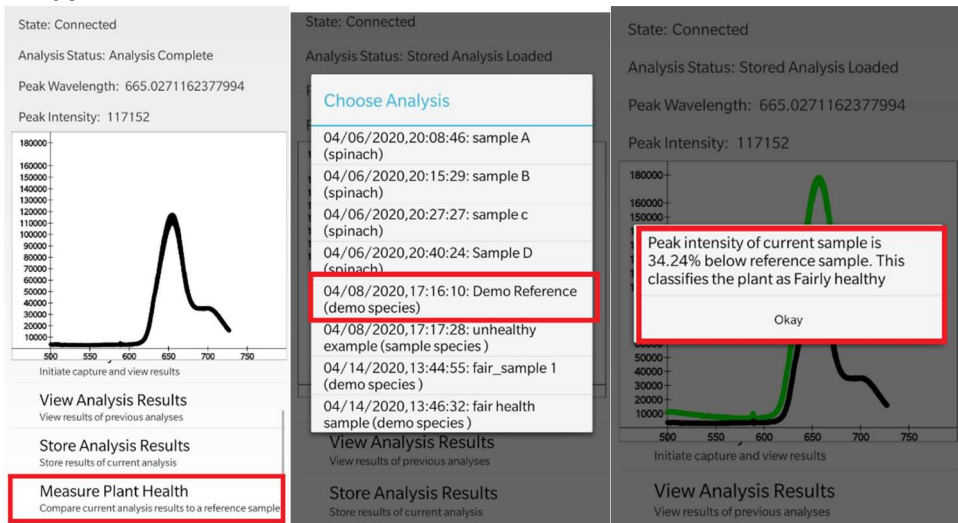


Figure 69. Measuring Plant Health in the CFS Application

- To compare the currently loaded analysis results to a reference sample to measure plant health, expand the “Analysis Options” menu at the bottom of the screen, scroll down, and press “Measure Plant Health”. You will be prompted to select a reference sample to compare your current sample to. After you select your reference sample, you will be able to see the health of the current sample in the popup window, as well as compare the two spectrums on the main page. This process can be seen in Figure 69.

8. Administrative

The section herein describes the administrative content not pertinent to the overall design, construction, or research for the CFS. Covered in this section are milestones and timelines for the group, budget for the project, avenues of financing, and division of labor.

8.1 Milestones

To ensure the Chlorophyll Fluorescence Spectrometer was designed properly and met various design and timing constraints, several deadlines were enacted. The necessary objectives to be completed for each deadline appear in Table 32.

Table 32. Milestones for the CFS

Objective	Start Date	End Date	Status	Lead
Administrative				
Project Concept	8/26/2019	8/30/2019	Complete	Group 1
Role Assignment	8/30/2019	9/5/2019	Complete	Group 1
Initial Research	9/5/2019	9/19/2019	Complete	Group 1
D&C Document	9/9/2019	9/20/2019	Complete	Group 1
Component Research	9/21/2019	10/31/2019	Complete	Group 1
Initial Document	9/25/2019	11/1/2019	Complete	Group 1
Component Ordering	11/2/2019	11/14/2019	Complete	Group 1
Draft Document	11/5/2019	11/15/2019	Complete	Group 1
Initial Optics Design	11/5/2019	12/1/2019	Complete	PSE
Initial PCB Design	11/5/2019	12/1/2019	Complete	EE
Initial Software Design	11/5/2019	12/1/2019	Complete	CE
Final Draft Document	11/16/2019	12/4/2019	Complete	Group 1
Final Optics Design	1/6/2020	1/30/2020	Complete	PSE
Final PCB Design	1/6/2020	1/30/2020	Complete	EE
Final Software Design	1/6/2020	1/30/2020	Complete	CE
CDR Presentation	1/6/2020	1/28/2020	Complete	Group 1
Instructor Review	1/31/2020	1/31/2020	Complete	Group 1
Mid-Term Demo	2/1/2020	3/20/2020	Complete	Group 1
Conference Paper	3/18/2020	4/12/2020	Complete	Group 1
Final Demo	4/6/2020	4/12/2020	Complete	Group 1
Final Presentation	4/13/2020	4/13/2020	Complete	Group 1
Final Documentation	4/21/2020	4/21/2020	Complete	Group 1
Exit Interview	4/21/2020	4/21/2020	Complete	Group 1
Research and Design				
Optical Housing	11/1/2019	11/20/2019	Complete	PSE
Sensor Research	10/1/2019	10/23/2019	Complete	PSE

Device Housing	11/1/2019	12/1/2019	Complete	PSE
PCB Design	11/5/2019	11/29/2019	Complete	EE
Mobile App UI	11/5/2019	12/1/2019	Complete	CE
Wireless Components	11/5/2019	12/1/2019	Complete	CE
Parts Ordered	11/5/2019	11/15/2019	Complete	Group 1
Parts Tested	11/18/2019	11/30/2019	Complete	Group 1
Sample Preparation	11/19/2019	11/19/2019	Complete	PSE
Software Testing	1/6/2020	4/9/2020	Complete	CE
PCB Testing	1/31/2020	4/8/2020	Complete	EE
Optics Calibration	1/31/2020	4/2/2020	Complete	PSE
Sensor-Optic Testing	3/16/2020	4/6/2020	Complete	PSE, CE
Integration Testing	3/16/2020	4/10/2020	Complete	CE, PSE

8.2 Budget and Avenues of Financing

The University did not provide any funding for our materials. We asked several companies if they would be willing to sponsor us with any amount of funding, but none responded to our queries. This project was funded entirely by the four students who built it.

Table 33 shows details of the budget for this project. Since this project had no external funding, we tried to minimize the cost for the CFS while meeting our design constraints and standards. We borrowed a few components for testing, such as the longpass filter, that were not included in our budget or bill of materials.

Table 33. Budget details for CFS

Component	Area of Device	Provided By	Quantity	Price per unit	Total Price
Housing Material	Housing	Students/UCF	2	\$0.00	\$0.00
Laser Source	Pump Housing	Students	1	\$9.00	\$40.38
Quartz Cuvette	Pump Housing	Students	2	--	\$20.00
Mirrors	Optical Housing	Students	2	\$60.34	\$120.68
Diffraction Grating	Optical Housing	Students	1	\$89.00	\$89.00
Imaging Sensor	Optical Housing	Students	4	\$8.38	\$34.68
CPU	PCB	Students	2	\$4.41	\$8.82
Development Board	PCB	Students	1	\$8.79	\$8.79
Bluetooth Module	PCB	Students	1	\$15.40	\$29.85
PCB Order	PCB	Students	3	\$10.85	\$46.00
Total					\$398.20

It should be noted that the budget shown above does not match the bill of materials shown in Table 25. This is because certain parts were omitted from this list since they were not used in the final integration stage of the project.

8.3 Division of Labor

Shown below is Table 34 is the division of labor for the task of building, designing, and executing the CFS. Table 34 shows all tasks attempted, the primary executor, the secondary executors, the workload involved in completing the task, and the college major associated with each task.

Table 34. Division of labor for the CFS

Task	Primary	Secondary	Workload	Major
Pump section design	Robert	Samuel	Medium	PSE
Sample holder design	Robert	Samuel	Medium	PSE
Spectroscopy section design	Samuel	Robert	High	PSE
Sensor testing	David, Luke	Robert, Luke	High	CE, EE, PSE
Integration testing	Samuel, David	Robert	High	PSE, CE
CFS housing design	Samuel	Robert	Medium	PSE
PCB testing and design	Luke	David	High	EE, CE
Power circuit	Luke	David	Low	EE
Embedded software design	David	Luke	High	CE
Mobile application design	David	Luke	Medium	CE

9. Project Summary/Conclusion

The design of the chlorophyll fluorescence spectrometer is a result of overcoming design challenges, meeting engineering requirements, collaborating with different fields of engineering, and agreeing on standards, constraints, and compromises. The engineering requirement specifications that started out as a design table on a screen has evolved into a device capable of observing fluorescence from samples and categorizing them based on intensity.

The CFS consists of four major components: the source housing, the spectroscopy housing, the PCB, and the embedded software. The source housing excites a chlorophyll sample to fluorescence using low-visible light at 405nm. The spectroscopy section splits the fluorescence into its component wavelengths using a diffraction grating and two concave mirrors and directs it to an imaging sensor. The PCB powers every component of the CFS, reads data from the sensor, and transmits said spectroscopy data to a user via a mobile app for ease of review and consideration. The embedded software transforms the imagery into a line spectrum which can be interpreted by the user as a measure of relative plant health.

The group consensus is that the work included herein is a result of individuals collaborating to produce an idea of original design and implementation. The project shown in this document was successfully produced within two semesters and worked according to our specifications.

Problems occurred during the second semester included electronic leads snapping off, scheduling conflicts, and the COVID-19 shutdown. Time was a large consideration in regard to these problems. When leads snapped, we were unable to conduct integration testing for several days. When our schedules conflicted, we were unable to meet as a group and resolve issues quickly. The COVID-19 shutdown prevented the CFS from being finished in its entirety and the device could only be operated in a dark room. In this respect, the CFS failed to meet the Robust Quality goal outlined in 2.2 Project Goals and Objectives. The PCB was also not completed in a timely manner and we discovered later that the drive source for the laser on the PCB was voltage-controlled instead of being current-controlled, an issue that the photonics team should have told the electronics team about and failed to do so. We were unable to fully integrate the PCB into our project due to this and the COVID-19 shutdown and ended up using a backup demo setup for our final demonstration.

A brief discussion can be made about the engineering requirement specifications and whether the CFS met the specifications listed in 2.3 Requirement Specifications and 2.4 Engineering Trade-Off Matrix. The dimensions needed to be less than or equal to 4000 cm³ and the power consumption needed to be less than or equal to 5 Watts. The CFS should have cost under 500 USD to build, should have used Bluetooth 4.0 Bluetooth Low Energy technology, and should have been able to analyze a sample in less than 60 seconds. It should also have had a radio power consumption less than or equal to 50 mW and should have been able to analyze a spectrum from at least 600 to 700 nm.

As described in 6.6 , the dimensions requirement was satisfied since the device was 19.2 x 12 x 8.5 cm or 1958.4cm³ in volume. Our requirement specification stated a maximum of 5 Watts for total system power consumption and the sum of peak power consumption for each of our major components was 3.61 Watts. The power consumption requirement was satisfied. According to both Table 25 and Table 33, the CFS was under the required 500 USD budget and met the cost requirement specification. The CFS was designed to use Bluetooth 4.0 Bluetooth Low Energy technology for its wireless communications and did so, meeting this requirement. The device performed analyses in 45 seconds which was under the required 60 seconds, meeting this requirement. The CFS had a radio power consumption of 39.6 mW which was under the required 50 mW, meeting this requirement. And finally, the CFS was able to image a light spectrum from approximately 500 to 740 nm, meeting and exceeding the requirement that it image at least 600 to 700 nm.

It is also important to remember that the CFS was designed to meet or exceed commercially available products. The Spectral Evolution spectrometer discussed in 4.1 Similar Products can be used as a benchmark for comparison. Due to budget limitations, this device was not purchased by the group, but it is reasonably well documented online and has been used by several third-party groups to conduct research and study. Research into Spectral Evolution's broadband UV-Vis-NIR spectrometer showed that our CFS beat it only in cost, with the CFS costing ~400 USD and the Spectral Evolution chlorophyll spectrometer costing ~2300 USD. Given that our CFS was designed to be low-cost, this is not surprising, but it is nice to know our device exceeded a commercially available product in one metric.

With the extent of the work done on the CFS, the team feels confident that the device was the best performance possible given the problems highlighted previously. Problems with the optical design were addressed before the final presentation, issues were brought up and documented, and all relevant standards were met and implemented. The CFS was a successful senior design project that operates according to specifications and performs as outlined in this report.

The team responsible for the optical design of the CFS would like to thank Dr. David Hagan, Hao-Jung "Wilbur" Chang, Mr. Richard Zotti, Dr. Kyle Renshaw, and Dr. Kyu Young Han from CREOL, the College of Optics and Photonics at the University of Central Florida for assisting with and mentoring the design process.

Appendix A – References

[MC.aprs] Measurement Computing. *TechTip: Accuracy, Precision, Resolution, and Sensitivity*. <https://www.mccdaq.com/TechTips/TechTip-1.aspx>

[TL.dfg] Thor Labs. *Optics Catalog: Introduction to Diffraction Gratings*. <https://www.thorlabs.com/catalogpages/802.pdf>

[TgO.Dnk] Dereniak, Eustace L.; Dereniak, Teresa D. *Geometrical and Trigonometric Optics*. 2008.

[MD.WUUES] Micro Digital. *Ways to Use USB in Embedded Systems*. http://www.smxrtos.com/articles/usb_art/waysusb.htm

[ARM.CPU] Arm Ltd. *Classic Processors*.
<https://www.arm.com/products/processors/classic/arm7/index.php>

[EET.I2C] EETech Media, LLC. *Introduction to the I2C Bus*. <https://www.allaboutcircuits.com/technical-articles/introduction-to-the-i2c-bus/>

[EET.UART] EETech Media, LLC. *Back to Basics: The Universal Asynchronous Receiver/Transmitter (UART)*. <https://www.allaboutcircuits.com/technical-articles/back-to-basics-the-universal-asynchronous-receiver-transmitter-uart/>

[EET.SPI] EETech Media, LLC. *Back to Basics: SPI (Serial Peripheral Interface)*. <https://www.allaboutcircuits.com/technical-articles/spi-serial-peripheral-interface/>

[LFI] LightForm, Inc. *Prism and Diffraction Grating Spectral Properties Compared*. <https://lightforminc.com/prism-grating/>

[Hct] Hecht, Eugene. *Optics*. 4ED.

[HL.A] Healthline; reviewed by Xixi Luo, MD. *Acetone Poisoning*. <https://www.healthline.com/health/acetone-poisoning#symptoms>

[OFC] Keiser, Gerd. Optical Fiber Communication, Fourth Edition. McGraw-Hill, New York, NY. 2011.

[LE] Kuhn, Kelin J. Laser Engineering. Prentice-Hall, Inc. Upper Saddle River, NJ. 1998.

[HGIC] Blake, James H.; Kluepfel, Marjan; Williamson, Joey (ed.). Clemson Cooperative Extension Home & Garden Information Center.
<https://hgic.clemson.edu/factsheet/houseplant-diseases-disorders/>

[ONS.AR0130] SCILLC dba ON Semiconductor. *AR0130CS Datasheet*.
<https://www.onsemi.cn/PowerSolutions/document/AR0130CS-D.PDF>

[Qck.Htn] Quick, W.P.; Horton, P. *Studies on the induction of chlorophyll fluorescence in barley protoplasts. I. Factors affecting the observation of oscillations in the yield of chlorophyll fluorescence and the rate of oxygen evolution.*

<https://www.jstor.org/stable/35689>

[Pond] Poniedzialek, Barbara & Falfushynska, Halina & Rzymiski, Piotr. (2017). "Flow cytometry as a value tool to study cyanobacteria: A mini-review." *Limnological Review*. 17. 89-95. 10.1515/limre-2017-0009.

[Ice] The UC Berkeley IceCube Group. (2014). "Fluorescence; Astrobiology." IceCube Neutrino Observatory; University of California, Berkeley. <<http://icecube.berkeley.edu/~bramall/work/astrobiology/fluorescence.htm>>

[Braz] M. S. Lopes, Jefferson & G. C. Moreira, Sanclayton & M. Barbosa Neto, Newton. (2020). "Selective Inner-Filter on the Fluorescence Response of Chlorophyll and Pheophytin Molecules Extracted from *Caesalpinia echinata* Leaves." *Journal of the Brazilian Chemical Society*. 31. Online publication. 10.21577/0103-5053.20190150.

Appendix B – Permissions

Permission for [TgO.Dnk]

Re: Requesting Permission to Use Material



Eustace Dereniak <eustace@optics.arizona.edu>
To: Samuel Knight

Reply Reply All Forward ...
Wed 10/23/2019 6:57 PM

Sure,
Yes

Sent from my Verizon, Samsung Galaxy smartphone

----- Original message -----

From: Samuel Knight <knights@Knights.ucf.edu>
Date: 10/23/19 3:50 PM (GMT-07:00)
To: Eustace Dereniak <eustace@optics.arizona.edu>
Cc: Robert Bernson <bermson91@Knights.ucf.edu>, David Maria <DavidMaria@Knights.ucf.edu>
Subject: Requesting Permission to Use Material

Dr. Dereniak,

Hello; I'm an undergraduate student at CREOL at the University of Central Florida. I'm enrolled in my senior design capstone course and I'm working on a project about chlorophyll fluorescence spectrometry. I'm emailing you today to request your permission to use Figure 4.8 from Geometric and Trigonometric Optics, first edition, in my capstone course's research paper with the appropriate citation included in the references. The paper will not be published for monetary gain.

Regards,
Samuel Knight

Permission for [MD.WUUES]

RE: Request for Permission



David Moore <davidm@smxrtos.com>
To: David Maria
Cc: Samuel Knight; Robert Bernson; Luke Preston

Sat 10/26/2019 7:38 PM

Hi David,

Sure that's fine. You might get a better quality image if you open the PDF version (link in upper right of web page), zoom in, and then use the Windows Snipping Tool to lift it.

David Moore
Vice President

Micro Digital Inc www.smxrtos.com
Voice 714-437-7333 ext 304

From: David Maria [<mailto:DavidMaria@Knights.ucf.edu>]
Sent: Saturday, October 26, 2019 2:20 PM
To: davidm@smxrtos.com; yingbohu@smxrtos.com
Cc: Samuel Knight; Robert Bernson; Luke Preston
Subject: Request for Permission

Hello,

I'm an undergraduate student in the College of Engineering and Computer Science at the University of Central Florida. I'm working on a research paper for my senior design capstone course and I was wondering if I could use one of your figures in my paper, which will not be published for monetary gain. The image is Figure 1 on this page: http://www.smxrtos.com/articles/usb_art/waysusb.htm. I will cite the source appropriately, as well, and state that the image was republished with permission.

Regards,
David Maria

Permission for [EET.UART], [EET.I2C], [EET.SPI]

Re: Request for Permission



Adam LaBarbera <adam@eetech.com>

To: David Maria

Cc: admin@eetechmedia.com

We removed extra line breaks from this message.

Thanks for asking.

You are permitted to use AAC content.
Best of luck.

Best,
Adam

> On Oct 27, 2019, at 12:25 PM, David Maria <davidjmaria@knights.ucf.edu> wrote:
>
> University of Central Florida
> 7542343157
> Hello,
>
> I'm an undergraduate student in the College of Engineering and
> Computer Science at the University of Central Florida. I'm working on
> a research paper for my senior design capstone course and I was
> wondering if I could use some of your figures in my paper, which will
> not be published for monetary gain. The figures will come from the following pages:
> [https://nam02.safelinks.protection.outlook.com/?url=https%3A%2F%2Fwww.allaboutcircuits.com%2Ftechnical-articles%2Fspi-serial-peripheral-inte](https://nam02.safelinks.protection.outlook.com/?url=https%3A%2F%2Fwww.allaboutcircuits.com%2Ftechnical-articles%2Fspi-serial-peripheral-interface%2F&data=02%7C01%7Cdavidjmaria%40knights.ucf.edu%7Cc456f998ad%55454e2b6708d75b17829f%7C5b16e18278b3412c919668342689eeb7%7C0%7C1%7C63%7078028854830384&data=BI1dEI5Nm18%2FgiwGrXvc%2BuHgl%2BtTwa7Hfh856%2tOdM%3D&reserved=0)
> [rface%2F&data=02%7C01%7Cdavidjmaria%40knights.ucf.edu%7Cc456f998ad](https://nam02.safelinks.protection.outlook.com/?url=https%3A%2F%2Fwww.allaboutcircuits.com%2Ftechnical-articles%2Fspi-serial-peripheral-inte)
> [55454e2b6708d75b17829f%7C5b16e18278b3412c919668342689eeb7%7C0%7C1%7C63](https://nam02.safelinks.protection.outlook.com/?url=https%3A%2F%2Fwww.allaboutcircuits.com%2Ftechnical-articles%2Fspi-serial-peripheral-inte)
> [7078028854830384&data=BI1dEI5Nm18%2FgiwGrXvc%2BuHgl%2BtTwa7Hfh856](https://nam02.safelinks.protection.outlook.com/?url=https%3A%2F%2Fwww.allaboutcircuits.com%2Ftechnical-articles%2Fspi-serial-peripheral-inte)
> [d2tOdM%3D&reserved=0](https://nam02.safelinks.protection.outlook.com/?url=https%3A%2F%2Fwww.allaboutcircuits.com%2Ftechnical-articles%2Fspi-serial-peripheral-inte),

Permission for [LFI]

Re: Request for Permission



jlerner lightforminc.com <jlerner@lightforminc.com>

To: Samuel Knight; jlerner lightforminc.com

Cc: Robert Bernson; David Maria

Reply Reply All Forward

Thu 10/24/2019 5:09 PM

Bandpass-QE_Composite.xlsx 36 KB Effic_Curves_Composite.xlsx 28 KB Spectral_Imaging_Hardware.pdf 4 MB

Action Items

Get more add-ins

Hi Sam,

Fine with me.

I think the bandpass spreadsheet contains the figure you are looking for. I used the data in the spreadsheets in the attached paper and subsequently my website. Use, tweak it / them however you wish.

The second spreadsheet compares the efficiency of various devices used in imaging spectroscopy.

Should you publish please be so kind as to send me a copy, or a link to the final publication.

If you need more or different just ask.

Good luck!!

Jeremy

Cell: (908)963-4262

On 10/24/2019 4:18 PM, Samuel Knight wrote:

Hello,

I'm an undergraduate student at CREOL at the University of Central Florida. I'm working on a research paper for my senior design capstone course and I was wondering if I could use one of your images in my paper, which will not be published for monetary gain. The image is Figure 3 on this page: <https://lightforminc.com/prism-grating/>. I will be using it to highlight the differences between gratings and prisms in spectrometers. I will cite the source appropriately, as well, and state that the image was republished with permission. I was also hoping, if permission was granted, that there is a higher resolution copy available for use in my paper, and if I could have access to it.

Regards,
Samuel Knight

Proof of permission request for Young's double slit and [Hct] Request for Permission



Samuel Knight

To: hecht@adelphi.edu

Cc: Bobby Bernson; davidjmaria@knights.ucf.edu; lukepreston@knights.ucf.edu

Reply

Reply All

Forward



Mon 10/28/2019 2:00 PM

Dr. Hecht,

I'm an undergraduate student at CREOL at the University of Central Florida. I'm working on a research paper for my senior design capstone course and I was wondering if I could use some images from your book *Optics* 4th Edition. My paper will not be published for monetary gain. I will be using the images in chapter 10 to highlight the differences between gratings and prisms in spectrometers. I will cite the source appropriately, as well, and state that the images were republished with permission. If I need to use other pictures in my paper, I will be sure to email you before adding them.

Regards,
Samuel Knight

Proof of permission from Scott Prahl



Scott Prahl <Scott.Prahl@oit.edu>

Wed 10/30/2019 12:11 AM

Robert Bernson

You have permission

On Oct 29, 2019, at 9:03 PM, Robert Bernson <rberkson91@knights.ucf.edu> wrote:

Hello Scott,

My name is Robert Bernson and I would like to use the figures you made for the absorption and emission spectra of Chlorophyll A you made and posted on the following page: <https://omlc.org/spectra/PhotochemCAD/html/1122.html>

I will be using them for my capstone course's research paper on chlorophyll fluorescence spectroscopy and will use proper citation.

Sincerely,
Robert

Proof of permission from Greg Sun

RE: Requesting permission to use figures



Greg Sun <Greg.Sun@umb.edu>

Wed 10/30/2019 8:32 AM

Robert Bernson

Dear Robert,

Please go ahead with the figure. Thanks for checking.

Greg

From: Robert Bernson [mailto:rberkson91@Knights.ucf.edu]

Sent: Wednesday, October 30, 2019 4:25 AM

To: Greg Sun <Greg.Sun@umb.edu>

Subject: Requesting permission to use figures

[EXTERNAL SENDER]

Greg,


My name is Robert Bernson and I would like to use Figure 1 in your paper "Intersubband approach to silicon based lasers—circumventing the indirect bandgap limitation."

I will be using it for my capstone course's research paper on chlorophyll fluorescence spectroscopy and will use proper citation.

Sincerely,
Robert

Proof of permission from Edmund Optics

Edmund Optics Technical Support - Photo Permission

 Austin O'Neill <AO'Neill@edmundoptics.com>
Thu 10/31/2019 2:15 PM
Robert Bernson; Gretchen Morris <GMorris@edmundoptics.com>

Hi Robert,

Thank you for contacting Edmund Optics Technical Support.


I have CC'd our Director of Creative Services, Gretchen Morris, she will be happy to work with you to get the correct permissions for use in your research paper.

Good Luck in your academic endeavors!

Best Regards,

Austin O'Neill | Product Support Technician

Edmund Optics® Headquarters
p: +1 856.547.3488 ext. 6143



The Future Depends on Optics

From: eo-service@edmundoptics.com <eo-service@edmundoptics.com>
Sent: Thursday, October 31, 2019 1:55 PM
To: Technical Support USA <techsup@edmundoptics.com>
Subject: Edmund Optics: Technical Support : EN - 15798

Edmund Optics: Technical Support : EN - 15798

Reason for Contact:	Technical Support
Country:	United States
First Name:	Robert
Last Name:	Bernson
Company:	UCF
Job Title:	Student
Phone Number:	4109716713
Ext:	
Email Address:	rbernson91@knights.ucf.edu
Military/Defense Related?:	False
Comments:	My name is Robert Bernson and I am a student at the University of Central Florida working on a research paper. I would like to use the image comparing shortpass, longpass, and bandpass filters on this page: https://www.edmundoptics.com/campaigns/high-performance-optical-filters/ . This image will be properly cited and the paper will not be used for monetary gain. Sincerely, Robert Bernson https://www.edmundoptics.com/contact-support/

Referring Page URL:
User Agent:
UserIp:

This email has been automatically generated. Please do not reply to this message.

(10/31/2019 05:54 PM EST)

Permission for [ONS.AR0130]

Re: Request for Permission SR#241395



Steve West <Steve.West@onsemi.com>
To: David Maria
Cc: Steve West

Tue 11/26/2019 6:15 PM

Hello David,

Please consider this email as official permission from ON Semiconductor (Semiconductor Components Industries, LLC) to use Figure 29 from the AR0130CS/D data sheet in your capstone research paper as indicated in the information outlined below. Please make sure to provide the following attribution statement: *Used with permission from SCILLC dba ON Semiconductor.*

In the future, any and all copyright requests may be sent directly to me.

Best Regards,
Steve



Steve West | ON Semiconductor
Global Technical Publications Manager
Marketing Communications
602.616.5816 (W)
480.619.0930 (M) | 866.435.1399 (F)
steve.west@onsemi.com

Follow us: [Twitter](#) | [Facebook](#) | [LinkedIn](#) | [YouTube](#) | [Blog](#)

Proof for Richardson grating efficiency curve

Request to use grating curve in a paper



Samuel Knight
To gratings@newport.com
Cc Bobby Bernson; davidjmaria@knights.ucf.edu; Luke Preston

Reply Reply All Forward ...

Sat 11/30/2019 5:36 PM

Hello,

I am an undergraduate student at CREOL, the College of Optics and Photonics, at the University of Central Florida. I'm doing a chlorophyll fluorescence spectrometer for my senior design capstone project and I'd like to use your efficiency curve from your 53-*270R data sheet as part of my report since I used this same grating in my design. This report will not be published for monetary gain but will be hosted online for peer review. I will cite the source appropriately and give reference to the owner.

Regards,
Samuel Knight

Proof for ON Semiconductor sensor efficiency

First Name	Samuel
Last Name	Knight
Company name	N/A
Phone	*
Email Address	knightsc@knights.ucf.edu
Country	UNITED STATES
Product Type	Sensors
Part Number	AR0130CS
Estimated Annual Usage	3
Subject	Request for permission
Description (max. 2000 characters)	Hello, I am an undergraduate student at <u>CREOL</u> , the College of Optics and <u>Photonics</u> , at the University of Central Florida. I'm doing a chlorophyll fluorescence spectrometer for my senior design capstone project and I'd like to use your monochromatic efficiency curve from your <u>AR0130CS</u> data sheet as part of my report since I used the monochrome sensor in my design. This report will not be published for
First Name	Samuel
Last Name	Knight
Company name	N/A
Phone	*
Email Address	knightsc@knights.ucf.edu
Country	UNITED STATES
Product Type	Sensors
Part Number	AR0130CS
Estimated Annual Usage	3
Subject	Request for permission
Description (max. 2000 characters)	I'm doing a chlorophyll fluorescence spectrometer for my senior design capstone project and I'd like to use your monochromatic efficiency curve from your <u>AR0130CS</u> data sheet as part of my report since I used the monochrome sensor in my design. This report will not be published for monetary gain but will be hosted online for peer review. I will cite the source appropriately and give reference to the owner.

Appendix C – Extra Tables and Figures

Table 35. (Appendix) Efficiency and loss at relevant interfaces

	600nm	683nm	700nm
Sensor quantum efficiency (%)	78	69	68
Sensor loss (dB)	1.0790	1.6115	1.6749
Concave mirror reflectance (%)	97	98	98
Concave mirror loss (dB)	0.1323	0.0877	0.0877
Grating spectral efficiency (%)	73	63	62
Grating spectral loss (dB)	1.3668	2.0066	2.0761

Loss calculated using $10 \log_{10} \left(\frac{1}{\Gamma} \right)$, where Γ is the quantum efficiency/reflectance/spectral efficiency in decimal form. Modified from $10 \log_{10} \left(\frac{P_0}{P_f} \right)$ where P_0 is the incident power and P_f is the power after the surface interaction. Table 35 assumes the only loss at that surface comes from the efficiency or reflectance and thus does not include losses from scratches, digs, or settled surface particles.